

Studies on the Measurement of Differential
Luminosity using Bhabha Events at the
International Linear Collider

Diplomarbeit

Humboldt-Universität zu Berlin
Mathematisch-Naturwissenschaftliche Fakultät I
Institut für Physik

eingereicht von

André Philippe Sailer
geboren am 29.11.1983 in Berlin

Abstract

The International Linear Collider (ILC) is an electron-positron-collider with a variable center-of-mass energy \sqrt{s} between 200 and 500 GeV. The small bunch sizes needed to reach the design luminosity of $L_{\text{Peak}} = 2 \cdot 10^{34} \text{ cm}^{-2}\text{s}^{-1}$ necessary for the physics goals of the ILC, cause the particles to radiate beamstrahlung during the bunch crossings. Beamstrahlung reduces the center-of-mass energy from its nominal value to the effective center-of-mass energy $\sqrt{s'}$. The spectrum of the effective center-of-mass energy $\sqrt{s'}$ is the differential luminosity $dL/d\sqrt{s'}$, which has to be known to precisely measure particle masses through threshold scans.

The differential luminosity can be measured by using Bhabha events. The real differential luminosity is simulated by the GuineaPig [1] software. The energy spectrum of the Bhabha events is measured by the detector and compared to the energy spectrum of Monte Carlo (MC) Bhabha events with a known differential luminosity given by an approximate parameterization. The parameterization is used to assign each MC event a weight. By re-weighting the events, until the energy spectra from the real and the MC Bhabha events match, the differential luminosity can be measured.

The approximate parameterization of the differential luminosity is given by the Circe parameterization introduced by Ohl [2], which does not include the correlation between the particle energies due to beamstrahlung. The Circe parameterization is extended to include the correlation and better describe the differential luminosity. With this new parameterization of the differential luminosity it is possible to predict the observed production cross section of a MC toy particle with a mass of $250 \text{ GeV}/c^2$ to a precision better than 0.2%.

Using the re-weighting fit with the extended parameterization also allows the measurement of the beam energy spreads of $\sigma_E/E = 0.0014$ for electrons and $\sigma_E/E = 0.0010$ for positrons with a precision of a few percent.

The total error from the measured differential luminosity and beam energy spreads on the mass of a toy particle measured in a production threshold scan is found to be $7 \text{ MeV}/c^2$ for a $250 \text{ GeV}/c^2$ particle, with an integrated luminosity of 5fb^{-1} per scanning point.

Zusammenfassung

Der International Linear Collider (ILC) ist ein Beschleuniger für Elektronen und Positronen mit einer variablen Schwerpunktsenergie \sqrt{s} zwischen 200 und 500 GeV. Die Abmessungen der Teilchenpakete im ILC müssen sehr klein sein, um die geplante Luminosität von $L_{\text{Peak}} = 2 \cdot 10^{34} \text{ cm}^{-2}\text{s}^{-1}$ zu erreichen. Diese Luminosität wird benötigt, um die physikalischen Ziele des ILC zu verwirklichen.

Während des Kreuzens der Teilchenpakete im Wechselwirkungspunkt produzieren die Elektronen und Positronen Beamstrahlung bevor sie annihilieren. Durch die Beamstrahlung verringert sich allerdings die nominelle Schwerpunktsenergie auf die effektive Schwerpunktsenergie $\sqrt{s'}$. Die Verteilung von Annihilationsereignissen je effektiver Schwerpunktsenergie wird differentielle Luminosität $dL/d\sqrt{s'}$ genannt. Diese muss exakt bekannt sein, um die Massen von Elementarteilchen durch Schwellenscans bestimmen zu können.

Die differentielle Luminosität kann mit Hilfe der Bhabha-Streuung gemessen werden. Zunächst wird die wahre differentielle Luminosität mit Hilfe des Simulationsprogramms GuineaPig [1] generiert. Das Energiespektrum der Monte Carlo (MC) Bhabha-Ereignisse folgt einer bekannten differentiellen Luminosität, welche durch eine angenäherte Parametrisierung beschrieben wird. Diese Parametrisierung wird benutzt, um jedem MC Bhabha-Ereignis ein Gewicht zuzuweisen. Dieses simulierte Energiespektrum wird dann mit dem vom Detektor gemessenen Energiespektrum der Bhabha-Ereignisse verglichen. Die differentielle Luminosität wird dabei gemessen, indem die Ereignisse wiederholt neu gewichtet werden, bis das gemessene Energiespektrum mit dem simulierten Energiespektrum übereinstimmt.

Für die Parametrisierung wird zunächst die von Ohl eingeführte Circe-Parametrisierung [2] benutzt. Damit lässt sich allerdings nicht die Korrelation zwischen den Energien der streuenden Teilchen beschreiben. Deshalb wird die Circe-Parametrisierung mit weiteren freien Parametern ergänzt, um die differentielle Luminosität besser zu beschreiben. Die neue Parametrisierung ermöglicht es, die beobachteten Produktions-Querschnitte eines MC Teilchens mit einer Masse von $250 \text{ GeV}/c^2$ mit einer Abweichung von weniger als 0,2% vorherzusagen.

Mit Hilfe des Rewichtens und der erweiterten Parametrisierung ist es außerdem möglich, die Energieunschärfe der Elektronen von $\sigma_E/E = 0,0014$ bzw. Positronen von $\sigma_E/E = 0,0010$ mit einer Genauigkeit von einigen Prozent zu messen. Der gesamte Fehler, der sich durch die gemessene differentielle Luminosität und Strahlenergieunschärfen auf die Masse des MC Teilchens überträgt, ist $7 \text{ MeV}/c^2$ bei einer Masse von $m = 250 \text{ GeV}/c^2$ und einer integrierten Luminosität von 5fb^{-1} pro Messpunkt des Schwellenscans.

Dedication

The following thesis could not have been done without the help by many people. I would like to thank the LC group at DESY Zeuthen for the extremely positive working environment, especially Klaus Mönig for giving me this interesting topic and guiding my work and Michele Viti for the discussions that deepened my understanding of what I was actually doing.

I would like to thank all the teachers, friends and relatives for encouraging and nurturing my curiosity and showing interest in my work.

Most of all I would like to thank my parents without your unwavering support, dedication and love none of this had been possible.

Contents

1	Introduction	1
2	The International Linear Collider	5
2.1	Baseline Design	5
2.2	Luminosity and Beam Parameters	6
2.3	Detector	7
2.3.1	Detector Resolution	9
3	Beamstrahlung	13
3.1	Forces inside a Bunch	13
3.1.1	Disruption	15
3.1.2	Beamstrahlung	15
3.1.3	Beamstrahlung and Disruption at the ILC	16
3.2	Simulating Beamstrahlung	16
3.3	Correlation between the Energy of Scattering Particles	16
4	Differential Luminosity	19
4.1	Particle Energy Spectrum	19
4.1.1	Beam Energy Spread	19
4.1.2	Beamstrahlung	20
4.1.3	Initial and Final State Radiation	20
4.2	Threshold Scan	21
4.2.1	Cross Section of the MC Toy Particle	22
4.2.2	Threshold Scan with Beam Energy Spread	22
5	Circe Parameterization for Beamstrahlung	25
5.1	Particle Energy Parameterization	25
5.2	Parameterization for the Differential Luminosity	26
5.3	Transformation of the Parameterization	27
5.3.1	Producing a Spectrum According to the Parameterization	29
5.4	Fitting the GuineaPig Spectrum	30
5.4.1	Fit to the One-Dimensional Spectrum	30
5.4.2	Fit to the Two-Dimensional Spectrum	30
5.4.3	Effective Center-of-Mass Energy Spectrum	33
5.4.4	Directly Fitting the Effective Center-of-Mass Energy	34

5.4.5	Threshold Scan	34
6	Parameterization including Correlation	37
6.1	Differences due to Correlation	37
6.1.1	Probability Parameters	37
6.1.2	Beta-Distribution Parameters	38
6.2	Correlated Parameterization (CoPa)	39
6.2.1	Fitting CoPa to GuineaPig	39
6.2.2	Differences between CoPa and GuineaPig	40
6.3	Differing Beam Parameters - Asymmetric Parameterization (Asym)	41
7	Measuring the Center-of-Mass Energies of Bhabha Events	45
7.1	Bhabha Scattering	45
7.1.1	Simulation Software BHWide	45
7.1.2	Acceptance Region and Cross Section	46
7.2	Effective Center-of-Mass Energy	46
7.2.1	Measurement using the Tracker	46
7.2.2	Measurement by the Calorimeter	48
8	Measuring the Differential Luminosity	51
8.1	Re-weighting Fit	51
8.1.1	One-Dimensional Histogram	52
8.1.2	Two-Dimensional Histogram	52
8.1.3	Three-Dimensional Histogram	52
8.1.4	Calculating the Chi-Square	53
8.2	Data and Monte Carlo Bhabha Events	53
8.3	Determining the Circe Parameters	53
8.3.1	Fitting Circe to Circe	54
8.3.2	Fitting Circe to GuineaPig	55
8.4	Determination of the CoPa Parameters	58
8.4.1	Fitting CoPa to CoPa	59
8.4.2	Fitting CoPa to GuineaPig	59
8.5	Measuring with the Asymmetric Parameterization	64
8.5.1	Re-weighting Fit with the Three-Dimensional Histogram	64
8.5.2	Measuring the Asymmetric Spectrum with the Symmetric Parameterizations	65
9	Measuring a Luminosity Spectrum including Beam Energy Spread	67
9.1	Adding the Beam Energy Spread to the Re-Weighting Fit	67
9.1.1	Effect on Measured Energy Spectra	68
9.2	Measuring a Symmetric Beam Energy Spread	69
9.2.1	Threshold Scan with Beam Energy Spread	69
9.3	Measuring the real Beam Energy Spread	70
9.4	Mass Measurement	71

10 Conclusion	75
A Calculating the Effective Center-of-Mass Energy from the Angles	77
Bibliography	81
List of Figures	83
List of Tables	87

Chapter 1

Introduction

The Standard Model (SM) of particle physics is one of the best tested physical theories today and in almost all cases the predictions of the SM have been confirmed within theoretical and experimental uncertainties. The only particle predicted by the Standard Model that has not been found so far is the Higgs boson, responsible for the masses of all particles. It is expected that the Higgs boson will be found in the near future by the Large Hadron Collider (LHC) somewhere around $m_H \approx 140 - 200 \text{ GeV}^1$ and thus completing the particle spectrum of the Standard Model. There is compelling evidence for new physics beyond the Standard Model like Super-Symmetry (SuSy), which predicts at least one partner for each SM particle. Some of the lighter SuSy particles are also expected to be within the reach of the LHC. The lightest SuSy particle could be a candidate for dark matter.

Because the LHC collides protons, the initial state of the interactions of the proton constituents are not well defined and the resolution of the mass measurements will be a few GeV. Unlike the LHC the International Linear Collider (ILC) collides electrons and positrons. These point-like particles carry the full momentum instead of a fraction of the energy like the constituents of protons. This means that the initial state of the interaction is better known at the ILC than at the LHC.

The ILC will be a precision machine to determine the mass and quantum numbers of the Higgs boson, SuSy particles or other particles demanded by physics beyond the Standard Model. It will be able to determine the mass of the top quark to a precision of less than 100 MeV .

In order to achieve these high precisions, the nominal electron/positron beam energy has to be variable between 200 and 500 GeV, and the nominal energy must be measurable to a precision of $\delta E/E \approx 10^{-4}$ [3]. The ILC must further provide a very high peak luminosity of $L_{\text{Peak}} = 2 \cdot 10^{34} \text{ cm}^{-2}\text{s}^{-1}$ to produce the particles at a high enough rate. This peak luminosity is reached by using very small bunches with a high charge density. Dense charge distributions, causing high field strengths and strong forces on the particles of the opposite bunches, generate two important effects. The first one is the focusing of the bunches. The particles are attracted by the opposite charges and pulled inwards. This pinch increases the luminosity by a factor of 1.3

¹Throughout the thesis a system of units with $\hbar = c = 1$ is used.

to 2.0. The other effect is known as beamstrahlung. Because of the deflection the particles radiate and therefore lose energy. Individual electrons can lose up to 40% of their energy, while the whole bunch loses about 3% of the total energy. The second effect is of course undesirable, but the need for a high luminosity makes it unavoidable. The initial state of the interactions at the nominal center-of-mass energy \sqrt{s} is smeared out by the beamstrahlung into the effective center-of-mass energy $\sqrt{s'}$. The spectrum of the events per $\sqrt{s'}$ is called the differential luminosity $dL/d\sqrt{s'}$.

The spectrum of the particle energies due to beamstrahlung is neither directly accessible, because the energies of the particles are further changed by Initial and Final State Radiation (ISR/FSR), nor can it be predicted easily, because the geometry of the bunches can be severely changed in the accelerator. It is also not enough to measure the resulting beamstrahlung photons, because while all particles could radiate beamstrahlung, only some particles will be able to annihilate, if the bunch is deformed into a banana shape for example. Thus the energy spectrum of the colliding bunches has to be extracted by measuring the acollinearity and the energy of Bhabha events. The energy spectrum is the convolution of beamstrahlung, ISR and FSR. To extract the differential luminosity the energy spectra have to be compared to energy spectra with a known differential luminosity. A study done by Mönig [4], where the known energy spectrum after beamstrahlung was created according to the approximate parameterization introduced by Ohl called Circe [2], showed that the correlation between the energies of scattering particles due to beamstrahlung is an important effect and has to be included for a precise description of the differential luminosity.

In this thesis a re-weighting fit is used, where the data from the detector is compared with a sample of simulated Bhabha events with a known differential luminosity given by a parameterization. The weights of the simulated events are re-weighted until the simulated energy spectrum matches the energy spectrum of the data. The resulting parameters should describe the differential luminosity due to beamstrahlung of the data events.

The unknown differential luminosity due to beamstrahlung is given by the program GuineaPig [1] that simulates the bunch crossings in a linear collider. The known differential luminosity of the Bhabha events is at first given by the Circe parameterization, which is extended to also include the correlation between the energies of the scattering particles.

The thesis is organized as follows. In chapter 2 a brief overview over the ILC, one of its detectors and the beam properties at the interaction point is given. This is a very short summary of the recently published reference design report (RDR) [5], which describes the baseline design of the accelerator, the detector concepts and the physics goals of the ILC.

Chapter 3 describes the effects of the small bunch sizes known as disruption and beamstrahlung, as well as the software to simulate bunch crossings and why there is some correlation between the energies of scattering particles.

The differential luminosity is further detailed in chapter 4, where other contri-

butions to the energy spectrum of the Bhabha events are briefly discussed. The effect of the differential luminosity on the interacting particles is visualized with the threshold scan for the hypothetical toy particle with a mass of 250 GeV.

Chapters 5 and 6 introduce parameterizations to describe the differential luminosity due to beamstrahlung. At first the Circe parameterization is described. The parameters best describing the differential luminosity produced through GuineaPig are found by fitting the parameterization directly to the differential luminosity. It is shown that Circe does not suffice to properly describe the energy spectrum of the particles before scattering. Chapter 6 expands the Circe parameterization to reduce the difference between the simulated and parameterized differential luminosity by accounting for the correlation of the energy of interacting particles. Because it includes correlation, this parameterization is called Correlated Parameterization (CoPa). This parameterization is expanded for the most general case, where two beams with different beam parameters collide. Because of the asymmetry of the resulting spectrum this parameterization is called “Asym”.

Chapter 7 explains how the Bhabha events are used to measure the energy spectra in the detector using the acollinearity of outgoing particles and the energy deposited in the calorimeters.

The re-weighting method is explained in chapter 8 and the one-, two- and three-dimensional histograms that are used to extract the beamstrahlung parameterizations out of the measured Bhabha events are introduced. The re-weighting method is used to extract the parameters of the Circe parameterization and from this starting point the other parameterizations are also extracted out of the energy spectra of the Bhabha events. To describe the real differential luminosity for the ILC the beam energy spread is included in the generation of the Bhabha events and measured as described in chapter 9. The measured differential luminosity and beam energy spread is then used to determine the mass of the MC toy particle.

Finally a brief summary and some conclusions are presented in chapter 10.

Chapter 2

The International Linear Collider

The International Linear Collider (ILC) is a proposal for the next large electron-positron collider at the terascale. Its first stage will offer a variable center-of-mass energy \sqrt{s} between 200 and 500 GeV, an upgrade could offer up to 1 TeV. This energy range is expected to cover the range where the Higgs boson as well as supersymmetric particles, like dark matter candidates, can be produced and studied. It will also be possible to measure the mass of the top quark to a precision of at least a factor of ten better than possible at the LHC [6].

2.1 Baseline Design

The electrons and positrons are accelerated in a linear accelerator, because the synchrotron radiation in a ring collider would cause an enormous energy loss. The energy loss per revolution is [7]:

$$E_{\text{loss}}[\text{GeV}] = 8.85 \cdot 10^{-5} \frac{(E_{\text{Beam}}[\text{GeV}])^4}{r[\text{m}]} \quad (2.1)$$

This loss has to be replaced by radio frequency (RF) power. However for a reasonably sized ring collider the lost energy at 250 GeV would be much larger than the RF power. A circular collider with the same tunnel length as the ILC (33 km) would mean that the particles lose 66 GeV per revolution. A much larger radius would be needed, which means higher costs for the excavation of the tunnel. A linear accelerator thus becomes cheaper than a ring collider even though much more RF cavities are needed in this case.

The main parts of the ILC (Figure 2.1) are

- a polarized electron source based on a photo-cathode,
- an undulator based positron source that uses the 150 GeV electrons from the main linear accelerator (linac),
- two damping rings with a 6.7 km circumference to cool the electrons and positrons down at a beam energy of 5 GeV,

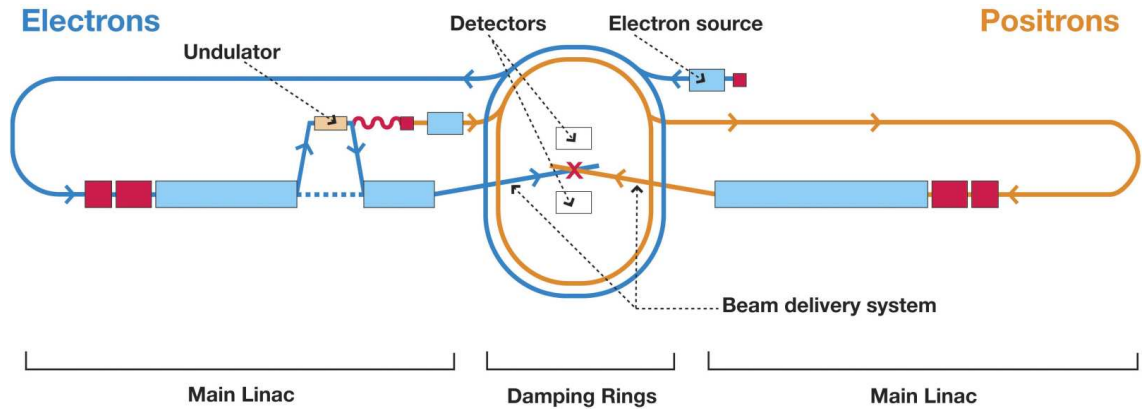


Figure 2.1: Layout of the ILC [8].

- two beam transportation lines to transport the bunches from the damping rings to the beginning of the main linacs,
- two 11 km long main linacs using superconducting radio frequency (SCRF) cavities at a gradient of 31.5 MV/m (about 16000 cavities are needed for 500 GeV center-of-mass energy),
- a 4.5 km long beam delivery system that houses diagnostics and brings the beams into collision at a 14 mrad crossing angle,
- a single interaction point that is shared by two detectors in a “push-pull” configuration.

The crossing angle is necessary to keep the outgoing bunches from one beam away from the incoming bunches of the other beam. In order to keep the bunches overlapped during the bunch crossing the bunches are rotated accordingly and move sideways towards the other bunch. This is called “crab-crossing”.

2.2 Luminosity and Beam Parameters

Cross sections are inversely proportional to the center-of-mass energy, which means that the cross sections at high energies become very small. In order to produce the interesting events with the ILC, the peak luminosity

$$L_{\text{Peak}} = f_{\text{rep}} n_b \frac{N^2}{4\pi\sigma_x\sigma_y} H_D \quad (2.2)$$

has to be large. The design luminosity at the ILC is $L_{\text{Peak}} = 2 \cdot 10^{34} \text{ cm}^{-2}\text{s}^{-1}$. Such a high luminosity can only be achieved with a large number of particles N and small bunch sizes $\sigma_{x/y}$, because the bunch train repetition rate f_{rep} and the number of bunches per train are limited by the power output in the accelerator and the necessary cooling time in the damping ring [9]. H_D is the luminosity enhancement

factor caused by the focusing of the bunches due to electromagnetic forces of the bunches (See Chapter 3). The nominal beam parameters necessary to reach the design luminosity are found in Table 2.1. The integrated luminosity is expected to reach $L_{\text{int}} = 500\text{fb}^{-1}$ in the first four years of operation.

To overcome some foreseeable problems inside the accelerator several different beam parameter sets exist. Each parameter set (Table 2.1) yields the same peak luminosity. In the “Low N” set for example the number of particles per bunch is reduced, if the larger number of charged particles causes instabilities in the accelerator. By increasing the number of bunches, and making the bunches smaller the design luminosity is still reached [3].

2.3 Detector

At the release of the ILC reference design report (RDR) there were four concepts for detectors at the ILC. Two of those are now merging into a single concept, the International Large Detector (ILD). All detectors are evolving and are being optimized. This study used a version of the simulation software for the Large Detector Concept (LDC) that is now part of the ILD. The LDC detector is designed with the concept of “particle-flow” in mind to achieve a good jet energy resolution. Particle flow means that the four-vectors of all visible particles in an event are reconstructed and their energy is measured by the tracker. The energy measured for neutral particles, like photons, is taken from the calorimeter. To separate the clusters from charged particles a high granularity of the calorimeter is more important than the energy resolution or the calorimeter, any cluster associated to the track of a charged particle is no longer available for the energy of a neutral particle [10].

The detector subsystems of the LDC from the interaction point (IP) outwards (Figure 2.2) are [11]

- silicon pixel and strip detectors for vertex detection and tracking,
- a Time Projection Chamber (TPC) for further tracking,
- a granular silicon-tungsten (SiW) electromagnetic calorimeter,
- a granular iron-scintillator hadronic calorimeter,
- a large volume superconducting coil with a longitudinal B-field of 4 Tesla,
- an instrumented iron return yoke that serves as the muon filter and detector,
- the corresponding detectors in the end-caps and detectors to monitor luminosity and collision quality in the very forward region.

Table 2.1: Beam parameters for the ILC at $\sqrt{s} = 500$ GeV [3].

Parameter	Symbol/Units	Nominal	Low	N	Large	Y	Low	P
Repetition rate	f_{rep}/Hz	5	5	5	5	5	5	5
Particles per Bunch	$N/10^{10}$	2	1	2	2	2	2	2
Number of bunches per pulse	n_b	2625	5120	2625	2625	2625	1320	1320
Bunch interval in the Main Linac	t_b/ns	369.2	189.2	369.2	369.2	369.2	480.0	480.0
RMS horizontal bunch size at IP	σ_x^*/nm	639	474	474	474	474	474	474
RMS vertical bunch size at IP	σ_y^*/nm	5.7	3.5	9.9	9.9	9.9	3.8	3.8
Normalized emittance at IP	$\gamma\epsilon_{x'}^*/\text{mm} \cdot \text{mrad}$	10	10	10	10	10	10	10
Normalized emittance at IP	$\gamma\epsilon_{y'}^*/\text{mm} \cdot \text{mrad}$	0.04	0.03	0.08	0.08	0.08	0.036	0.036
Beta function at IP	β_x^*/mm	20	11	11	11	11	11	11
Beta function at IP	β_y^*/mm	0.4	0.2	0.6	0.6	0.6	0.2	0.2
RMS Bunch length	$\sigma_z/\mu\text{m}$	300	200	500	500	500	200	200
Luminosity enhancement factor	H_D	1.71	1.48	2.18	2.18	2.18	1.64	1.64
Geometric luminosity	$L_{\text{geo}}/(10^{34} \text{ cm}^{-2} \text{ s}^{-1})$	1.20	1.35	0.94	0.94	0.94	1.21	1.21
Luminosity	$L/(10^{34} \text{ cm}^{-2} \text{ s}^{-1})$	2	2	2	2	2	2	2
Energy spread at IP for e^-/e^+	$\sigma_E/E \cdot 10^{-3}$	1.4/1.0	1.4/1.0	1.4/1.0	1.4/1.0	1.4/1.0	1.4/1.0	1.4/1.0

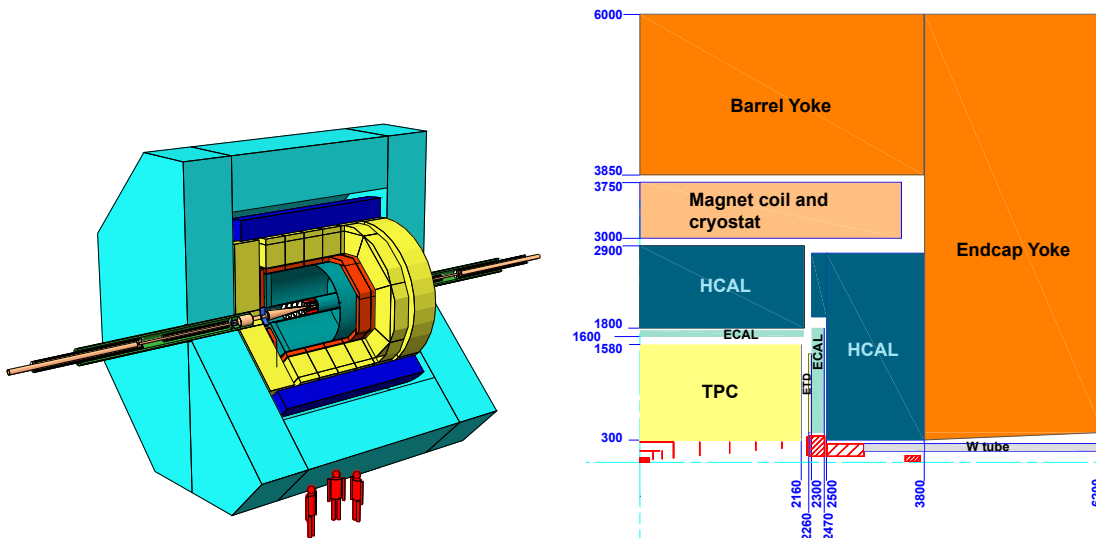


Figure 2.2: An overview of the LDC detector [11].

2.3.1 Detector Resolution

The detector is designed to reach an energy resolution in the electromagnetic calorimeter of

$$\frac{\sigma_e}{E} = \frac{15\%}{\sqrt{E}}, \quad (2.3)$$

equalling a resolution of about 1% for 250 GeV electrons. To confirm this, the geant4 [12] based detector simulation software “Mokka” [13] with the detector model “LDCPrime02Sc” and the reconstruction software “Marlin” [14] were used. 130,000 Bhabha events were simulated and reconstructed. Two problems were found during the analysis of the simulation results. One problem was a small error in the simulation software that made hits in the forward tracker at about 10° and 170° very unlikely, so that almost no events in this region were reconstructed (Figure 2.3). This problem has since been fixed and the tracking works properly in this region.

The cause of the other problem is not yet clear. It was found that some particles were reconstructed with energies of more than 300 GeV (Figure 2.4). In the standard reconstruction done by the Particle Flow Algorithm (PFA) in Marlin the reconstructed energy is dominated by the tracking. The resolution of the reconstructed energies could be improved by relying on the energies measured by the calorimeter instead. This changed the reconstructed particle energy spectrum from the left in Figure 2.5 to the right. The effective detector resolution in the later case is roughly 1.3%. It can be expected that the energy resolution of the reconstruction will be improved and for this reason an energy resolution for the electrons and positrons of 1% is assumed in this thesis.

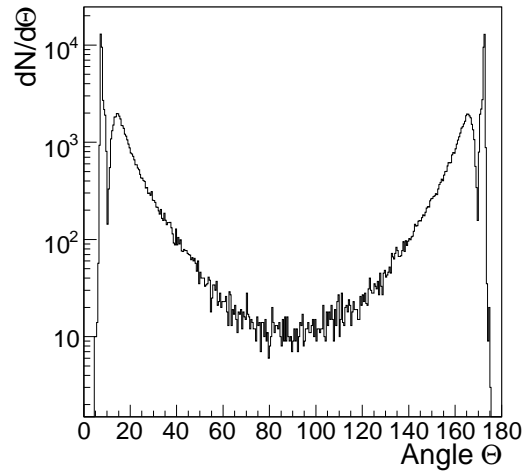
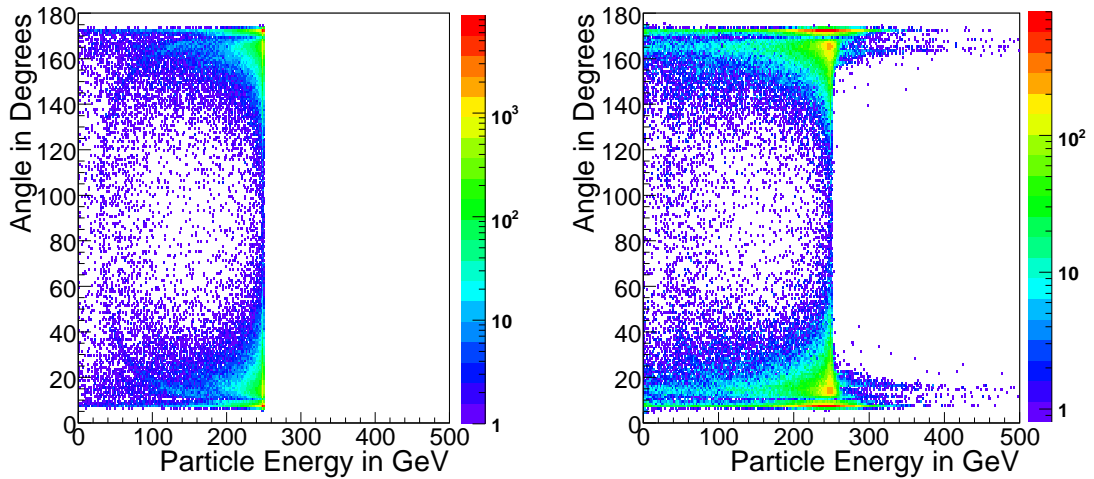


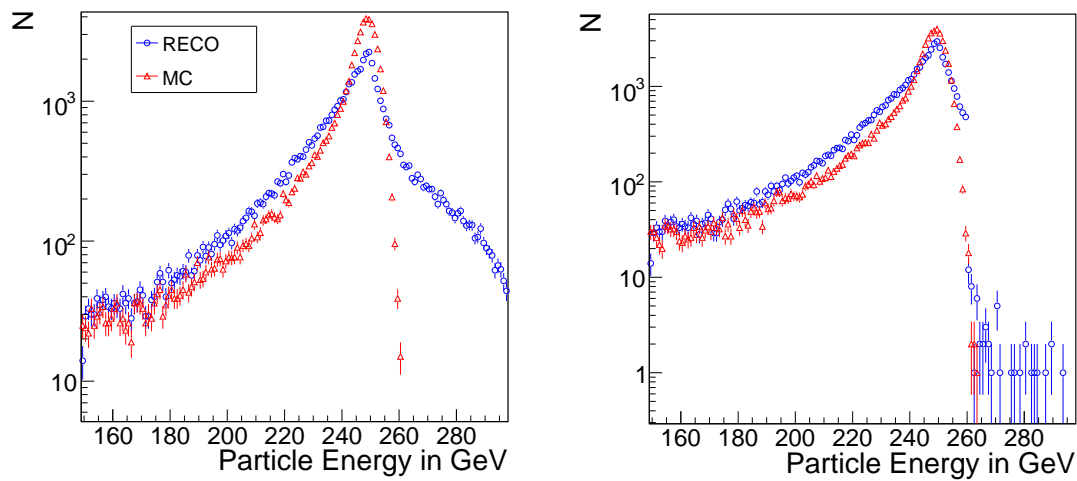
Figure 2.3: The polar angle of the reconstructed events. The dips at 10° and 170° were caused by a bug in the simulation software.



(a) Polar angle and energy used as the input for the simulation.

(b) Polar angle and energy after simulation and reconstruction.

Figure 2.4: Polar angles and energies of the Bhabha events before and after simulation and reconstruction. The reconstructed events with particle energies above 300 GeV and the problems for 10° and 170° are visible. The gap in the polar angle distribution is visible on the left as well, because only events are shown, that could be reconstructed.



(a) Reconstructed particle energy by Marlin and particle energy before the simulation.

(b) Particle energy reconstructed by using the calorimeter information and the particle energy before the simulation.

Figure 2.5: RECO refers to the energy reconstructed by Marlin originally (left) and by using the energy deposited in the calorimeter (right). MC refers to the energies of the Monte Carlo particles smeared with a 1.3% Gaussian to compare the resolution with the resolution from the detector simulation and reconstruction.

Chapter 3

Beamstrahlung

The demands for high luminosity and the extremely small beam sizes necessary at the ILC give rise to the phenomena known as disruption and beamstrahlung. The strong fields inside a bunch deflect the particles of the other bunch and causes them to emit radiation and vice versa.

3.1 Forces inside a Bunch

To qualitatively understand the effects of small bunch sizes during a bunch crossing the model of a homogeneous, cylindrical bunch geometry is sufficient. Analogous calculations are found in [15; 16; 1]. For a cylindrical bunch of N electrons with charge $-e$, of length L and radius R the homogeneous charge distribution ρ_0 inside the bunch limits is

$$\rho_0 = \frac{-Ne}{\pi R^2 L}. \quad (3.1)$$

The bunch moves in z -direction at a speed $v \approx c = 1$ in the laboratory system. To calculate the electric $E(r)$ and magnetic $B(r)$ fields inside the bunch at a distance $r < R$ from the center Gauss' and Ampère's law and the respective loops and surfaces shown in Figure 3.1 are used. The fields are

$$\vec{E}(r) = \vec{e}_r \frac{-Ne}{\epsilon_0 2\pi L R^2} r, \quad (3.2)$$

$$\vec{B}(r) = \vec{e}_\phi \frac{-Ne}{2\pi L R^2} \mu_0 v r. \quad (3.3)$$

The electric field points in the radial direction along unit vector \vec{e}_r and the magnetic field is directed azimuthally around the cylinder axis along unit vector \vec{e}_ϕ . The Lorentz force on an electron inside the bunch is

$$\vec{F}_{\text{intern}} = -e(\vec{E} + \vec{v} \times \vec{B}) = \vec{e}_r \frac{Ne^2}{\epsilon_0 2\pi L R^2} (1 - v^2) r = \vec{e}_r \frac{Ne^2}{\gamma^2 \epsilon_0 2\pi L R^2} r, \quad (3.4)$$

with $\gamma = (1 - v^2)^{-1/2}$ and $\epsilon_0 \mu_0 = 1$. For highly relativistic bunches the forces on the particles of the same bunch nearly cancel, because of $\gamma = E_{\text{beam}}/m_e = 5 \cdot 10^5$ at

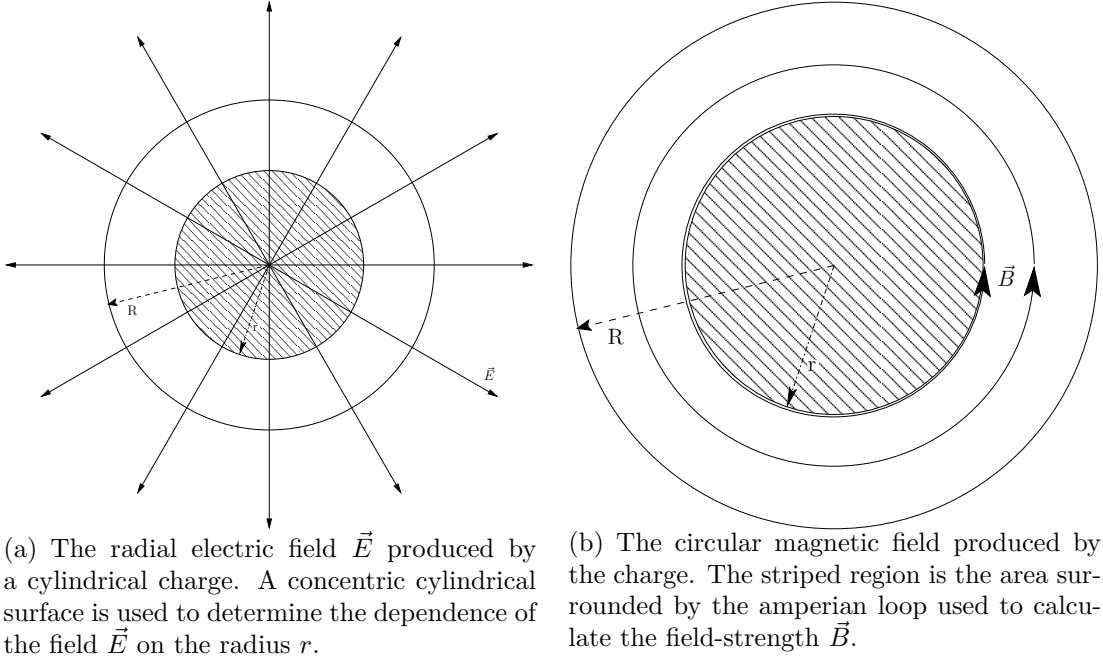


Figure 3.1: Gauss surface and Amperian loop.

250 GeV. The forces add up for a single oncoming positron with charge e passing through the bunch with $v \approx c = 1$ to

$$\vec{F}_{\text{extern}} = e(\vec{E} - \vec{v} \times \vec{B}) = -e\vec{e}_r \frac{Ne^2}{\epsilon_0 2\pi LR^2} (1 + v^2) r \approx -e\vec{e}_r \frac{Ne^2}{\epsilon_0 2\pi LR^2} 2r. \quad (3.5)$$

In the case of a homogeneous, cylindrical charge distribution the particle will perform a harmonic oscillation around the beam axis only depending on the absolute distance to the cylinder axis r . Let the particle enter the bunch at a distance $r_0 = r(0)$ from the center at $t = 0$, then from the equation of motion

$$\gamma m_e \ddot{r}(t) = -\frac{Ne^2}{\epsilon_0 \pi LR^2} r(t) \quad (3.6)$$

follows for the position

$$r(t) = r_0 \cos\left(\sqrt{\frac{Ne^2}{\pi \epsilon_0 m_e LR^2 \gamma}} t\right). \quad (3.7)$$

Or in terms of the longitudinal position $z = ct$ inside the bunch:

$$r(z) = r_0 \cos\left(\sqrt{\frac{Ne^2 L}{\pi \epsilon_0 m_e R^2 \gamma}} \frac{z}{L}\right) \quad (3.8)$$

3.1.1 Disruption

The period of the motion (3.8) is used to define the so called disruption parameter D [15]:

$$D = \frac{1}{\sqrt{3}} \frac{4Nr_e L}{R^2 \gamma}, \quad (3.9)$$

$r_e = \frac{e^2}{4\pi\epsilon_0 m_e}$ is the classical electron radius. The disruption parameters for a beam with Gaussian profiles $\sigma_x \neq \sigma_y$ are [16]

$$D_x = \frac{2Nr_e \sigma_z}{\sigma_x(\sigma_x + \sigma_y)\gamma} \quad \text{and} \quad D_y = \frac{2Nr_e \sigma_z}{\sigma_y(\sigma_x + \sigma_y)\gamma}. \quad (3.10)$$

The value of D is an indicator for the disruption of the bunch during a bunch crossing. $D \ll 1$ means small disruption where the particles are only pulled inwards and do not oscillate (Pinch effect). $D > 1$ corresponds to a large disruption causing the particles to oscillate around the center during the bunch crossing. The disruption parameter is related to the luminosity enhancement factor H_D (See Table 2.1). H_D can only be determined through simulations for $D \gg 1$ [16].

3.1.2 Beamstrahlung

The mean field strength \bar{F} averaged over the impact parameter r can be used to define a global beamstrahlung parameter Υ [16]:

$$\Upsilon = \gamma \frac{\bar{F}}{B_C} \quad (3.11)$$

with the Schwinger critical field $B_C = m_e^2/e$. The global beamstrahlung parameter for the homogeneous cylinder is

$$\Upsilon = \frac{4\gamma r_e^2 N}{\alpha LR}, \quad (3.12)$$

with the fine-structure constant $\alpha = e^2/4\pi\epsilon_0$. The global beamstrahlung parameter for beams with Gaussian profiles is [16]

$$\Upsilon = \frac{5}{6} \frac{N\gamma r_e^2}{\alpha \sigma_z(\sigma_x + \sigma_y)}. \quad (3.13)$$

This global beamstrahlung parameter can describe some important aspects of beamstrahlung. The average energy loss $\bar{\epsilon}$ of a particle due to beamstrahlung is [15]

$$\bar{\epsilon} \propto \begin{cases} \Upsilon^2 & \text{for } \Upsilon \ll 1 \\ \Upsilon^{2/3} & \text{for } \Upsilon \gg 1. \end{cases} \quad (3.14)$$

Υ should be as small as possible to limit the radiation loss through beamstrahlung.

3.1.3 Beamstrahlung and Disruption at the ILC

In order to minimize beamstrahlung while keeping the luminosity at the desired level very flat bunches with $\sigma_y \ll \sigma_x$ are used at the ILC. For the nominal beam parameters (Table 2.1, $N = 2 \cdot 10^{10}$, $\sigma_x = 639\text{nm}$, $\sigma_y = 5.7\text{nm}$) the disruption parameters are

$$D_x = 0.16 \quad \text{and} \quad D_y = 18.4, \quad (3.15)$$

which means that the particles oscillate several times in direction y and are only focused in direction x . The global beamstrahlung parameter for the nominal beam parameters is

$$\Upsilon = 0.05.$$

The beamstrahlung parameter for a round bunch geometry $\sigma_x = \sigma_y$ with the same design luminosity would be $\Upsilon = 0.5$, which would mean a much larger energy loss due to beamstrahlung.

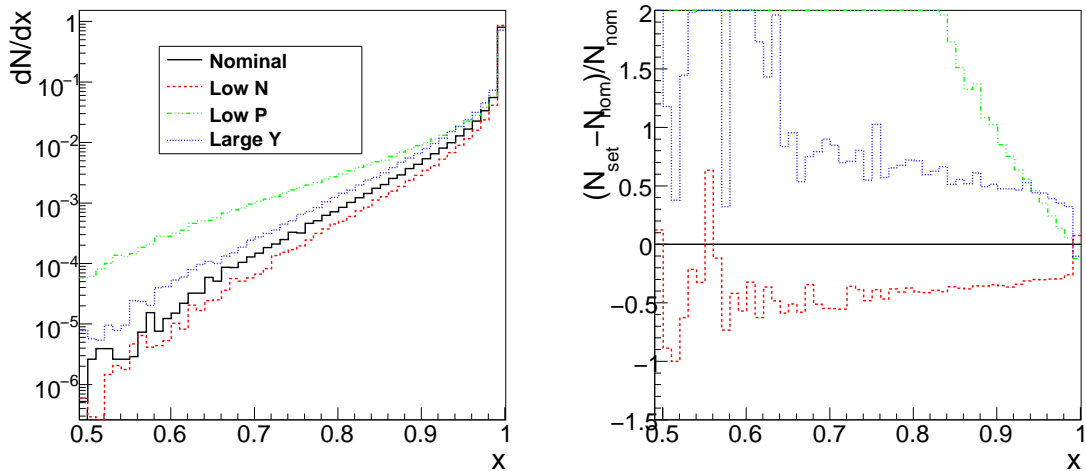
3.2 Simulating Beamstrahlung

The program GuineaPig [1] is used to simulate the beam-beam interaction during bunch crossings. GuineaPig will take the beam parameters (Table 2.1) and simulate the crossing of two bunches including disruption and beamstrahlung. To accomplish this in a reasonable computing time several thousand macroparticles are used instead of the $N \propto 10^{10}$ actual particles. During the simulation GuineaPig records the energies of annihilation or scattering events. For each pair undergoing annihilation the energy of the electron E_{e-} and the positron E_{e+} as well as the time and place of the scattering is recorded.

Figure 3.2 shows the energy spectra for all beam parameter sets considered at the ILC (Table 2.1) simulated by GuineaPig. The effect the different beam parameters have on the beamstrahlung is evident. The largest amount of beamstrahlung loss happens for “Low P” set, because of the smaller bunch sizes. The set “Low N” has similar bunch sizes, but because of the smaller number of particles per bunch the least amount of beamstrahlung is produced in this case.

3.3 Correlation between the Energy of Scattering Particles

The amount of beamstrahlung produced by two particles before scattering is slightly correlated for two reasons. One is the dependence of the amount of beamstrahlung radiated on the time the particle spent in the field of the other bunch: The later the annihilation occurs the higher the probability for the radiation of beamstrahlung becomes (Figure 3.3). At the beginning of the bunch crossing the probability for an annihilation event to occur where one or both particles produced beamstrahlung is small. For events happening later during the bunch crossing the probability for the



(a) Energy spectra after Beamstrahlung.

(b) Relative difference of the different energy spectra to the spectrum from the nominal parameters.

Figure 3.2: Energy spectra simulated with GuineaPig for the different beam parameter sets from Table 2.1. The legend from the plot on the left applies to the plot on the right as well.

radiation of beamstrahlung to happen before scattering becomes larger. The other reason is due to the dependence of beamstrahlung on field strength. The stronger the field, affecting the particles, is the more they radiate. This causes particles at the edge of the bunch to radiate more than particles at the center [4].

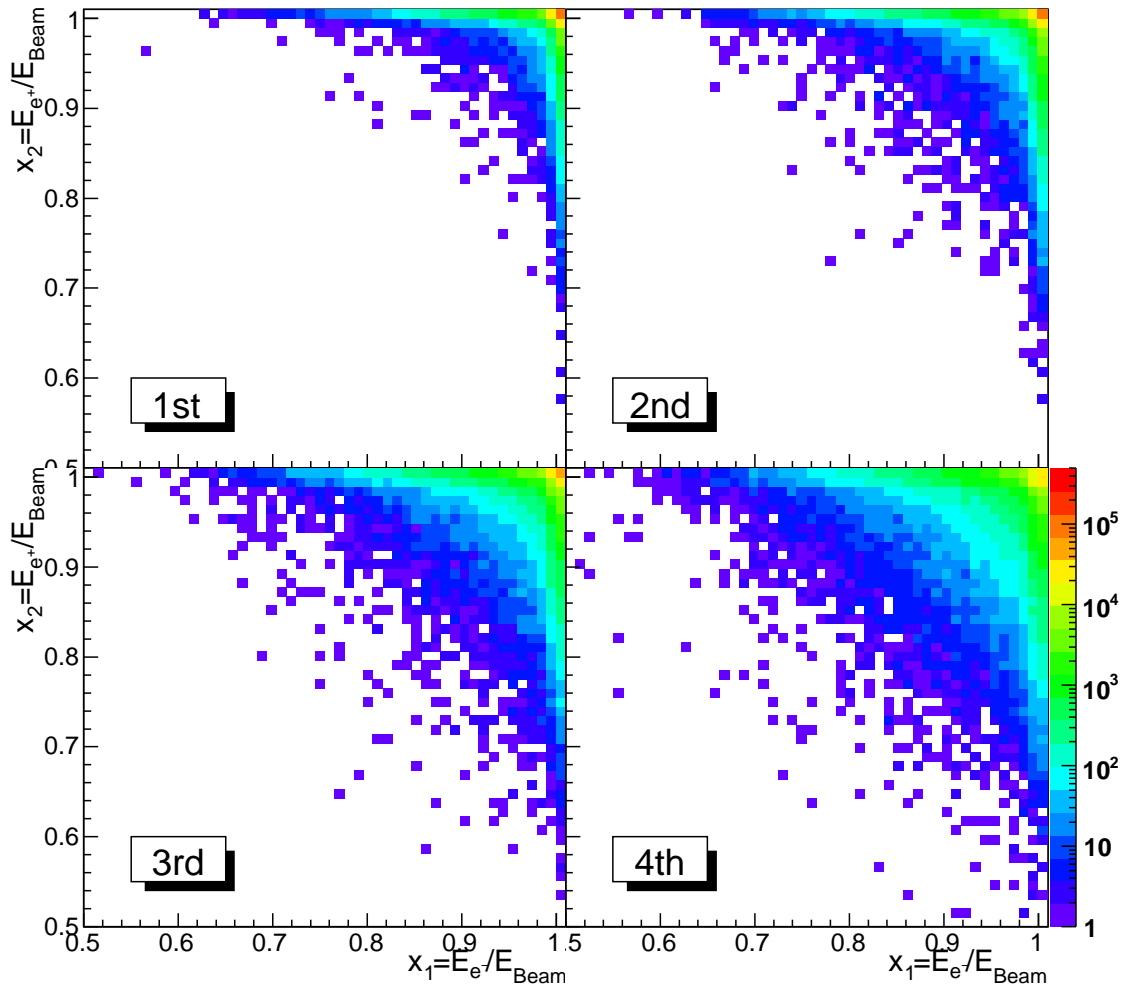


Figure 3.3: These plots show the time slices of a simulated bunch crossing. The histograms show events that happen during the first, second, third and fourth quarter of the bunch crossing respectively. The particles show a larger probability to radiate for events occurring later during the bunch crossing.

Chapter 4

Differential Luminosity

The main advantage of a lepton collider like the ILC over a hadron collider like the LHC is that the initial state of the interaction between the leptons is in principle exactly known, because leptons are point-like particles, unlike protons that consist of three constituent quarks, sea-quarks and gluons. Because of this, every interaction at the ILC should occur at the nominal center-of-mass energy \sqrt{s} . The nominal energy, however, is smeared out by the beam energy spread and beamstrahlung to the effective center-of-mass energy $\sqrt{s'}$. The resulting distribution of annihilation events per effective center-of-mass energy is called the differential luminosity $\frac{dL}{d\sqrt{s'}}$. The differential luminosity has to be known precisely for some physics analyses like threshold scans.

4.1 Particle Energy Spectrum

The differential luminosity is the combination of the particle energy spectra of two colliding bunches. Two effects, described in the following, cause the energy of a particle E' to deviate from the nominal beam energy E_{Beam} before scattering.

4.1.1 Beam Energy Spread

The beam energy spread σ_E occurs because the particles in a bunch do not all see the same accelerating phase and therefore some particles receive more energy than the others and a spread in the energy appears. The energy spread at the interaction point is $\frac{\sigma_E}{E} = 0.1\%$ for positrons and $\frac{\sigma_E}{E} = 0.14\%$ for electrons. The beam energy spread of the electrons is larger than that of the positrons, because the electrons pass an undulator, where they emit photons to create the positrons [3]. The beam energy spread is assumed to be Gaussian, although the shape of the beam energy spread is not known and could have a non-Gaussian shape [4]. The beam energy spread is very small compared to the effect of beamstrahlung (Figure 4.1(b)).

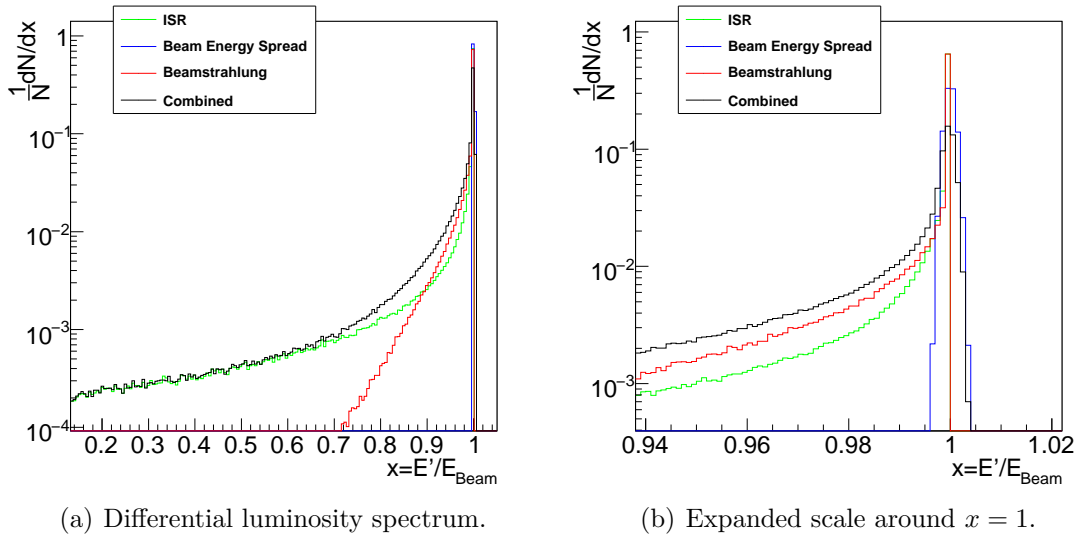


Figure 4.1: Beamstrahlung, beam energy spread, initial state radiation and the combination into the particle energy spectrum.

4.1.2 Beamstrahlung

Beamstrahlung was discussed in chapter 3. It dominates the energy loss close to the nominal beam energy and takes at most 40% of the energy of a colliding particle. This effect depends on the bunch geometry and can only be calculated or simulated if the geometries are well known. Beamstrahlung is produced by all particles, whether they annihilate or not. If the tail of the bunch is moved by wake fields in the beam pipe, the particles at the edge of the distribution might produce beamstrahlung, but have no chance to interact with particles from the other bunch. For this reason, the beamstrahlung photons measured after the bunch crossing do not represent the spectrum of the scattering particles. The beamstrahlung photons also do not represent the correct particle energy spectrum, because the interaction between two particles happens on average after half a bunch crossing. But the photon spectrum is the spectrum integrated over the whole bunch crossing. Therefore annihilation data from Bhabha events have to be used to extract the energy spectrum due to beamstrahlung, which is the same for all annihilation and scattering events.

4.1.3 Initial and Final State Radiation

The energy of the scattering particles is also changed by the emission of photons through a higher order QED process. This is called Initial and Final State Radiation (ISR/FSR) or internal Bremsstrahlung. The distribution of the bremsstrahlung photons can be calculated by QED, because it only depends on the effective center-of-mass energy. The emitted photons can be extremely hard and take away a large fraction of the particle energy (Figure 4.1). Because the contribution of ISR and FSR to the cross sections can be calculated, it does not have to be measured and

the effect is excluded from the differential luminosity.

4.2 Threshold Scan

The effective center-of-mass energy $\sqrt{s'}$ for a scattering event depends on the energies of the interacting particles E'_1 and E'_2 . The effective center-of-mass energy is

$$\sqrt{s'} = \sqrt{4E'_1E'_2} = \sqrt{x_1x_24E_{\text{Beam}}} = \sqrt{x_1x_2s}, \quad (4.1)$$

with the fractional beam energy $x_{1/2} = E'_{1/2}/E_{\text{Beam}}$ of the interacting particles. If the particle energy spectrum is functionally described by $f(x_{1/2})$, then the differential luminosity $dL/d\sqrt{s'}$ can be described by a function depending on the fractional energies of two interacting particles $L(x_1, x_2)$.

To visualize the effect of the differential luminosity a threshold scan is used. The pairs of particles with a mass m can only be produced if the effective center-of-mass energy is above the production threshold of $\sqrt{s'} > 2m$. The expected cross section σ_L is given by the differential luminosity $L(x_1, x_2)$ and the cross section $\tilde{\sigma}(\sqrt{s})$ by

$$\sigma_L(\sqrt{s}) = \int dx_1 dx_2 L(x_1, x_2) \tilde{\sigma}(\sqrt{x_1 x_2 s}). \quad (4.2)$$

The reference differential luminosity is given by the energy spectra of the scattering particles simulated by GuineaPig. All expected cross sections σ_L calculated with the functional descriptions of the differential luminosity are compared to the observed reference cross section

$$\sigma_{GP} = \frac{1}{N} \sum_{i=1}^N \tilde{\sigma}(\sqrt{x_1^i x_2^i s}), \quad (4.3)$$

with $N = 10^6$ scattering events from GuineaPig. In this way the differential luminosity function can be compared to the real differential luminosity, given by GuineaPig, independent of the binning of a histogram. The “resolution” is only dependent on the steps in the nominal energy of the threshold scan. The differential luminosity is assumed to be independent of the nominal center-of-mass energy. This means the same GuineaPig scattering events and the same parameters of the differential luminosity functions are used to calculate the cross sections for every point of the threshold scan.

Because the difference in the observed cross sections is generally smaller than 1%, the relative difference $\rho(\sqrt{s})$ between the cross sections is plotted instead of the absolute cross sections. The relative difference is

$$\rho(\sqrt{s}) = \frac{\sigma_{GP}(\sqrt{s}) - \sigma_L(\sqrt{s})}{\sigma_{GP}(\sqrt{s})}. \quad (4.4)$$

The statistical errors on the cross sections will be ignored, and only the error of the parameters of the differential luminosity function will be taken into account for the error on the relative difference. The variance on the cross section $(\Delta\sigma_L)^2$ is:

$$(\Delta\sigma_L)^2 = \left(\sigma_L(\sqrt{s}; a_j - \Delta_j) - \sigma_L(\sqrt{s}) \right) C_{jk} \left(\sigma_L(\sqrt{s}; a_k - \Delta_k) - \sigma_L(\sqrt{s}) \right) \quad (4.5)$$

Where $\sigma_L(\sqrt{s}; a_j - \Delta_j)$ means that the the j -th parameter of the differential luminosity L in (4.2) is changed by one standard deviation of the parameter. C_{jk} is the correlation matrix for the parameters and the Einstein convention for sums is used. From the error propagation follows the error on the relative difference

$$\Delta\rho = \frac{\Delta\sigma_L}{\sigma_{GP}}. \quad (4.6)$$

The errors for the scan points of the threshold scan are correlated, because the differential luminosity for the reference cross sections from GuineaPig and the differential luminosity function are the same for each point.

4.2.1 Cross Section of the MC Toy Particle

The particle used for the threshold scan is a simple Monte Carlo toy particle, that could be a chargino χ^\pm for example. This spin $\frac{1}{2}$ particle has a differential production cross section [17, Chapter 39]

$$\frac{d\sigma}{d\Omega} = \frac{\alpha^2}{4s} \beta [1 + \cos^2 \Theta + (1 - \beta^2) \sin^2 \Theta], \quad (4.7)$$

with

$$\beta = \frac{p}{E_{\text{Beam}}} = \sqrt{\frac{E_{\text{Beam}}^2 - m^2}{E_{\text{Beam}}^2}} = \sqrt{1 - \frac{4m^2}{s}}, \quad (4.8)$$

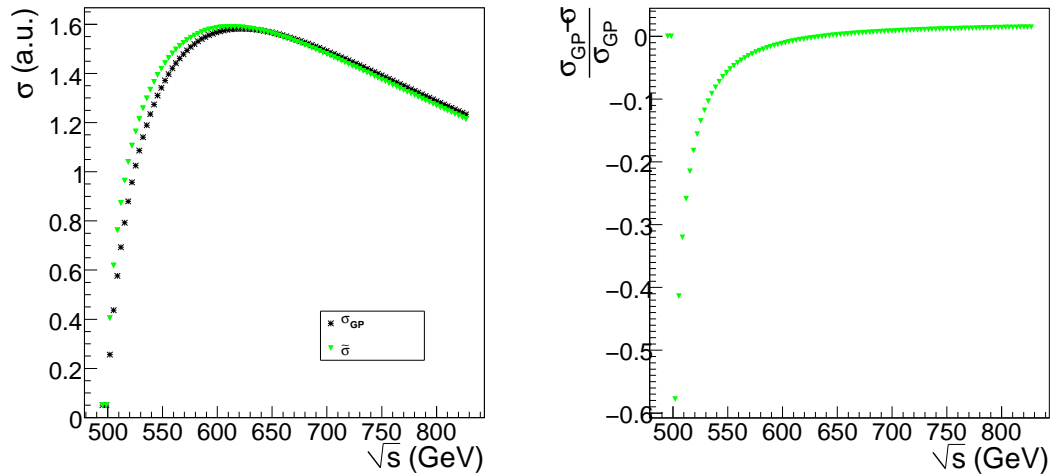
which is much smaller than 1 for $m \approx E_{\text{Beam}}$. The mass of the particle is set to 250 GeV. The cross section is in first order of β and integrated over the solid angle

$$\begin{aligned} \tilde{\sigma}_{e^+e^- \rightarrow \chi^+\chi^-}(s) &= \frac{2\pi\alpha^2}{s} \cdot \beta = \frac{2\pi\alpha^2}{s} \cdot \sqrt{1 - \frac{4m_\chi^2}{s}} \\ &\approx \frac{130\text{nb}}{s(\text{GeV}^2)} \cdot \beta. \end{aligned} \quad (4.9)$$

The differences between the observed cross section from the GuineaPig spectrum and the prediction by the luminosity model $L(x_1, x_2)$ can become large, if the model deviates from the real spectrum. Figure 4.2 shows the extreme case of what happens, if a constant luminosity spectrum of $L(x_1, x_2) = \delta(1 - x_1)\delta(1 - x_2)$ is used instead of the spectrum coming from the beamstrahlung. The two cross sections differ by about 60% right after the threshold. The cross section without beamstrahlung would allow all interacting pairs to produce a chargino pair. But with beamstrahlung 40% of the annihilating particles lost energy and can no longer produce a toy particle pair. In order to correctly predict the observed cross section, a very precise functional description of the differential luminosity is needed.

4.2.2 Threshold Scan with Beam Energy Spread

To include the beam energy spread into the threshold scan the differential luminosity from the parameterization $L(x_1, x_2)$ has to be convoluted with the parameterization



(a) Cross sections.

(b) Relative difference between the cross sections.

Figure 4.2: Threshold scan with (σ_{GP}) and without ($\tilde{\sigma}$) beamstrahlung.

of the beam energy spread $B(x_{1/2})$. The differential luminosity with beam energy spread $\tilde{L}(x_1, x_2)$ is

$$\tilde{L}(x_1, x_2) = \int_{-\infty}^{\infty} d\epsilon_1 \int_{-\infty}^{\infty} d\epsilon_2 B(\epsilon_1) B(\epsilon_2) L(x_1 - \epsilon_1, x_2 - \epsilon_2). \quad (4.10)$$

The convoluted luminosity is also assumed to be independent of the nominal energy. It can therefore be calculated independently of the cross sections to save computing time by calculating the convolution once and then numerically integrating the cross sections weighted with this differential luminosity. For the calculation of the expected cross sections the differential luminosity $L(x_1, x_2)$ in (4.2) is replaced by \tilde{L} from (4.10). The beam energy spread smears the production threshold, so that some particle pairs are created below $\sqrt{s} = 2m_\chi$ (Figure 4.3).

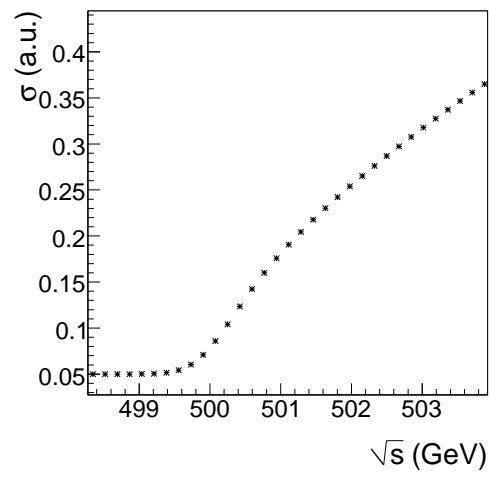


Figure 4.3: Threshold scan with beamstrahlung and beam energy spread.

Chapter 5

Circe Parameterization for Beamstrahlung

The Circe parameterization for beamstrahlung can be used as a functional description of the differential luminosity. It is used to describe the energy spectrum of the particles of a bunch after the radiation of beamstrahlung. It assumes that there is no correlation between the energies of the interacting particles and that the spectra are the same for electrons and positrons [2].

5.1 Particle Energy Parameterization

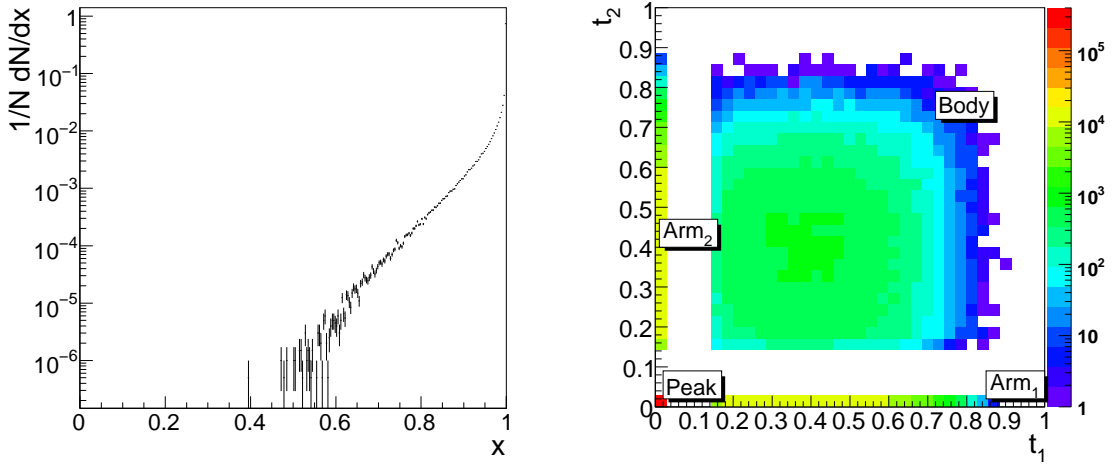
The parameterization for the particle energy is a one-dimensional parameterization of the energy E' of the particles after beamstrahlung. This energy is normalized to the nominal beam energy E_{Beam} , x is the fraction of energy the particles have after beamstrahlung.

$$x = \frac{E'}{E_{\text{Beam}}}$$

The energy spectrum after beamstrahlung (Figure 5.1(a)) has a very pronounced peak and a steep slope for $x \rightarrow 1$ for the particles that did radiate beamstrahlung, because the probability for scattering events to happen, after large amounts of beamstrahlung have been radiated, is very small. The distribution can be approximated by a beta-distribution

$$B(x; a_2, a_3) = x^{a_2}(1-x)^{a_3}, \quad (5.1)$$

with two free parameters here called a_2 and a_3 . This distribution is used, because the particle energy spectrum has physical limits at both ends: The energy of the particle is limited by the nominal energy E_{Beam} and cannot become negative. To describe the characteristics of the energy spectrum, the peak for $x \rightarrow 1$ and vanishing for $x \rightarrow 0$, $0 < a_2$ and $-1 < a_3 < 0$ have to be fulfilled. Particles that did not produce beamstrahlung ($x = 1$) before scattering are described by a δ -function and a factor a_0 giving the probability with $0 < a_0 < 1$. For the unphysical case without beam energy spread all particles that did not produce beamstrahlung are at $x = 1$ and



(a) Spectrum of the energies of electrons and positrons after beamstrahlung. (b) Two-dimensional spectrum of particle energies transformed using (5.8).

Figure 5.1: Particle energy spectrum after beamstrahlung. 10^6 scattering events from GuineaPig are used. This means $N = 2 \cdot 10^6$ for the one-dimensional histogram.

all particles that did radiate beamstrahlung have $x < 1$, the cutoff for the δ -peak is given by the numerical precision of the generator. The output files from GuineaPig have a precision of 0.001 GeV, which means that the cutoff for the beta-distribution is $x = 0.99996$. The complete one-dimensional Circe parameterization for the particle energy spectrum after beamstrahlung is

$$f(x)dx = a_0\delta(1-x) + (1-a_0)a_{\text{norm}}x^{a_2}(1-x)^{a_3}. \quad (5.2)$$

The parameters (a_0 , a_2 and a_3) are free parameters, a_{norm} is used for normalization so that

$$\int_0^1 f(x)dx = 1. \quad (5.3)$$

The integral of the beta-distribution is known as the beta-function [18]

$$\int_0^1 x^{a_2}(1-x)^{a_3}dx = B(1+a_2, 1+a_3) = \frac{\Gamma(1+a_2)\Gamma(1+a_3)}{\Gamma(2+a_2+a_3)}. \quad (5.4)$$

And the normalization parameter is therefore

$$a_{\text{norm}} = \frac{1}{B(1+a_2, 1+a_3)}. \quad (5.5)$$

5.2 Parameterization for the Differential Luminosity

To create the parameterization for the differential luminosity the functions for one bunch $f(x_1)$ is multiplied with the spectrum of the other bunch $f(x_2)$. The center-

of-mass energy after beamstrahlung is

$$\sqrt{s'} = \sqrt{x_1 x_2 s}. \quad (5.6)$$

The luminosity spectrum after beamstrahlung is described by the two dimensional distribution:

$$\begin{aligned} \frac{L_{\text{circe}}(x_1, x_2)}{dx_1 dx_2} &= f(x_1) f(x_2) \\ &= a_0^2 \delta(1 - x_1) \delta(1 - x_2) \\ &\quad + a_0 (1 - a_0) a_{\text{norm}} \delta(1 - x_1) x_2^{a_2} (1 - x_2)^{a_3} \\ &\quad + a_0 (1 - a_0) a_{\text{norm}} x_1^{a_2} (1 - x_1)^{a_3} \delta(1 - x_2) \\ &\quad + (1 - a_0)^2 a_{\text{norm}}^2 x_1^{a_2} (1 - x_1)^{a_3} x_2^{a_2} (1 - x_2)^{a_3} \end{aligned} \quad (5.7)$$

The leading factors in (5.7) give the probability for the pairs, where

$$\begin{array}{ll} \text{neither particle produced beamstrahlung} & a_0^2, \\ \text{only one particle produced beamstrahlung} & a_0 (1 - a_0), \\ \text{both particles produced beamstrahlung} & (1 - a_0)^2. \end{array}$$

The normalization parameters a_{norm} in (5.7) are calculated according to (5.5), so that $L(x_1, x_2)$ is normalized to 1. Due to the factorized ansatz, there is no correlation between x_1 and x_2 .

5.3 Transformation of the Parameterization

To remove the singularity of the beta-distribution as $x \rightarrow 1$ and the very steep slope a variable transformation is used. This transformation is also beneficial to the integration and fitting procedures. The transformation from x to t is

$$t = (1 - x)^{1/\eta}. \quad (5.8)$$

The transformed beta-distribution (Figure 5.2(b)) becomes:

$$f_B(t) = (1 - a_0) a_{\text{norm}} \eta t^{\eta-1} (1 - t^\eta)^{a_2} t^{\eta a_3} \quad (5.9)$$

η must be large enough to suppress the singularity for $x \rightarrow 1$ or for $t \rightarrow 0$ and therefore

$$\eta > \frac{1}{1 + a_3}. \quad (5.10)$$

$\eta = 5$ is sufficient as long as $a_3 > -0.8$, which is true for all cases in this thesis. The δ -part is only moved from $x = 1$ to $t = 0$. The transformed Circe parameterization is:

$$f(t) = a_0 \delta(t) + (1 - a_0) a_{\text{norm}} \eta t^{\eta-1} (1 - t^\eta)^{a_2} t^{\eta a_3} \quad (5.11)$$

Using the transformation shows (Figure 5.3) that the beta-distribution is not able to

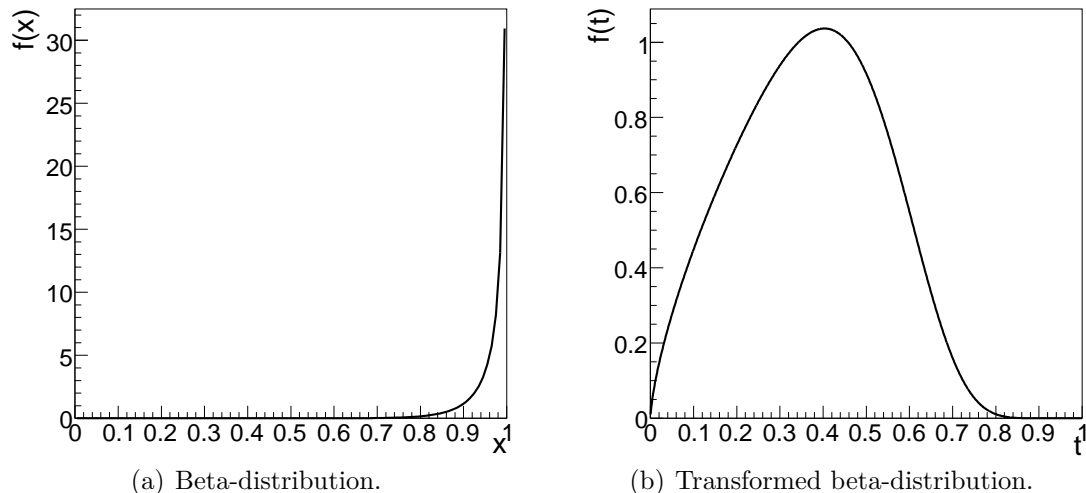


Figure 5.2: The beta-distribution part of the Circe parameterization without and with the transformation $t = (1 - x)^{1/5}$.

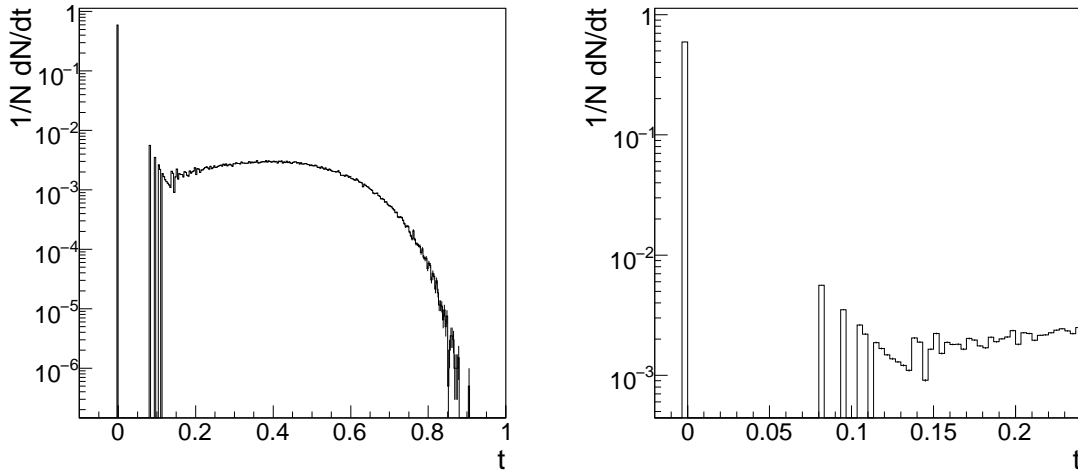
describe the continuous energy spectrum generated by GuineaPig up to $x = 0.999996$ and a different cutoff for the beta-distribution has to be used. The transformed beta-distribution is expected to fall off for $t \rightarrow 0$ (Figure 5.2(b)), but the transformed energy spectrum from GuineaPig shows a different behavior. For this reason, all the particles that lost less than 0.01% of their energy to beamstrahlung are now considered to have not radiated beamstrahlung at all. Because the continuous part of the distribution now only describes the range from 0 to 0.9999, the normalization has to be adjusted as well. The incomplete integral over the beta-distribution is known as the (unregularized) incomplete beta-function [19]

$$B(y, 1 + a_2, 1 + a_3) = \int_0^y x^{a_2} (1 - x)^{a_3} dx. \quad (5.12)$$

The change in the normalization is of the order of 10%. For the parameters $a_2 = 12$ and $a_3 = -0.6$ the two integrals are

$$\begin{aligned} B(1.0, 1 + a_2, 1 + a_3) &= 0.802, \\ B(0.9999, 1 + a_2, 1 + a_3) &= 0.740, \end{aligned} \quad (5.13)$$

which would cause a significantly wrong fitting result. The transformation separates the two-dimensional spectrum into four separate regions analogous to the four terms of the two-dimensional parameterization (5.7). The resulting four regions are going to be called peak, where neither particle radiated beamstrahlung, arms, where only one of the particles radiated beamstrahlung and body, where both radiated beamstrahlung (Figure 5.1(b)).



(a) Transformed spectrum.

(b) Zoom on the discontinuity of the spectrum.

Figure 5.3: Transformed spectrum simulated by GP using $t = (1 - x)^{1/5}$. On the right the discontinuity below $t \approx 0.15$ is clearly visible. The first bin with entries at $t = 0.08$ belongs to the particles with $E' = 249.999$ GeV

5.3.1 Producing a Spectrum According to the Parameterization

The particle energy spectrum according to the chosen parameters of the parameterization is produced by first picking a random uniformly distributed number $0 < r \leq 1$ to decide in which region (peak, arm or body; Figure 5.1(b)) the event belongs:

$$\begin{aligned}
 0 < r \leq a_0^2 & \rightarrow \begin{cases} x_1 = 1 \\ x_2 = 1 \end{cases} \\
 a_0^2 < r \leq a_0^2 + a_0(1 - a_0) & \rightarrow \begin{cases} x_1 = 1 \\ x_2 \in B(a_2, a_3) \end{cases} \\
 a_0^2 + a_0(1 - a_0) < r \leq a_0^2 + 2a_0(1 - a_0) & \rightarrow \begin{cases} x_1 \in B(a_2, a_3) \\ x_2 = 1 \end{cases} \\
 a_0^2 + a_0(1 - a_0) < r \leq 1 & \rightarrow \begin{cases} x_1 \in B(a_2, a_3) \\ x_2 \in B(a_2, a_3) \end{cases}
 \end{aligned} \tag{5.14}$$

The distributions for x_1 and x_2 are chosen depending on the region. If the event falls into a region where one particle did not produce beamstrahlung, its fractional energy is $x_i = 1$. For particles that did produce beamstrahlung the fractional energy is chosen through the `TF1::GetRandom()` method from ROOT [20], which can produce a random variate for every integrable function. The upper limit of the random variate $x_{1/2}$ is 0.9999 corresponding to the redefined upper limit of the continuous part of the GuineaPig distribution.

5.4 Fitting the GuineaPig Spectrum

The parameters are found by a least square fit of the one- or two-dimensional parameterization to the transformed spectrum dN/dt or dN/dt_1dt_2 respectively. For the one dimensional fit to the spectrum both the transformed energy of the electrons t_1 and the transformed energy of the positrons t_2 are filled into one histogram (Figure 5.4(a)). Both energies follow the same distribution, because the same beam parameters were used for both beams. Using both particle energies increases the statistics. For the minimization of the χ^2 the Minuit [21] implementation in ROOT [20] is used.

5.4.1 Fit to the One-Dimensional Spectrum

The fit to the one-dimensional particle energy spectrum is stable and almost independent of the binning. The parameters only vary within one σ for the three fits with 35, 50 and 65 bins. But the function with the parameters returned from the fit is only partially able to reproduce the spectrum of the particle energy spectrum from GuineaPig (Figure 5.4(b)). This is expressed in the large ratio of the χ^2 to the degrees of freedom N_{df} between 10 and 20. The χ^2 is so large, because the errors on the entries of the bins are underestimated by relying on the Poissonian statistics. The real error coming from the MC generation is larger, because of the macroparticles that are used. The use of macroparticles means that small fluctuations in the simulation affect the outcome more significantly than can be expected from Poissonian statistics. The real error coming from the MC generation is unavailable, but it is visible in the fitting results for the second GuineaPig sample (GP2) created with the same beam parameters (Table 5.1), where the a_0 parameter differs by 2σ to the parameter found for the sample GP1. Another reason for the large χ^2/N_{df} is the very simple ansatz for the Circe parameterization that can describe the characteristics of the particle energy spectrum qualitatively and only to some degree quantitatively.

The correlation matrix for the parameters shows a large correlation between the two parameters of the beta-distribution and only a very small correlation between these parameters and a_0 .

$$C_{\text{direct}} = \begin{pmatrix} 1 & 0.02 & 0.04 \\ 0.02 & 1 & 0.72 \\ 0.04 & 0.72 & 1 \end{pmatrix} \quad (5.15)$$

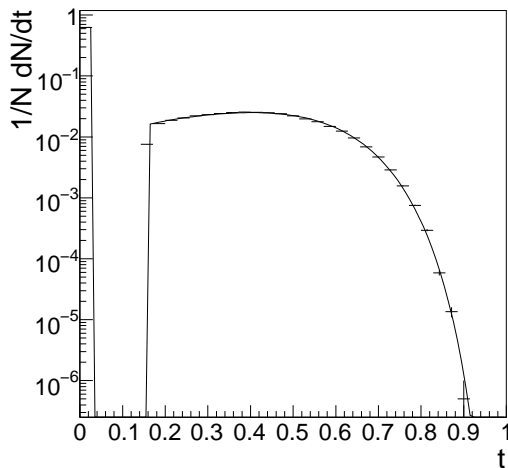
This comes as no surprise because a_0 is most important where the other parameters have no influence on the distribution.

5.4.2 Fit to the Two-Dimensional Spectrum

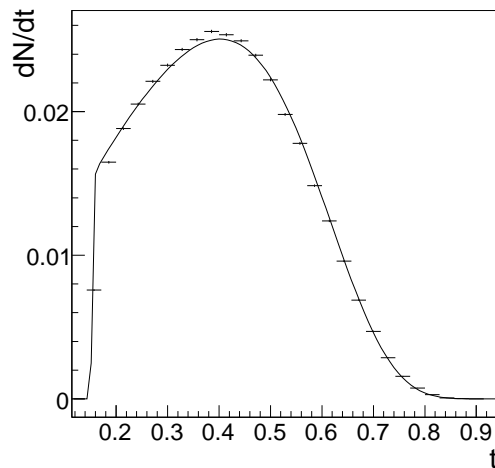
The fit to the two-dimensional spectrum is also stable, but the resulting parameters differ significantly from the parameters found by the one-dimensional fit (Table 5.1). The ratio between the χ^2 and the degrees of freedom has become smaller

Table 5.1: Results for fitting the 1D and 2D Circe parameterization to two particle energy spectra produced by GuineaPig. Both GuineaPig samples were produced with the same beam parameters. The bins are per axis, which means that the bins for the two-dimensional histograms are N_{Bins}^2 . Some of the bins are empty, because of the merging of the bins below $t \approx 0.15$.

N_{Bins}	35		50		65		
	GP1	GP2	GP1	GP2	GP1	GP2	Error
1D							
a_0	0.6287	0.6293	0.6288	0.6295	0.6284	0.6291	0.0003
a_2	11.79	11.94	11.81	12.00	11.78	11.97	0.04
a_3	-0.6739	-0.6744	-0.6733	-0.6723	-0.6753	-0.6749	0.0009
χ^2	525	566	458	566	459	570	
N_{df}	24		35		46		
2D							
a_0	0.6298	0.6301	0.6299	0.6306	0.6301	0.6307	0.0004
a_2	11.92	12.05	11.96	12.13	11.97	12.12	0.04
a_3	-0.6732	-0.6738	-0.6724	-0.6717	-0.6741	-0.6742	0.0009
χ^2	2744	2533	3157	3054	3752	3666	
N_{df}	665		1219		2017		

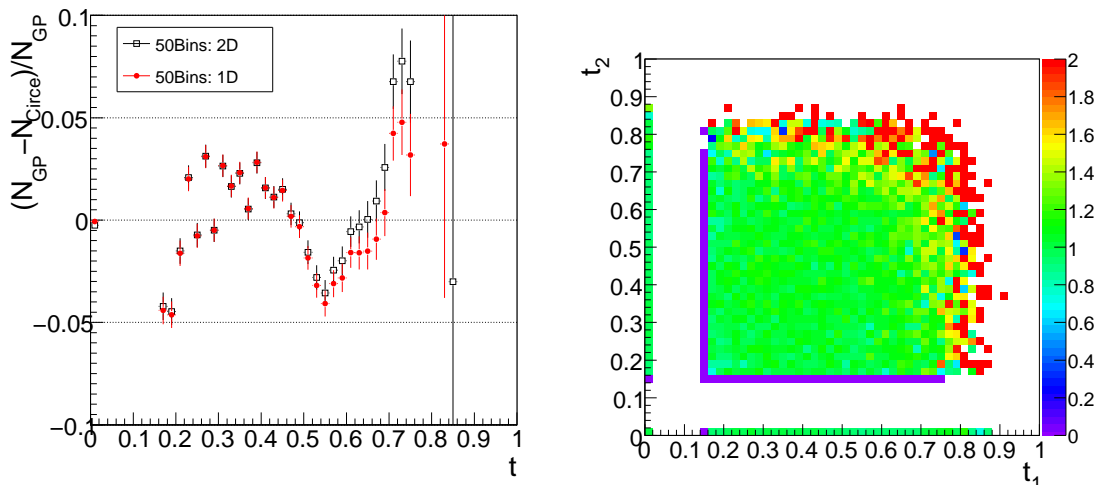


(a) Fit on the e^+/e^- -spectrum.



(b) Close up of the continuous part of the distribution.

Figure 5.4: The energy distribution of electrons and positrons simulated by GuineaPig and the fitted Circe function for 35 bins.



(a) Relative difference between GuineaPig and Circe for the particle energy spectrum found by the fits to the one and two-dimensional histograms with 50 bins per axis.

(b) Ratio N_{GP}/N_{Circe} between the 2 dimensional distributions of Circe and GuineaPig. The ratio for $t_1 = 0.15$ or $t_2 = 0.15$ is wrong, because of the cutoff, which lies inside the bins.

Figure 5.5: Differences between Circe and GuineaPig

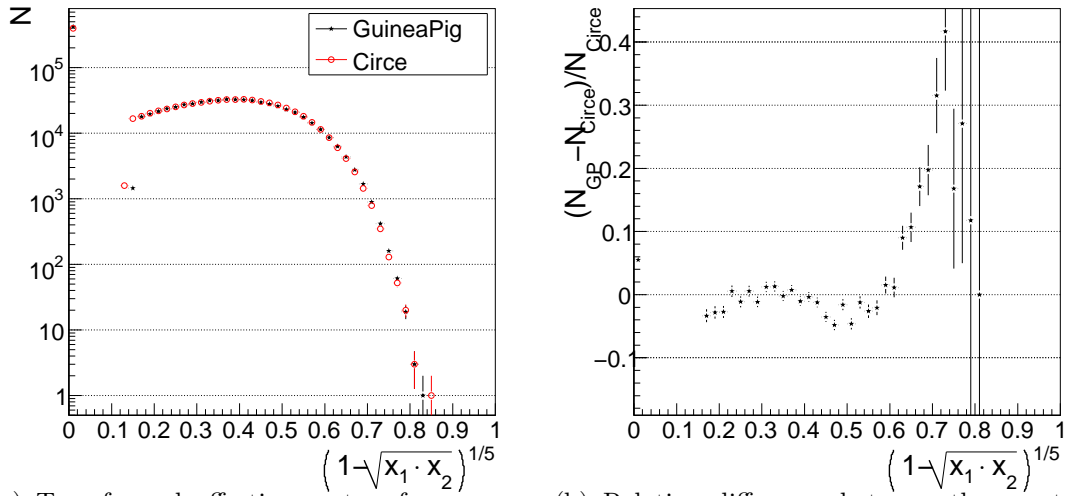
and is between 2 and 4. The problem of the neglected Monte Carlo errors and the simple ansatz still exist and the two-dimensional function is still not able to properly describe the distribution from GuineaPig.

The parameters for the 1D and 2D parameterization differ, because the a_0 parameter corresponds to the entries of the bin at $t_{1/2} = 0$ and the entries for the continuous distribution correspond to $1 - a_0$. For the 2D fit the a_0^2 should correspond directly to the entries in the bin at $t_1 = t_2 = 0$ and the entries for the arms should correspond to $a_0(1 - a_0)$. This, however, is not the case, because the particle energy spectrum is not a factorization.

The differences in the results for the parameters a_2 and a_3 emerge from a similar origin. They only have to describe a single slope in the 1D case. But in the 2D case two slopes for the arms and the body regions exist, which means that the resulting parameters average the slopes in this region.

This difference in the parameters is only seen for the a_0 parameter in the particle energy spectrum for the bin at $t_{1/2} = 0$ (Figure 5.5(a)). For all other bins the difference between the two spectra from the parameterization in one and two dimensions is small compared to the difference to the spectrum from GuineaPig.

The ratio between the two-dimensional function and the two-dimensional spectrum from GuineaPig in Figure 5.5(b) shows that Circe is somewhat able to reproduce the spectrum in two dimensions. The fluctuations at the edges for $t_{1/2} \rightarrow 1$ in the two dimensional spectrum, where the ratio is larger than 2 are caused by statistical fluctuations, because only very few events are in those bins.



(a) Transformed effective center-of-mass energy spectrum after beamstrahlung.

(b) Relative difference between the spectra from Circe and GuineaPig.

Figure 5.6: The Circe spectrum is taken from a sample of random numbers generated according to the parameterization with the parameters found from the fit to the particle energy spectrum simulated by GuineaPig.

5.4.3 Effective Center-of-Mass Energy Spectrum

More important than the differences for the particle energies are the differences for the effective center-of-mass energy $\sqrt{s'}$. For $\sqrt{s'}$ the energy of both particles of the scattering pairs have to be taken into account and the correlation between the two particle energies plays a non-negligible role. Although the average energies agree perfectly

$$\begin{aligned}
 \left\langle \frac{\sqrt{s'}}{\sqrt{s}} \right\rangle_{\text{Circe}} &= \int_0^1 \int_0^1 dx_1 dx_2 f(x_1) f(x_2) \sqrt{x_1 x_2} \\
 &= 0.98920 \pm 0.00002, \\
 \left\langle \frac{\sqrt{s'}}{\sqrt{s}} \right\rangle_{\text{GuineaPig}} &= \frac{1}{N} \sum_{i=1}^N \sqrt{x_1^i x_2^i} \\
 &= 0.98920
 \end{aligned} \tag{5.16}$$

the differential distribution $dN/d\sqrt{x_1 x_2}$ (Figure 5.6) shows clear deviations for this distribution. Most important is the difference of about 5% for pairs without beamstrahlung at $(1 - \sqrt{x_1 x_2})^{1/5} = 0$. Additionally, smaller deviations are visible for the continuous part of the distribution. These differences cancel for the average. This only means that the average is not discriminative in judging the quality of the parameterization for the differential luminosity, because not the average, but the function itself is needed for threshold scans.

5.4.4 Directly Fitting the Effective Center-of-Mass Energy

The Circe parameterization can also be applied directly to the luminosity spectrum of $G(x = \sqrt{x_1 x_2} = \sqrt{s'/s})$ instead of the detour via the spectrum of the particle energies $f(x_{1/2})$. The two spectra are related by

$$G(x) = \int_0^1 \int_0^1 dx_1 dx_2 f(x_1) f(x_2) \delta(\sqrt{x_1 x_2} - x), \quad (5.17)$$

$$G(x) = a_0^* \delta(1 - x) + a_{\text{norm}}^* x^{a_2^*} (1 - x)^{a_3^*}. \quad (5.18)$$

The knowledge of $G(x)$, however does not give any insight in the distribution of the particles before the scattering interaction.

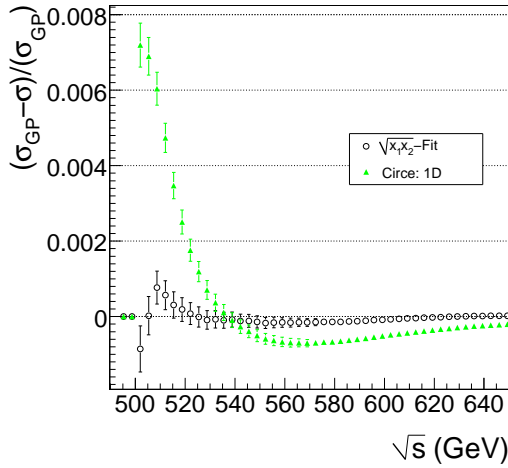
5.4.5 Threshold Scan

The threshold scan in Figure 5.7(a) shows that the fit to the $\sqrt{s'}$ spectrum with (5.17) would give a much better result than the parameterization of the particle energies. The $\sqrt{s'}$ -scan is only significantly different from the scan with GuineaPig-spectrum very close to the threshold, where the scan using the parameterization of the particle energies is much worse.

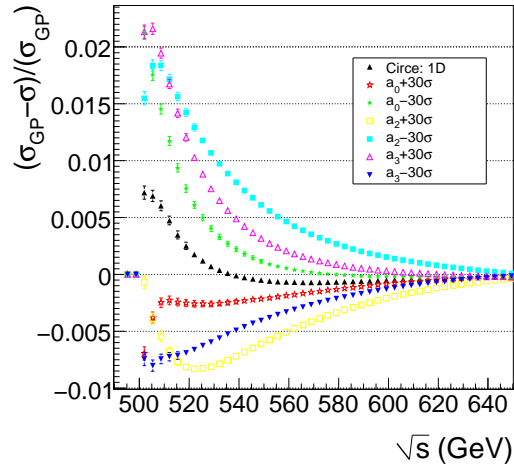
The difference of the threshold scan for parameters from the fit to the particle energy spectrum from GuineaPig can be attributed to the lack of correlation for the particle energies in the Circe parameterization. The GuineaPig sample can be de-correlated, if each particle energy is paired randomly with a different partner particle. This de-correlation results in a threshold scan that is almost identical to the 1D Circe scan. (Figure 5.7(c)). This figure also shows that the 2D Circe scan is already a bit better than the 1D version.

The parameters are definitely able to cover the whole range for the threshold scan if the parameters are changed. Figure 5.7(b) shows that even for a 30σ difference in the parameters the maximal divergence for the threshold scan is only 2%.

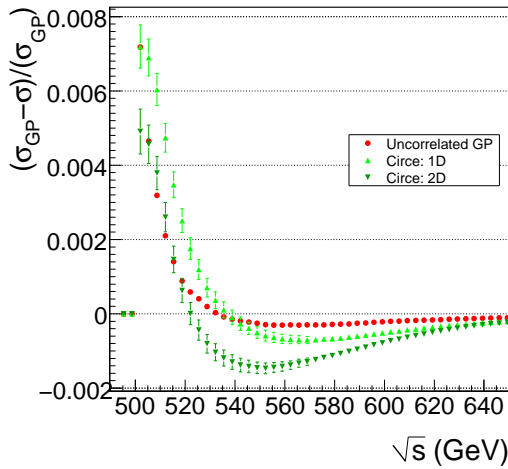
The problem of the macroparticles used by GuineaPig can be seen in Figure 5.7(d), where the threshold scans for the parameters found by the fit to the particle energies are compared to the two GuineaPig samples GP1 and GP2. The difference between the scan using the parameters from the fit to GP1 and the scan from GP1 is the same as the difference between the scan from the fit to GP2 and the scan using GP2. The fluctuations in the simulation cause a difference between the scans for GP1 and GP2 of more than 0.2% close to the threshold.



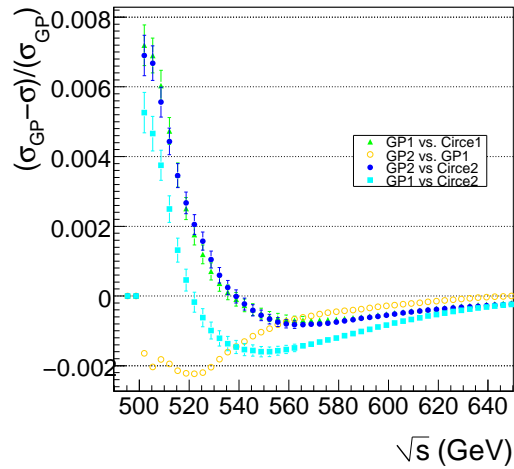
(a) 2D parameterization of the particle energy (2D-Fit) and the fit on the $\sqrt{s'}$ -spectrum ($\sqrt{x_1 x_2}$ -Fit, Section 5.4.4).



(b) Scans where the parameters have been changed as indicated.



(c) Comparison between Circe and an “uncorrelated” GuineaPig spectrum, where the particle energies were paired randomly.



(d) Comparison between two the two Samples from GuineaPig (GP1 and GP2) and their respective Circe parameters found by the fit.

Figure 5.7: Relative differences between the threshold scan using GuineaPig and scans, where a Circe parameterization was used as the differential luminosity.

Chapter 6

Parameterization including Correlation

Some of the differences between Circe and the spectrum from GuineaPig can be explained by the lack of correlation between the two particles in the Circe parameterization. The inclusion of correlation requires additional parameters in the parameterization.

6.1 Differences due to Correlation

The threshold scans resulting from the Circe parameters found by the fit to the particle energy spectrum can be nearly described by the de-correlated GuineaPig particle spectrum (Figure 5.7(c)). By accounting for the correlation between the particle energies a better description of the particle energy spectrum and therefore a better prediction of the observed cross sections should be possible. To include the correlation the two dimensional Circe parameterization is extended.

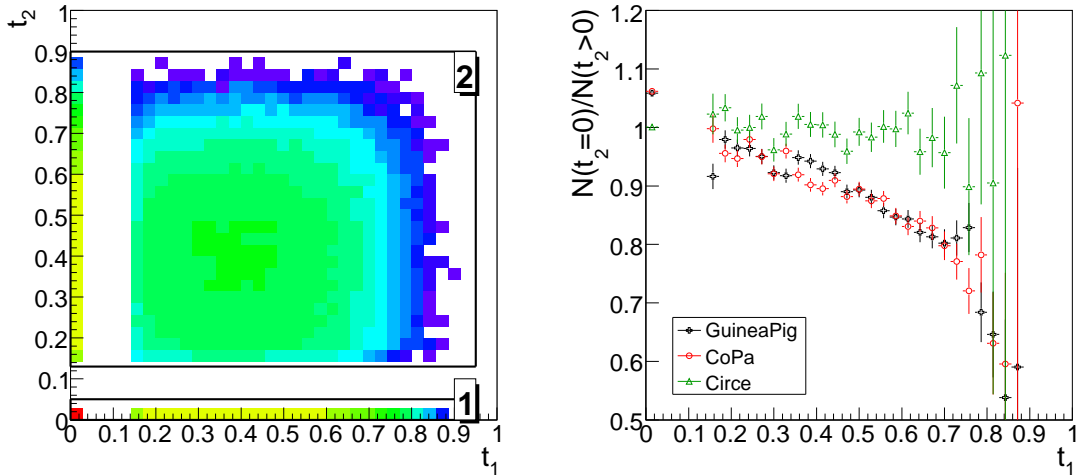
6.1.1 Probability Parameters

For Circe only the parameter a_0 describes the probability for events to lie in the particular regions. The probability for events without beamstrahlung (the peak) is described by a_0^2 , for events where only one particle produced beamstrahlung (the arms) the probability is $a_0(1 - a_0)$ and for events where both particles produced beamstrahlung (the body) the probability is $(1 - a_0)^2$. This single parameter is only able to describe the distribution of the events found in the GuineaPig distribution with a precision of 4% (Table 6.1). Even if the probability for one region were to be fixed to the correct value the probabilities for the other regions would still be wrong.

To properly describe the probabilities for the different regions new parameters are introduced. $a_{\text{peak}} \approx a_0^2$, $a_{\text{arm}} \approx a_0(1 - a_0)$ and $a_{\text{body}} \approx (1 - a_0)^2$. Because these three parameters also describe the probabilities only two of them are free parameters

Table 6.1: Probabilities for the different regions of the Energy spectrum due to Beamstrahlung.

Region	Circe Parameter	GuineaPig	Circe	GuineaPig/Circe
Peak	a_0^2	0.4032 ± 0.0005	0.3954	1.020
Arms	$2a_0(1 - a_0)$	0.4516 ± 0.0005	0.4668	0.967
Body	$(1 - a_0)^2$	0.1453 ± 0.0003	0.1378	1.054



(a) 2D particle energy spectrum. Area 1 contains all events, where particle 2 did not radiate ($t_2 = 0$) and Area 2 where it did radiate ($t_2 > 0$). The ratio of the projection of the areas on the t_1 -axis results in the plots on the right.

(b) The ratios between the two areas for Circe, GuineaPig and CoPa. All projections are normalized to 1. CoPa is clearly able to follow the characteristics of the GuineaPig ratio.

Figure 6.1: Effect of the correlation between the particle energies on the slopes of the beta-distribution.

and the third one is fixed by

$$a_{\text{Peak}} + 2a_{\text{Arm}} + a_{\text{Body}} = 1. \quad (6.1)$$

6.1.2 Beta-Distribution Parameters

Another difference between the spectrum according to the Circe parameterization and the spectrum from GuineaPig is the slope of the beta-distributions (Figure 6.1). For Circe both events, where the scattering partner did not produce beamstrahlung ($t_2 = 0$) and where the scattering partner did produce beamstrahlung ($t_2 > 0$), are described by the same beta-distribution for t_1 and vice versa for t_2 . This implies that the ratio of the distributions are always equal to one. But the same ratio calculated for the spectrum from GuineaPig is falling (Figure 6.1(b)). The spectrum

from GuineaPig shows a higher fraction of lower energetic particles at large t_2 where $t_1 > 0$. Therefore different parameters for the beta-distributions in the separate regions (arms and body) have to be used. If both beams have the same beam-parameters a symmetric radiation of beamstrahlung can be expected and only the parameters for arms and body should be different. Generally the two beams come out of different machines and could have different beam-parameters, so that all four beta-distributions should have their separate parameters.

The point at $t_1 = 0$ in Figure 6.1(b) also points to the use of more than one parameter for the probabilities for an event to fall in one of the regions.

6.2 Correlated Parameterization (CoPa)

The considerations of the previous section lead to the parameterization for the correlated energies due to beamstrahlung. This parameterization will be called Correlated Parameterization (CoPa):

$$\begin{aligned}
\frac{L_{\text{CoPa}}(x_1, x_2)}{dx_1 dx_2} &= a_{\text{peak}} && \delta(1-x_1) && \delta(1-x_2) \\
&+ a_{\text{arm}} & a_{\text{norm1}} && \delta(1-x_1) && x_2^{a_2} (1-x_2)^{a_3} \\
&+ a_{\text{arm}} & a_{\text{norm1}} & x_1^{a_2} (1-x_1)^{a_3} && \delta(1-x_2) \\
&+ a_{\text{body}} & (a_{\text{norm2}})^2 & x_1^{a_4} (1-x_1)^{a_5} && x_2^{a_4} (1-x_2)^{a_5}
\end{aligned} \tag{6.2}$$

The normalization parameters are calculated from the respective beta-parameters as before (5.16). The probability parameters for the regions a_{peak} , a_{arm} and a_{body} are normalized by (6.1) and L_{CoPa} is therefore normalized.

6.2.1 Fitting CoPa to GuineaPig

The parameters for CoPa are found by a least square fit to the two-dimensional particle energy distribution from GuineaPig (Table 6.2). The same restrictions to the particle energies above $x_i = 0.9999$ and the normalization using the incomplete beta-function apply to this fit. The χ^2 is a factor of 2 better than the χ^2 of the fits from Circe to the two-dimensional GuineaPig spectrum. The ratio between the $\chi^2/N_{df} \approx 2$ is only so large, because the errors on the bins are underestimated because the real error from the Monte Carlo is unknown, the differences between the two different GuineaPig samples shows this.

The correlation matrix for the parameters (a_{peak} , a_2 , a_3 , a_{arm} , a_4 , a_5) from the fit of the correlated parameterization to GuineaPig is

$$C_{\text{Direct}}^{\text{CoPa}} = \begin{pmatrix} 1 & 0.002 & 0.004 & -0.75 & 0.003 & 0.003 \\ 0.002 & 1 & 0.70 & -0.003 & 0 & 0 \\ 0.004 & 0.70 & 1 & -0.005 & 0 & 0 \\ -0.75 & -0.003 & -0.005 & 1 & 0.003 & 0.004 \\ 0.003 & 0 & 0 & 0.003 & 1 & 0.69 \\ 0.003 & 0 & 0 & 0.004 & 0.69 & 1 \end{pmatrix}. \tag{6.3}$$

The correlation is large between the parameters of the two beta-distributions of about 70%. a_{peak} and a_{arm} are negatively correlated.

Table 6.2: Results for fitting the correlated parameterization to two different GuineaPig samples produced with the same beam-parameters, with different numbers of bins per axis.

N_{Bins}	a_{peak}	a_2	a_3	a_{arm}	a_4	a_5	a_{body}	χ^2	N_{df}
GP1									
35	0.4039	12.09	-0.678	0.2252	11.56	-0.664	0.1455	1253	662
50	0.4042	12.13	-0.677	0.2253	11.62	-0.664	0.1452	1688	1216
65	0.4041	12.09	-0.679	0.2256	11.69	-0.664	0.1447	2421	2014
GP2									
35	0.4038	12.16	-0.680	0.2259	11.83	-0.663	0.1444	1288	662
50	0.4043	12.22	-0.678	0.2259	11.94	-0.661	0.1439	1827	1216
65	0.4041	12.17	-0.681	0.2262	11.97	-0.662	0.1435	2560	2014
Errors	0.0005	0.05	0.001	0.0002	0.05	0.001	fixed		

Table 6.3: Probabilities for the different regions of the Energy spectrum due to beamstrahlung.

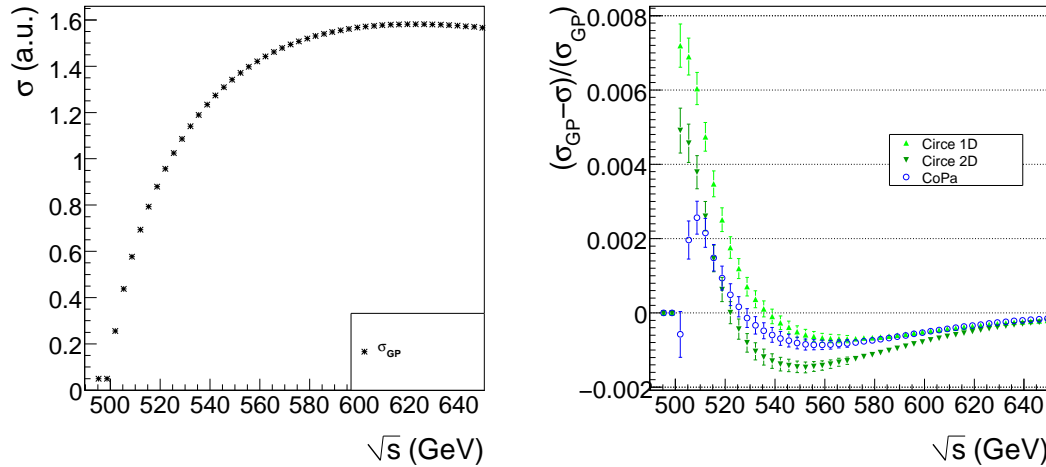
Region	CoPa-Parameter	GuineaPig	CoPa	GuineaPig/CoPa
Peak	a_{peak}	0.4032 ± 0.0005	0.4042	0.9975
Arms	$2a_{\text{arm}}$	0.4516 ± 0.0005	0.4506	1.0022
Body	a_{body}	0.1453 ± 0.0003	0.1452	1.0007

6.2.2 Differences between CoPa and GuineaPig

Because of the increased number of parameters the differences between the parameterization and GuineaPig becomes smaller. Table 6.3 shows the improvement over Circe (Table 6.1) for the probabilities of the events in the three regions. The probabilities are now closer than 0.3% to the probabilities expected from GuineaPig as opposed to a difference of about 2% for the Circe parameterization.

The different parameters for the beta-distribution directly improve the ratio drawn in Figure 6.1(b). But because of the greater number of parameters the error of the average energy becomes larger, and the difference to the GuineaPig value is larger than for the Circe parameterization, but not larger than one σ (see equation (5.16)):

$$\begin{aligned}
 \left\langle \frac{\sqrt{s'}}{\sqrt{s}} \right\rangle_{\text{CoPa}} &= \int_0^1 \int_0^1 dx_1 dx_2 L_{\text{Sym}}(x_1, x_2) \sqrt{x_1 x_2} \\
 &= 0.98928 \pm 0.00035 \\
 \left\langle \frac{\sqrt{s'}}{\sqrt{s}} \right\rangle_{\text{Circe}} &= 0.98920 \pm 0.00002 \\
 \left\langle \frac{\sqrt{s'}}{\sqrt{s}} \right\rangle_{\text{GP}} &= 0.98920
 \end{aligned} \tag{6.4}$$



(a) Threshold scan with GuineaPig for the differential luminosity.

(b) Differences between the GuineaPig and Circe or CoPa threshold scans respectively.

Figure 6.2: Threshold scans with Circe and CoPa.

For the threshold-scan (Figure 6.2(b)), CoPa shows a clear improvement over the Circe parameterization (either 1D or 2D). The difference is almost negligible close to the threshold at $\sqrt{s} = 500$ GeV, where the curve is dominated by the a_{peak} parameter. The largest difference is located where the slope of the threshold scan is very steep. But the difference is still smaller than for the Circe parameterization. Closer to the plateau all lines intersect and the difference is very small in all cases.

6.3 Differing Beam Parameters - Asymmetric Parameterization (Asym)

Until now it was assumed that the colliding bunches have equal properties, the same sizes, emittances, rotations and that they collide head on. But this does not have to be the case. For this simulation the size ($\sigma_{x/y}$) of one beam is increased by 5% and the size of the other decreased by the same amount.

Compared to the simulation for the symmetric beams one side produces more beamstrahlung while the other produces less, effectively moving events from one arm of the spectrum to the other. The difference between the number of events in the two arms is about 20%. Naturally the Circe and CoPa parameterizations are not able to properly describe this fact, because they assume a symmetric spectrum (Table 6.4).

In order to describe the spectrum with a parameterization additional parameters are needed: Two parameters for the arms and an additional 4 parameters for the different beta-distributions.

Table 6.4: The probabilities for the case of the asymmetric beam properties and the results for the different parameterizations.

Region	GuineaPig	Circe	CoPa	Asym
Peak	0.4053	0.4011	0.4084	0.4063
Arm ₁	0.2051	0.2322	0.2244	0.2052
Arm ₂	0.2457	0.2322	0.2244	0.2458
Body	0.1439	0.1345	0.1429	0.1427

The parameterization to describe the asymmetric spectrum (Asym) is:

$$\begin{aligned}
 \frac{L_{\text{Asym}}(x_1, x_2)}{dx_1 dx_2} &= a_{\text{Peak}} \delta(1-x_1) \delta(1-x_2) \\
 &+ a_{\text{arm1}} a_{\text{norm1}} \delta(1-x_1) x_2^{a_2} (1-x_2)^{a_3} \\
 &+ a_{\text{arm2}} a_{\text{norm2}} x_1^{a_4} (1-x_1)^{a_5} \delta(1-x_2) \\
 &+ a_{\text{body}} a_{\text{norm3}} a_{\text{norm4}} x_1^{a_6} (1-x_1)^{a_7} x_2^{a_8} (1-x_2)^{a_9}
 \end{aligned} \tag{6.5}$$

This parameterization is normalized with the constraint on the probability parameters $1 = a_{\text{peak}} + a_{\text{arm1}} + a_{\text{arm2}} + a_{\text{body}}$ and the usual normalizations for the beta-distributions.

Fitting the asymmetric spectrum is also possible with the other two parameterizations. But their χ^2 is much higher than the χ^2 of the asymmetric parameterization (Table 6.5), because they can not describe the distribution of the events properly (Table 6.4). The symmetric distributions are only able to average the different number of events per region, which is the main reason for the large χ^2 . For the asymmetric parameterization the ratio $\chi^2/N_{df} < 2$ is very good, considering the errors on the entries of the bins should still be larger due to the real Monte Carlo error from GuineaPig.

Looking at the different parameters for the beta-distributions in Asym (Table 6.5) shows that all the parameters are in fact needed to describe this spectrum. All pairs of beta-parameters show a very significant difference to the other pairs. The parameters for Circe or CoPa are merely averaging the parameters for four or two distributions respectively.

Despite the large differences, the threshold scans for the different parameterizations are only slightly deviating from the threshold scan with the asymmetric GuineaPig spectrum (Figure 6.3). Their respective characteristics show some differences. For Circe the absolute value between the largest differences is 0.5% and the difference to the cross section from GuineaPig is only slowly diminishing. The asymmetric parameterization is the only one that starts close to the cross section from GuineaPig near the threshold at $\sqrt{s} = 500$ GeV and is the fastest to come close to the correct cross section.

Table 6.5: Parameters to describe the asymmetric spectrum from all three parameterizations. The fits were done with 50 bins per axis.

	Circe	CoPa	Asym
$a_{\text{peak}} (a_0^2)$	0.4011 ± 0.0004	0.4084 ± 0.0005	0.4063 ± 0.0004
a_{arm1}		0.2244 ± 0.0002	0.2052 ± 0.0004
a_{arm2}			0.2458 ± 0.0004
a_2	12.21 ± 0.04	12.35 ± 0.05	12.95 ± 0.07
a_3	-0.668 ± 0.001	-0.674 ± 0.001	-0.681 ± 0.002
a_4		11.90 ± 0.06	11.44 ± 0.06
a_5		-0.657 ± 0.001	-0.667 ± 0.002
a_6			11.13 ± 0.07
a_7			-0.651 ± 0.002
a_8			12.51 ± 0.08
a_9			-0.665 ± 0.002
a_{body}		$0.1429 \pm \text{fixed}$	$0.1427 \pm \text{fixed}$
χ^2	8220	6667	1606
N_{df}	1278	1278	1278

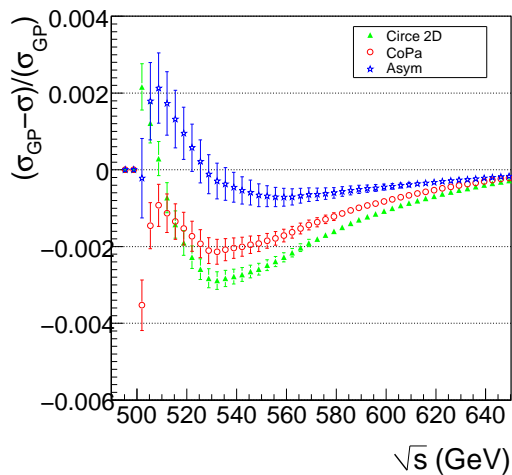


Figure 6.3: Relative difference between the threshold scans with Circe, CoPa and Asym and the threshold scan from the asymmetric GuineaPig sample.

Chapter 7

Measuring the Center-of-Mass Energies of Bhabha Events

The process $e^+e^- \rightarrow e^+e^-$ is called Bhabha scattering. It is used to measure the differential luminosity for three reasons, namely because the cross section can be calculated very precisely, because the cross section is relatively large and because of the clear signal electrons and positrons produce in the detector.

7.1 Bhabha Scattering

The first order differential cross section is given by

$$\frac{d\sigma_{\text{Bhabha}}}{d\theta} = \frac{2\pi\alpha^2}{s} \frac{\sin\theta}{\sin^4\theta/2} \quad (7.1)$$

with the fine-structure constant α , the center-of-mass energy \sqrt{s} and the scattering angle θ .

7.1.1 Simulation Software BHWide

To simulate the Bhabha scattering as well as the initial and final state radiation the wide angle Bhabha simulation software BHWide [22] is used. Beamstrahlung is included in the same way as it was done in [23]. Because the Bhabha cross section (7.1) depends inversely on s , the weight given for each event in BHWide is rescaled by $s/s' = 1/(x_1x_2)$, where $x_{1/2}$ is the fractional energy of the scattering particles and s' the effective center-of-mass energy squared. Thus events at a lower energy have a larger weight than events at the nominal energy. Besides the changed weight the four-vectors of the participating particles (electron, positron and photons) are rescaled to conserve energy and momentum. The four-vectors are rescaled by $\sqrt{s'/s} = \sqrt{x_1x_2}$ and boosted into the laboratory frame, which is no longer the same as the center-of-mass system. Because beamstrahlung can happen asymmetrically between the two leptons their center-of-mass system is boosted relative to the laboratory system.

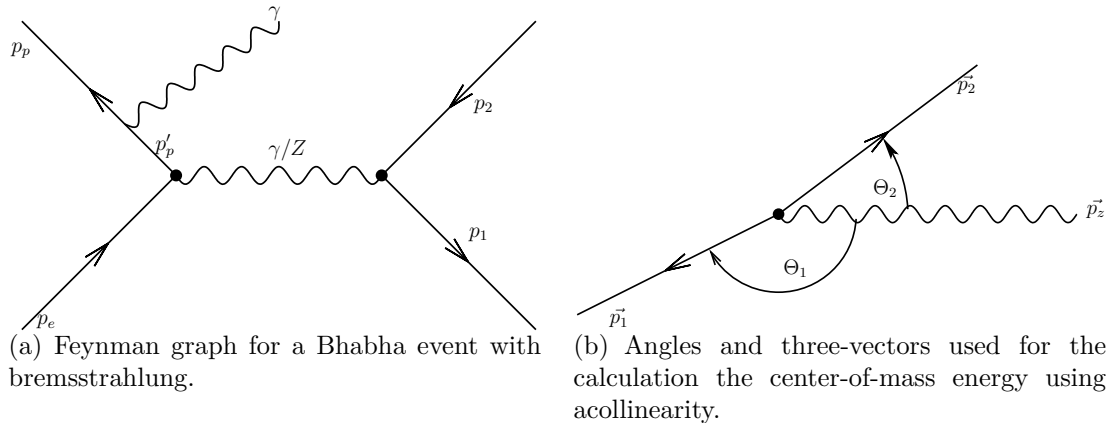


Figure 7.1: Diagrams for the calculation of $\sqrt{s_{\text{Rec}}}$ using acollinearity.

The fractional particle energies x_1 and x_2 are either taken from the energies of the scattering events simulated by GuineaPig or produced according to one of the parameterizations.

7.1.2 Acceptance Region and Cross Section

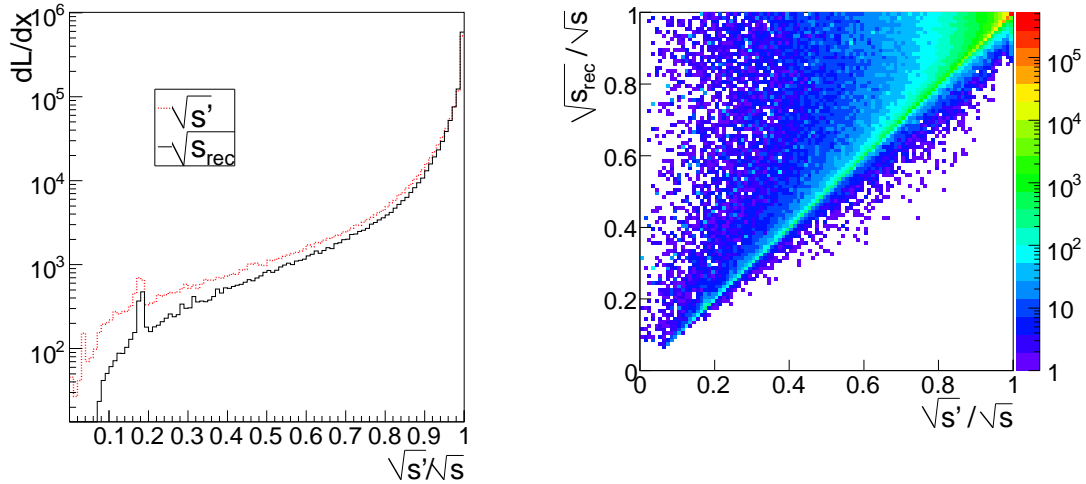
To measure the tracks of the electrons and positrons in the tracker the particles must have an angle of at least 7° above the beam pipe, corresponding to the lower edge of the tracker. This means that the total cross section for the Bhabha events is $\sigma_{\text{Bhabha}} = 0.33 \text{ nb}$ at $\sqrt{s} = 500 \text{ GeV}$. For a sample size of 10^6 events an integrated luminosity of $L_{\text{int}} = 3 \text{ fb}^{-1}$ is needed. This means about a month of data taking at the ILC, but precision physics measurements will also need an integrated luminosity of at least 5 fb^{-1} to 10 fb^{-1} .

7.2 Effective Center-of-Mass Energy

The detector will be used in two ways to determine the effective center-of-mass energy and the energy of the scattered particle of the Bhabha events. The effective center-of-mass energy can be reconstructed with the angles of the outgoing particles. The angles are measured by the vertex and tracking detectors. The absolute energy of the outgoing particles is measured by the electromagnetic calorimeter.

7.2.1 Measurement using the Tracker

Because of the very high angular resolution of the vertex and tracking detectors $\Delta\theta < 0.03 \text{ mrad}$ [4], planned for the ILC, a good way to measure the effective center-of-mass energy $\sqrt{s'}$ is measuring the angles of the outgoing electron-positron-pair.



(a) Reconstructed and actual effective center-of-mass energy.

(b) Reconstructed vs. real center-of-mass energy.

Figure 7.2: Energy spectra of Bhabha events. Center-of-mass energy reconstructed through the angles $\sqrt{s_{rec}}$ and taken from the four-vectors of the outgoing leptons and photons $\sqrt{s'}$ (see text).

Assuming that only one of the particles emits photons along the beam pipe, the effective center-of-mass energy can be reconstructed out of the angles Θ_1 and Θ_2 of the outgoing particles with respect to the beam pipe (Figure 7.1(b), Appendix A):

$$\frac{\sqrt{s_{rec}}}{\sqrt{s}} = \sqrt{\frac{\sin(\Theta_1) + \sin(\Theta_2) + \sin(\Theta_1 + \Theta_2)}{\sin(\Theta_1) + \sin(\Theta_2) - \sin(\Theta_1 + \Theta_2)}}. \quad (7.2)$$

If the nominal energy \sqrt{s} is known $\sqrt{s_{rec}}$ can be calculated. By construction the sum of the angles is $\Theta_1 + \Theta_2 > \pi$ and $\sqrt{s_{rec}}/\sqrt{s} \leq 1$. The effective center-of-mass energy reconstructed through the acollinearity $\sqrt{s_{rec}}$ differs from the real effective center-of-mass energy $\sqrt{s'}$, if the photons are not radiated along the beam pipe or if both particles emit radiation. If both particles radiate photons the acollinearity is reduced and the reconstructed energy $\sqrt{s_{rec}}$ is larger than the real effective center-of-mass energy $\sqrt{s'}$ (Figure 7.2(a)).

For Figure 7.2(a) the real effective center-of-mass energy $\sqrt{s'}$ is calculated out of the four-vectors of all outgoing particles of an event. Since the final state photons are mostly in the direction of the outgoing lepton, the angle measured through the tracker would only be changed marginally. The energy of the lepton, however, could be changed drastically. But the effective center-of-mass energy includes the energy of the final state photons. Therefore all photons within a cone of 3° around a lepton are added to the four-vector of the lepton. In some cases adding up the photons results in a real effective energy $\sqrt{s'}$ above the reconstructed energy $\sqrt{s_{rec}}$ (The small band for $\sqrt{s'/s} = 1$ and $\sqrt{s_{rec}/s} < 1$ in Figure 7.2(b)). Although the reconstructed energy has some problems for multiple photon radiation its main advantage is that

the angles can be measured very precisely and the resulting energy has a very high resolution.

7.2.2 Measurement by the Calorimeter

It is not possible to measure the absolute effective center-of-mass energy $\sqrt{s'}$ using the acollinearity. Only the relative difference in the particle energies can be measured $\sqrt{s_{\text{rec}}}$. The absolute size of the energy has to be measured with the electromagnetic calorimeter or through the bending radius in the tracker.

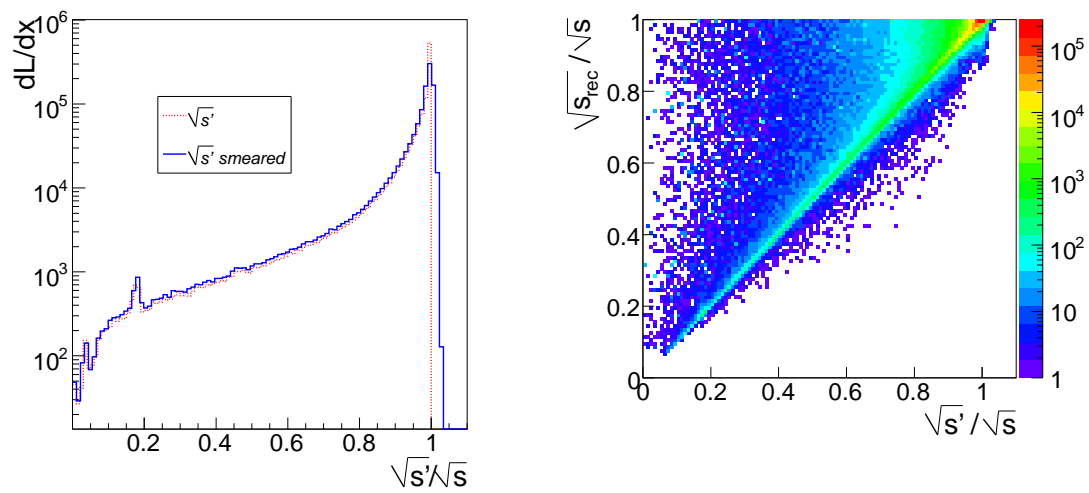
The absolute effective center-of-mass energy $\sqrt{s'}$ calculated from the four-vectors (Figure 7.1(a)) of the leptons p_1 and p_2 is

$$\sqrt{s'} = \sqrt{2p_1 \cdot p_2}, \quad (7.3)$$

with $m_e \ll \sqrt{s}$. The four-vectors of any photons within a small cone around the leptons are added to the four-vector of the respective lepton $\tilde{p}_{1/2} = p_{1/2} + p_\gamma$. The photon four-vectors are added after the angles for the acollinearity have been calculated.

To simulate the detector resolution the energies calculated from the four-vectors of the leptons are smeared with a 1% Gaussian instead of using the detector simulation and reconstruction (Section 2.3.1).

The detector resolution spreads the spectrum around the peak (Figure 7.3(a)) and effectively moves more events to lower energies. This mixes events without radiation at the peak and events with small amounts of radiative losses causing some complication for the measurement of the differential luminosity.



(a) Energy spectrum before and after smearing.

(b) Comparison between the reconstructed energies using acollinearity and the smeared energies measured in the calorimeter.

Figure 7.3: The smeared effective center-of-mass energies have been smeared with a 1% Gaussian to simulate detector resolution.

Chapter 8

Measuring the Differential Luminosity

The energy spectrum of the Bhabha events is affected by the initial and final state radiation as well as by beamstrahlung and by the beam energy spread. But while the bremsstrahlung can be calculated, the spectrum due to beamstrahlung is a priori unknown and has to be extracted out of the measured energies. This extraction is done by comparing the measured energy spectrum with the unknown amount of beamstrahlung, with a sample of simulated Bhabha events, where the amount of beamstrahlung is known. To measure the contribution of the beamstrahlung a re-weighting fit is used. The evolution of the re-weighting fit for determining the parameters of the Circe parameterization to the re-weighting fit able to determine the parameters of the asymmetric parameterization is described in the following chapter.

8.1 Re-weighting Fit

The parameterized spectra describe how likely an event is, where two particles have a certain energy x_1 and x_2 after beamstrahlung. The parameterization

$$L_A = L(x_1, x_2; A) \tag{8.1}$$

attributes a certain weight to each event. MC-events produced with this parameterization and the parameter set A can be transformed into events with parameter set B by re-weighting every event with a factor of

$$w = \frac{L_B(x_1, x_2; B)}{L_A(x_1, x_2; A)} \tag{8.2}$$

The Bhabha events of the data, with the beamstrahlung simulated by GuineaPig, follow their own differential luminosity. This differential luminosity can be described by the parameterization and an unknown parameter set C , which is at least unknown, if the differential luminosity is not directly accessible. Thus by re-weighting

the MC events the varied parameter set B should be equal to the unknown parameter set C once the χ^2 has been minimized and the beamstrahlung spectrum has been measured.

The re-weighting fit will produce the best results, when the MC generator is as close to the real world as possible. This requirement is fulfilled here, because the data and the MC events are both produced by the same generator.

The events from the data are filled into one histogram and the MC events are filled into a second histogram, but with the weight for each event given by w (8.2). The three different histograms that will be used for the comparison between data and MC events are described in the following.

8.1.1 One-Dimensional Histogram

The most precise value for the effective center-of-mass energy is the energy reconstructed using the acollinearity $\sqrt{s_{\text{rec}}}$ (7.2). Because the spectrum of the reconstructed energy has a very steep slope the same transformation is used that was used for the particle energy spectrum after beamstrahlung. The transformed energy

$$E_T = \left(1 - \frac{\sqrt{s_{\text{rec}}}}{\sqrt{s}}\right)^{1/5} \quad (8.3)$$

leads to an improved distribution of the events over the bins. For this variable the events are distributed between 0.0 and 1.0 and 100 bins are used.

8.1.2 Two-Dimensional Histogram

For additional information the absolute center-of-mass energy measured by the calorimeter $\sqrt{s'}$ can be used. This spectrum also has a very sharp peak, but because of the smearing due to the resolution and the fact that there is no defined maximum a slightly different transformation is used:

$$E'_T = \left(1.05 - \frac{\sqrt{s'}}{\sqrt{s}}\right)^{1/3} \quad (8.4)$$

This is not as effective as the other transformation, but because of the smearing only 50 bins are used.

8.1.3 Three-Dimensional Histogram

The absolute center-of-mass energy measured by the calorimeter can be replaced by the individually measured particle energies. The particle energies are transformed with the same transformation as the absolute center-of-mass energy,

$$\begin{aligned} E_T^+ &= \left(1.05 - \frac{E'_{e^+}}{E_{\text{Beam}}}\right)^{1/3}, \\ E_T^- &= \left(1.05 - \frac{E'_{e^-}}{E_{\text{Beam}}}\right)^{1/3}, \end{aligned} \quad (8.5)$$

and 50 bins for both variables are used. This histogram has 250,000 bins, but only about 24,000 of those are bins, where both the data and MC events have at least one entry, and only those are used to calculate the χ^2 .

8.1.4 Calculating the Chi-Square

If the χ^2 were to be calculated in the usual way by using the error of the bins from both histograms, the re-weighting would simply increase the weights to lower the χ^2 . The χ^2 is therefore calculated with the correct error from the data histogram $\sigma_{N_{\text{Data}}^i}$ and the error for the MC histogram $\sigma_{N_{\text{MC}}^i}$ is approximated by using the square root of the number of entries of a bin, instead of the square root of the sum of the squares of the weights of a bin. The χ^2 is:

$$\chi^2 = \sum_i \frac{(N_{\text{Data}}^i - N_{\text{MC}}^i)^2}{\sigma_{N_{\text{Data}}^i}^2 + \sigma_{N_{\text{MC}}^i}^2} \quad (8.6)$$

The sum is taken over all bins, N_{Data}^i is content of the bins of the data histogram and N_{MC}^i is the sum of the weights of the entries for the bins of the re-weighted histogram for the MC Bhabha events.

8.2 Data and Monte Carlo Bhabha Events

As long as the ILC is not running and taking data no Bhabha events with an unknown differential luminosity are available. Therefore both the data and the Monte Carlo Bhabha events are of course Monte Carlo events produced as described in Section 7.1.1. The difference between the two is that the data events are created with the differential luminosity given by the energies of the scattering events simulated by GuineaPig. The GuineaPig spectrum is of course known, but once the data is really being taken the differential luminosity due to beamstrahlung is unknown.

For the Monte Carlo Bhabha events the differential luminosity is given by one of the parameterizations. Because the GuineaPig spectrum is known the parameters found by the re-weighting fit can be compared to the parameters found by the direct fit to the GuineaPig spectrum and the quality of the result is judged by comparing the threshold scans with the parameters found by the re-weighting fit to the threshold scans resulting from the GuineaPig spectrum.

To see whether the re-weighting fit is stable enough to reproduce the GuineaPig spectrum without knowing a priori what the correct parameters are some energy distributions are created that are vastly different to the actual spectrum from GuineaPig.

8.3 Determining the Circe Parameters

The development of the re-weighting fit begins with the Circe parameterization as the function for the differential luminosity. The Circe parameterization and the

Table 8.1: Circe parameters for the differential luminosity input for BHWide (See Section 7.1.1).

Par.	Real	Arbitrary1	Arbitrary2
a_0	0.6288	0.6500	0.8000
a_2	11.81	12.00	14.00
a_3	-0.6733	-0.6400	-0.7400

histograms used are later replaced by the expanded parameterization to determine the parameters of the parameterizations including correlation.

Besides the free parameters of the given parameterization, a free scaling parameter is used to allow the integrated content of the histograms to stay the same size. This content could otherwise differ significantly because of the changed weights for the entries. This free scaling parameter would also allow the use of different numbers of events for the data or Monte Carlo events once real data has been taken.

Three Monte Carlo samples of Bhabha events were created with BHWide. The different parameters for the differential luminosity parameterized by Circe for the Bhabha events are found in table 8.1. The parameter sets are:

- Real: The parameters are taken from the direct fit to the GuineaPig spectrum (Chapter 5).
- Arbitrary1: The parameters are chosen to be slightly different to the real parameters.
- Arbitrary2: The parameters are chosen to be completely different to the real parameters.

The arbitrary parameter sets are used to determine whether the reproduction of the differential luminosity spectrum is possible without the a priori knowledge of the spectrum.

The data Monte Carlo sample was also created with BHWide, where the differential luminosity was given by the GuineaPig spectrum.

8.3.1 Fitting Circe to Circe

As a first check for the re-weighting fit the MC events were also used as the data-sample instead of the Bhabha events with the differential luminosity given by GuineaPig. If the fit is working properly, it should reproduce the exact parameters used for the Circe parameterization (Table 8.2). The only difference is that the size of the errors increases by a factor of two to four and the correlation between a_0 and the other parameters increases considerably compared to the almost nonexistent correlation before. Because all the events are now smeared out by the initial and final state radiation some information on the spectrum is lost and the errors increase. The smearing from the initial and final state radiation also causes the increased correlation between the parameters.

Table 8.2: The Circe parameters and the reproduced parameters using re-weighting to fit the MC onto the MC Sample.

Par.	Direct Fit	Re-weighting Fit	Correlation Matrix			
a_0	0.6288 ± 0.0004	0.6288 ± 0.0008	1.00	0.27	0.47	-0.02
a_2	11.81 ± 0.03	11.81 ± 0.10	0.27	1.00	0.78	-0.06
a_3	-0.6733 ± 0.0006	-0.6733 ± 0.0026	0.47	0.78	1.00	-0.03
Scale		1.000 ± 0.001	-0.02	-0.06	-0.03	1.00

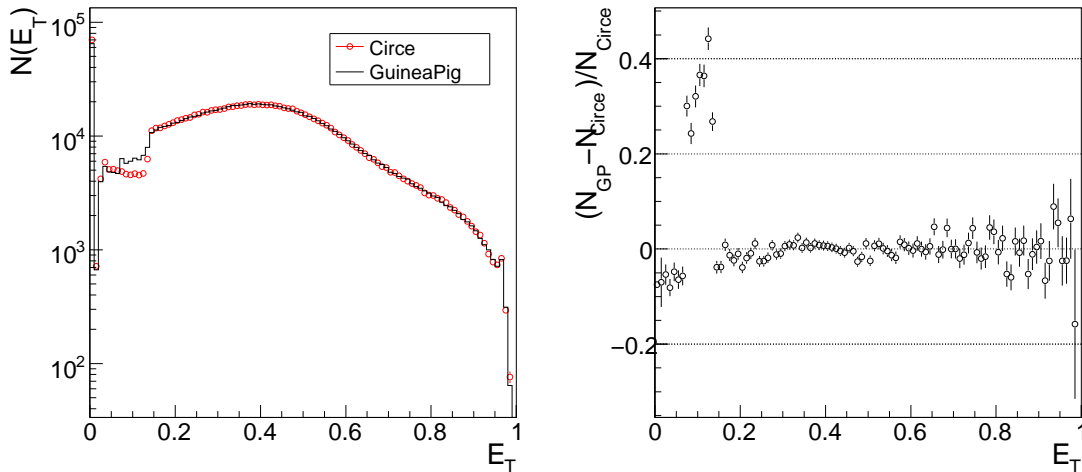


Figure 8.1: The two histograms after the re-weighting fit (left) and their relative difference (right).

8.3.2 Fitting Circe to GuineaPig

Consequently the Bhabha events with the GuineaPig distribution are used as the data and the histogram is fitted by the three samples of Bhabha events with the known beamstrahlung energy spectrum.

The histograms for GuineaPig and Circe show a significant difference for $E_T < 0.14$ (Figure 8.1). For events, where the combined energy loss is smaller than 0.0001 the number of entries in the bins differ by as much as 40%. The histogram for the Bhabha events with GuineaPig and Circe differ, because for GuineaPig events with an energy loss of less than 0.0001 due to beamstrahlung or initial state radiation exist. But for the Circe an energy loss that small is only caused by initial state radiation, because of the cutoff of at $x_{1/2} = 0.9999$.

The values of parameters a_0 and a_2 returned by the re-weighting fits for all MC sets are smaller than the parameters found by the direct fit to the particle energy spectrum from GuineaPig (Table 8.3). The value for the parameter a_3 is much smaller than the value found by the direct fit. The problematic bins also cause a very large χ^2 (Table 8.3).

If the bins for $E_T < 0.14$ are merged into a single bin that now contains all events

Table 8.3: Parameters reproduced by the re-weighting fit. The parameters found by the direct fit are $a_0 = 0.6288$, $a_2 = 11.81$ and $a_3 = -0.6733$.

Without the merging of the first bins			
Par.	Real	Arbitrary1	Arbitrary2
a_0	0.6260 ± 0.0012	0.6268 ± 0.0012	0.6254 ± 0.0014
a_2	11.51 ± 0.14	11.39 ± 0.14	11.56 ± 0.14
a_3	-0.6976 ± 0.0036	-0.6947 ± 0.0036	-0.6976 ± 0.0037
Scale	0.998 ± 0.001	0.999 ± 0.001	0.999 ± 0.001
χ^2/N_{df}	1992/95	1834/95	1643/95
With the merging of the first bins			
Par.	Real	Arbitrary1	Arbitrary2
a_0	0.6358 ± 0.0012	0.6355 ± 0.0012	0.6339 ± 0.0013
a_2	12.02 ± 0.15	11.83 ± 0.14	12.01 ± 0.14
a_3	-0.6741 ± 0.0037	-0.6739 ± 0.0037	-0.6772 ± 0.0039
Scale	0.999 ± 0.001	1.000 ± 0.001	1.000 ± 0.001
χ^2/N_{df}	127/81	113/81	124/81

where the energy loss is smaller than 0.0001 (Figure 8.3), the χ^2 of the re-weighting fits are reduced by a factor of ≈ 15 . At the same time the beta-parameters a_2 and a_3 are now reproduced, but a_0 is significantly increased (Table 8.3).

The threshold scans (Figure 8.4) show that the fits without the merging are slightly better than the fit with the merged bin, because parameter a_0 is the most important parameter close to the threshold. The parameters are determined almost independent of the initial distribution of the differential luminosity. All three MC samples of Bhabha events reproduce similar parameters that only fluctuate statistically.

The problem caused by the cutoff in the luminosity spectrum will be automatically removed once the beam energy spread is included in the analysis. The beam energy spread is a factor of 10 larger than the cutoff and all differences between GuineaPig and the parameterizations are smoothed over. For the development of the re-weighting fit without the beam energy spread the merging of the bins for $E_T < 0.14$ is kept.

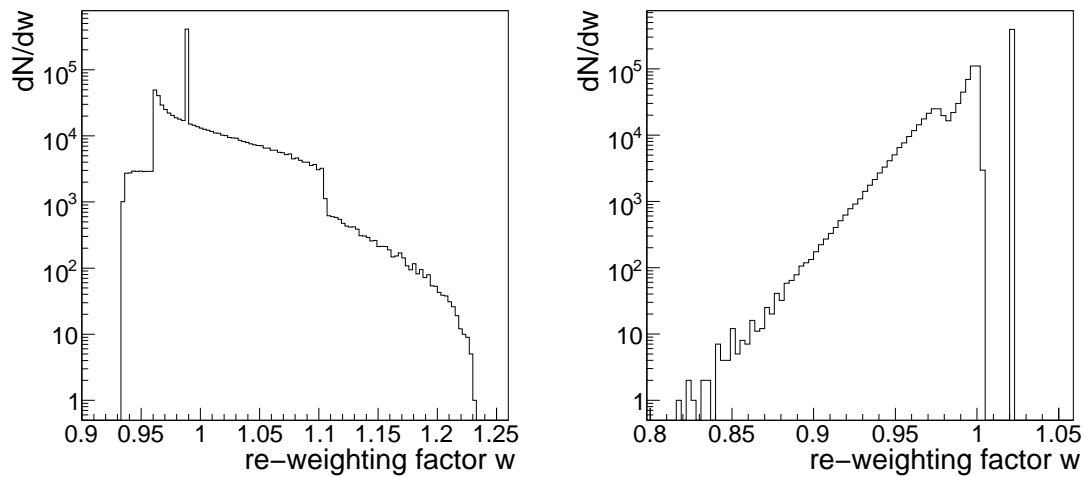


Figure 8.2: The weights for the MC histogram for the lowest χ^2 from the fit where the initial parameters were the real parameters without (left) and with (right) the merging. The large peak is from the events with $x_1 = x_2 = 1.0$.

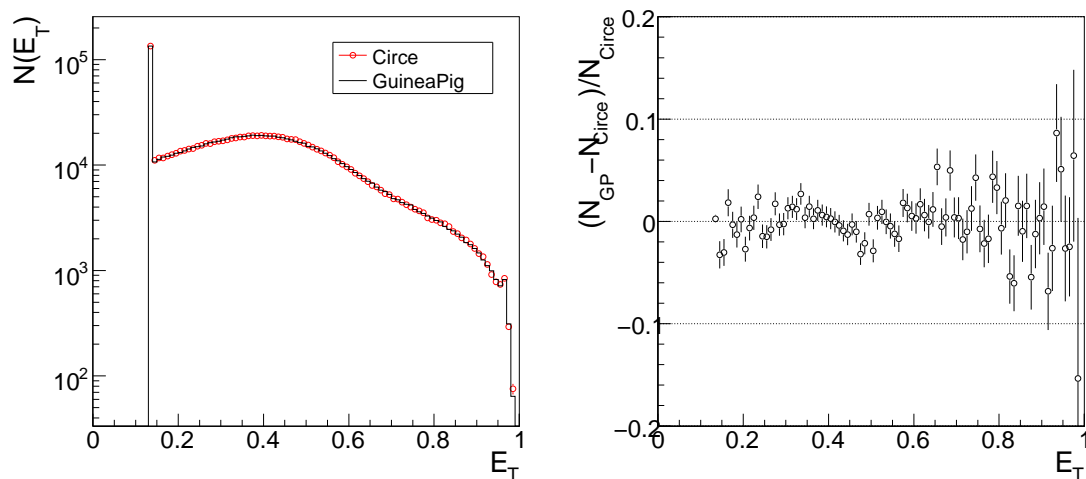


Figure 8.3: The two histograms after the re-weighting fit (left) and their relative difference(right), where the bins below $E_T = 0.14$ have been merged.

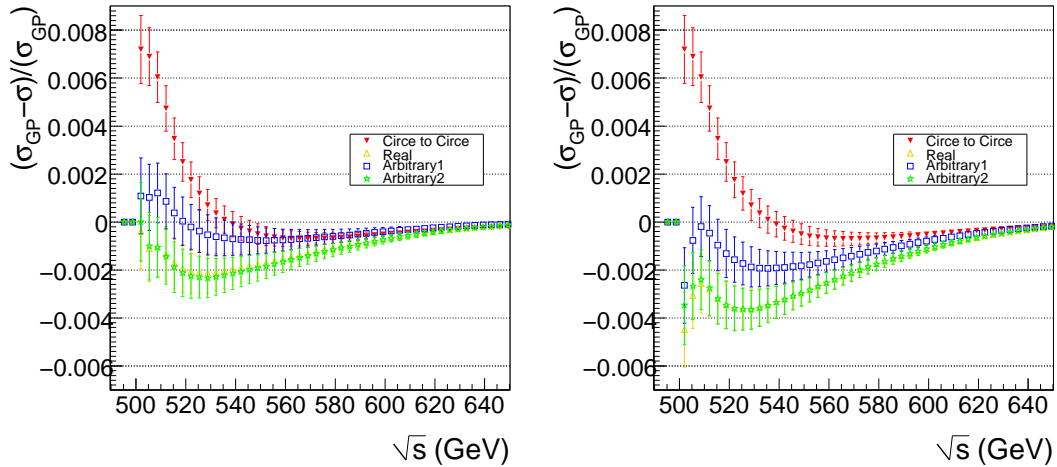


Figure 8.4: The resulting threshold scans for the fit without (left) and with (right) the merger.

Table 8.4: Parameters for the production of the parameterized energy spectra used as the initial energy for the generation of the Bhabha events.

Parameter	Real	Arbitrary1	Arbitrary2
a_{peak}	0.4042	0.4200	0.3000
a_2	12.13	12.50	14.00
a_3	-0.677	-0.700	-0.600
a_{arm}	0.2253	0.2000	0.2500
a_4	11.62	11.00	14.00
a_5	-0.664	-0.600	-0.600
a_{body}	0.1452	0.1800	0.2000

8.4 Determination of the CoPa Parameters

Instead of Circe CoPa is now used for the re-weighting of the MC histogram, to see whether better results can be obtained with this parameterization. Again three different parameter sets are chosen for the initial luminosity spectrum, one with the real parameters found by the direct fit of CoPa to particle energy spectrum from GuineaPig and two with arbitrary parameters different from the real parameters. In the parameter set “Arbitrary2” the distribution of the events is almost equal for the separate regions: 30% for the peak, 25% for each arm and 20% for the body (Table 8.4).

The luminosity spectra created with the parameters from Table 8.4 are used as the initial differential luminosity due to beamstrahlung for the generation of the MC Bhabha events.

Table 8.5: Comparison between the errors from the direct fit to the GuineaPig spectrum and the 1D and 2D-re-weighting fit from CoPa to CoPa.

	a_{peak}	a_2	a_3	a_{arm}	a_4	a_5	a_{body}
Real Parameter	0.4042	12.13	-0.677	0.2253	11.62	-0.664	0.1452
Errors from							
Direct Fit	0.0005	0.05	0.001	0.0002	0.05	0.001	fixed
1D re-weighting	0.0012	1.89	0.020	0.017	3.16	0.030	fixed
Results for the 2D-CoPa to CoPa re-weighting							
2D re-weighting	0.4043	12.69	-0.670	0.2144	10.33	-0.733	0.1668
Errors	0.0015	0.28	0.005	0.0029	0.40	0.014	fixed

8.4.1 Fitting CoPa to CoPa

As the first test of the re-weighting fit with CoPa both the data and the Monte Carlo Bhabha events are represented by the same Monte Carlo sample where the differential luminosity was created according to the CoPa parameterization with the real parameters.

It is possible to determine the CoPa parameters with the same one-dimensional histogram used to determine the Circe parameters. The errors, however, grow so large (Table 8.5, Figure 8.5(a)) that the result becomes meaningless.

Using the two-dimensional histogram (Figure 8.6(b)) enables the measurement of the parameters for CoPa with much smaller errors and more meaningful results. The data and MC histograms in this case only differ, because of the smearing of the absolute center-of-mass energy. These small statistical fluctuations cause a very small difference between the parameters used to create the spectrum and the parameters found by the re-weighting fit (Table 8.5). The small differences in the parameters do not represent a significant change for the threshold scan (Figure 8.5(b)).

8.4.2 Fitting CoPa to GuineaPig

The parameters reproduced by the fit with the two-dimensional histograms are found in Table 8.6. The probability parameters (a_{peak} , a_{arm}) all agree very well with the parameters from the direct fit. The beta-distribution parameters show large differences, but the resulting threshold scans (Figure 8.7 left) are all more or less the same, showing no large differences to the effective cross-sections for the GuineaPig differential luminosity. The scan from the “Arbitrary2” results reproduces the scan from the directly fitted parameters almost exactly, while the other two sets produce slightly larger effective cross sections.

This difference becomes more pronounced, if the three-dimensional histograms (Figure 8.8) are used for the re-weighting fit. The events, where no beamstrahlung is produced, described by parameter a_{peak} , are significantly overestimated (Table 8.7). Not even the fit from CoPa to CoPa, where the only difference between the

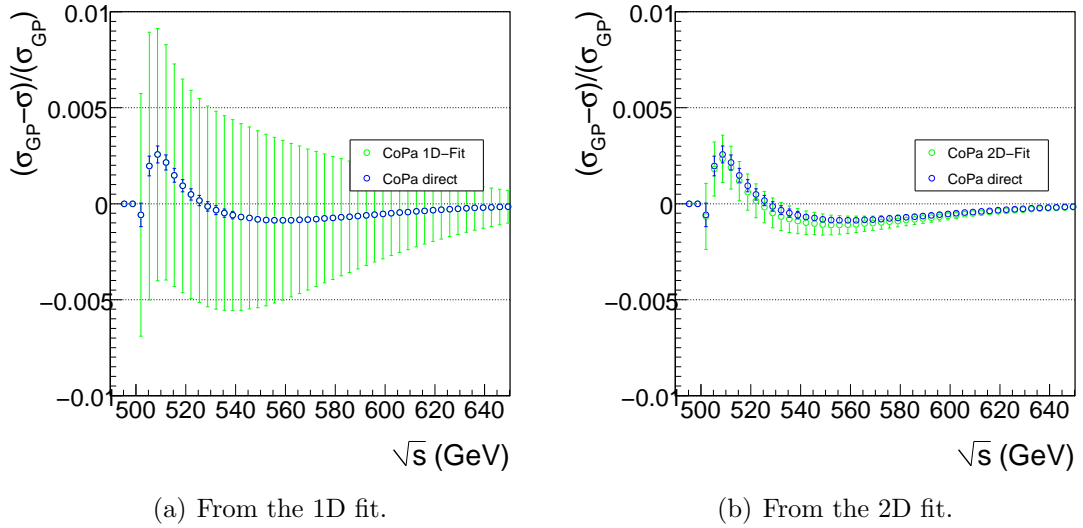


Figure 8.5: Threshold-scan resulting from the 1D and 2D re-weighting fit with CoPa.

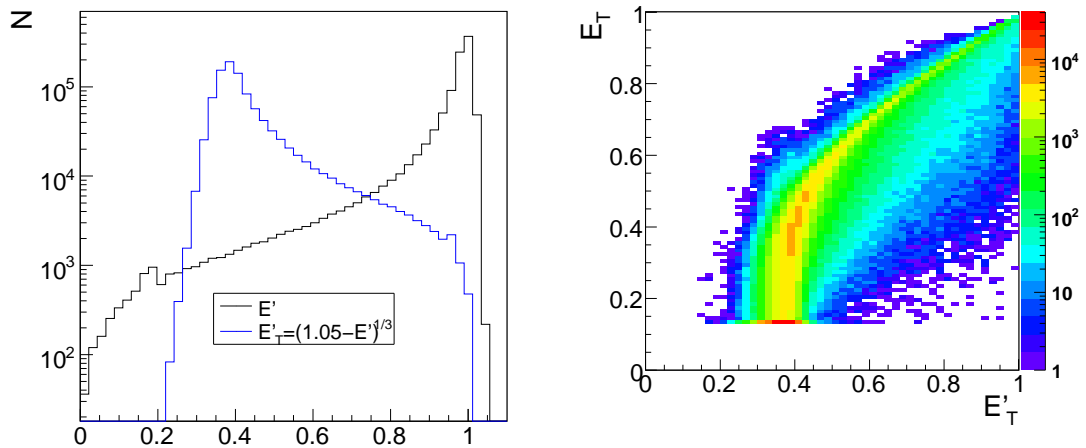


Figure 8.6: Histograms used for the 2D re-weighting fit to find the CoPa parameters. The sharp cutoff for $E_T = 0.14$ are due to the merging of the bins.

Table 8.6: Results for the measurement of the CoPa parameters from the re-weighting fit using two-dimensional histograms. Errors are approximately equal for all results.

	a_{peak}	a_2	a_3	a_{arm}	a_4	a_5	a_{body}
Direct Fit	0.4042	12.13	-0.677	0.2253	11.62	-0.664	0.1452
Real	0.4043	12.69	-0.670	0.2133	10.33	-0.733	0.1668
Arbitrary1	0.4054	13.11	-0.662	0.2179	9.95	-0.727	0.1588
Arbitrary2	0.4052	12.18	-0.676	0.2189	11.18	-0.697	0.1570
Errors	0.0015	0.28	0.005	0.0029	0.42	0.016	fixed

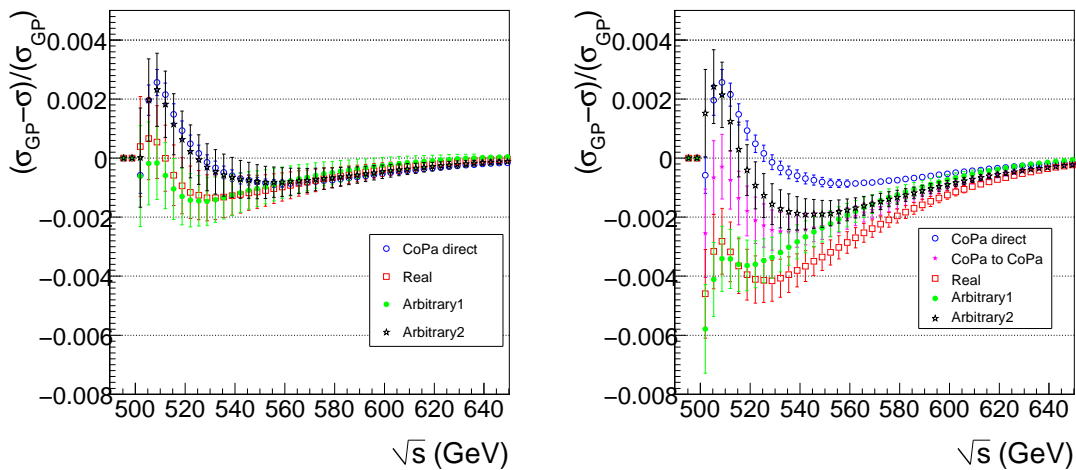


Figure 8.7: Left: Threshold scans for the results from the 2D fit. Right: Threshold scans for the results for the 3D fits without the demand of at least 20 entries for a bin.

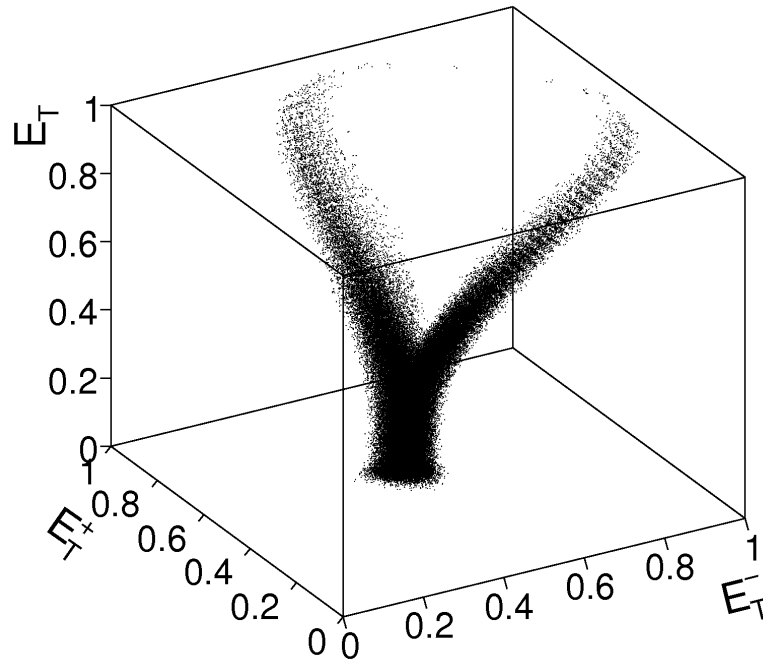


Figure 8.8: The three-dimensional histogram used for the re-weighting fit.

histograms comes from the smearing due to the detector resolution, reproduces correct results. The threshold scans (Figure 8.7 right) are all too large, except for the set “Arbitrary2”, where the initial distribution started with fewer events with no beamstrahlung.

In the three-dimensional histogram many bins ($\approx 20,000$) contain only very few or no entries, which means that statistical fluctuations make the re-weighting fit very unstable. If a bin of the histogram from the MC events is not empty, but the bin of data histogram is, the fit will try to reduce the weights for those entries. On the other hand, if the data histogram contains entries, but the MC histogram does not, the χ^2 for this bin is not changed by the re-weighting. To reduce the influence of these statistical fluctuations only those bins are used to calculate the χ^2 , where both histograms have at least 20 entries in the bins.

This requirement for the number of entries in a bin excludes 120,000 events from bins with less entries from the calculation of the χ^2 and instead of 25,000 bins only approximately 4,000 bins are used.

The CoPa to CoPa fit is now better able to reproduce the parameters within the error range (Table 8.8). Although there is still a small overestimation of the events without beamstrahlung, this effect has become smaller than 0.2% for the arbitrary parametersets. Shortly above the threshold the results are even better than the results for the two-dimensional scan (Figure 8.9). The results for the set “Arbitrary1” are even within one σ over almost the whole range of the scan.

Table 8.7: Results for the measurement of the CoPa parameters from the re-weighting fit using three-dimensional histograms without the requirement of at least 20 entries in a bin. Errors are approximately equal for all results.

	a_{peak}	a_2	a_3	a_{arm}	a_4	a_5	a_{body}
Direct Fit	0.4042	12.13	-0.677	0.2253	11.62	-0.664	0.1452
CoPa to CoPa	0.4059	12.11	-0.675	0.2223	11.93	-0.680	0.1475
Real	0.4060	12.38	-0.675	0.2238	12.00	-0.679	0.1462
Arbitrary1	0.4085	13.11	-0.671	0.2162	10.65	-0.706	0.1590
Arbitrary2	0.4024	12.01	-0.681	0.2191	12.01	-0.689	0.1594
Errors	0.0015	0.19	0.004	0.0015	0.28	0.009	fixed

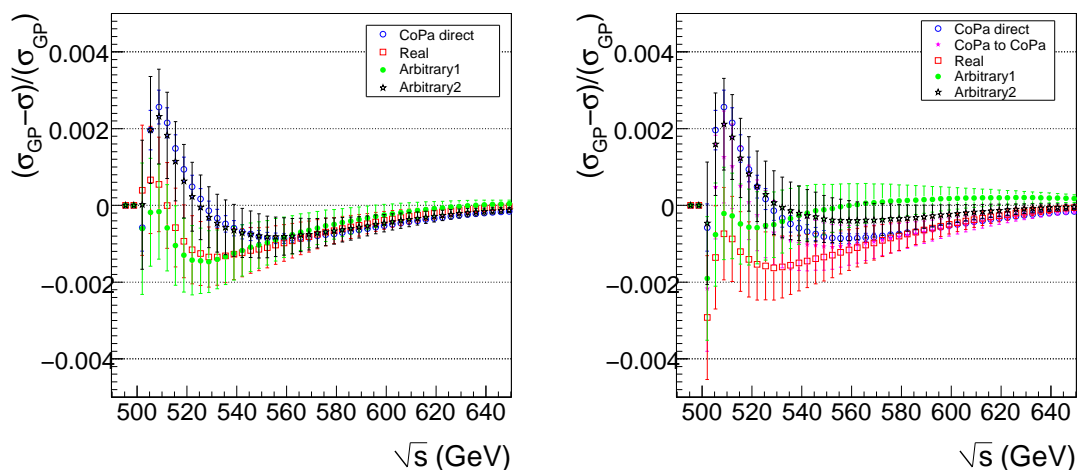


Figure 8.9: Left: Threshold scans for the results from the 2D fit. Right: Threshold scans for the results for the 3D fits with the demand of at least 20 entries for a bin.

Table 8.8: Results for the determination of the CoPa parameters from the re-weighting fit using the three-dimensional histograms with the requirement of at least 20 entries in a bin. Errors are approximately equal for all results.

	a_{peak}	a_2	a_3	a_{arm}	a_4	a_5	a_{body}
Direct Fit	0.4042	12.13	-0.677	0.2253	11.62	-0.664	0.1452
CoPa to CoPa	0.4051	12.27	-0.676	0.2257	11.5	-0.665	0.1435
Real	0.4043	12.56	-0.676	0.2219	10.8	-0.697	0.1518
Arbitrary1	0.4050	13.33	-0.665	0.2199	9.6	-0.714	0.1552
Arbitrary2	0.4053	12.40	-0.675	0.2168	10.6	-0.705	0.1611
Errors	0.0016	0.26	0.005	0.0022	0.4	0.013	fixed

Table 8.9: Parameters from the asymmetric parameterization for the production of the parameterized energy spectra.

Parameter	Real Asym	Arbitrary1	Arbitrary2
a_{peak}	0.4063	0.4200	0.3000
a_{arm1}	0.2052	0.2200	0.2500
a_{arm2}	0.2458	0.2200	0.2500
a_2	12.95	12.50	14.00
a_3	-0.681	-0.660	-0.60
a_4	11.44	12.50	14.00
a_5	-0.667	-0.660	-0.60
a_6	11.13	11.50	11.50
a_7	-0.651	-0.650	-0.60
a_8	12.51	11.50	11.50
a_9	-0.665	-0.650	-0.60
a_{body}	0.1427	0.12	0.20

8.5 Measuring with the Asymmetric Parameterization

The data Bhabha events are now created with the differential luminosity given by the GuineaPig sample created with the asymmetric beam parameters. The three Monte Carlo Bhabha events are created with a differential luminosity parameterized by the asymmetric parameterization and the parameters found by the direct fit, and two parameter sets that describe a symmetric distribution (Table 8.9). The arbitrary parameter sets are chosen to be symmetric, to make sure that the asymmetric parameterization is able to determine the correct distribution on its own through the re-weighting fit.

The three-dimensional histogram is used for the re-weighting fit to be able to distinguish the energies of the electrons and positrons.

8.5.1 Re-weighting Fit with the Three-Dimensional Histogram

Using the MC Bhabha events, where the differential luminosity was given by the asymmetric parameterization with the parameters found by the direct fit to the asymmetric GuineaPig sample, both for the data histogram and for the MC histogram for the re-weighting fit, shows that the re-weighting fit is able to reproduce the correct parameters within statistical fluctuations (Table 8.10, Asym to Asym).

The re-weighting fit on the data histogram from the Bhabha events with the differential luminosity given by the asymmetric GuineaPig reproduces the correct distribution of events for all Monte Carlo samples (Table 8.10). Independent of the initial distribution of the events, the correct distribution is reproduced within

Table 8.10: Results for the three-dimensional re-weighting fit for the asymmetric parameterization.

Par.	Asym to Asym	Real Asym	Arbitrary1	Arbitrary2	Error
a_{peak}	0.4078	0.4074	0.4096	0.4061	0.0015
a_{arm1}	0.2078	0.1996	0.1949	0.2028	0.0040
a_{arm2}	0.2441	0.2437	0.2440	0.2404	0.0043
a_2	12.82	13.46	12.89	13.58	0.47
a_3	-0.693	-0.669	-0.682	-0.675	0.015
a_4	11.64	11.09	12.02	12.32	0.38
a_5	-0.652	-0.685	-0.666	-0.663	0.013
a_6	11.41	11.26	10.42	9.84	0.53
a_7	-0.650	-0.671	-0.695	-0.681	0.023
a_8	12.51	11.61	12.41	10.64	0.60
a_9	-0.661	-0.704	-0.672	-0.722	0.022
a_{body}	0.1403	0.1494	0.1514	0.1507	

2σ . The beta-parameters show a somewhat larger spread in their values. The fact that the parameters $a_2 = 13.58$ and $a_8 = 10.64$ returned from the fit of the set “Arbitrary2” show a large difference, although they both belong to the variable x_2 , means that the 8 free parameters for the beta-distributions are necessary for the description of the differential luminosity.

The threshold sans for the parameter sets determined by the re-weighting fit are only slightly different from the threshold scan with the differential luminosity given by GuineaPig (Figure 8.10 right). Only a small significant offset right above the threshold is visible. The result for the set “Arbitrary2” is always within one σ of the threshold scan with GuineaPig.

8.5.2 Measuring the Asymmetric Spectrum with the Symmetric Parameterizations

By using the respective histograms and parameterizations, it is also possible to determine the parameters belonging to the symmetric parameterizations Circe or CoPa of the spectrum with a asymmetric energy spectrum due to Beamstrahlung. Although the resulting threshold scans are as good as the results from the re-weighting fit with the asymmetric parameterization (Figure 8.10 left), the real distribution of events cannot be determined.

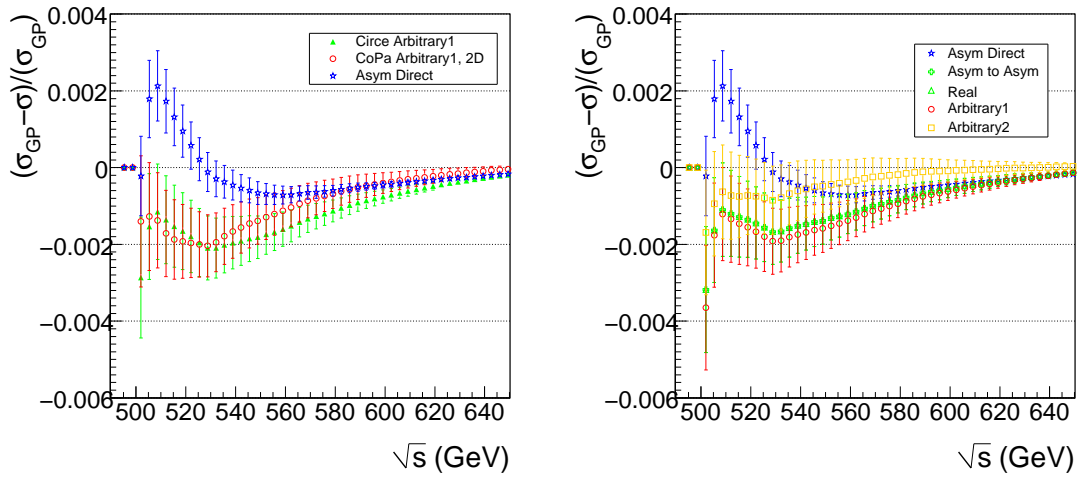


Figure 8.10: Resulting threshold scans for the an asymmetric differential luminosity measured with the symmetric parameterizations Circe and Copa (Left) and the asymmetric parameterization (Right).

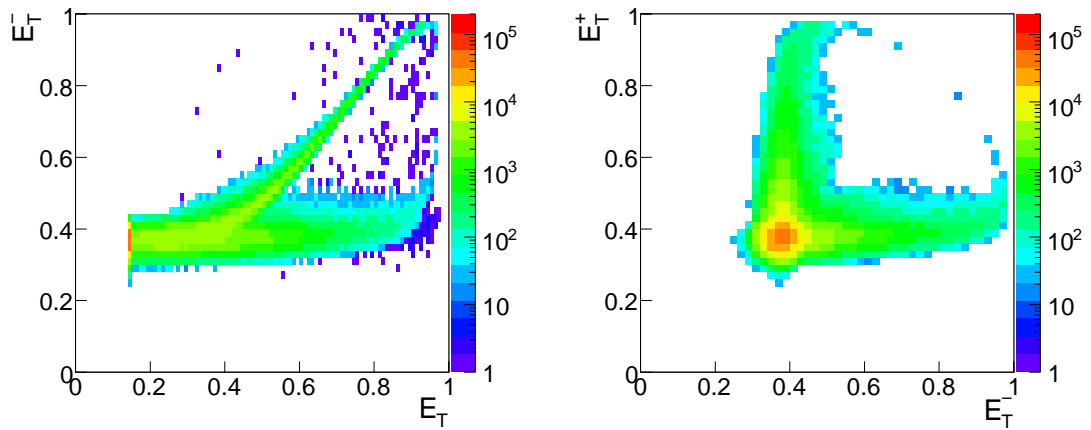


Figure 8.11: Projections of the three-dimensional histogram used for the re-weighting fit. Note that the events from bins with less than 20 entries have been removed prior to the projection, leaving some areas empty. Left: Projection showing the transformed reconstructed spectrum E_T versus the transformed energy spectrum of the positron E_T^- . Right: Projection showing the transformed energy spectrum of the electron E_T^- versus the energy spectrum of the positron E_T^+ .

Chapter 9

Measuring a Luminosity Spectrum including Beam Energy Spread

The re-weighting fit will now be expanded to include the beam energy spread for the measurement of the differential luminosity. Because the beam energy spread is inherently asymmetric due to the undulator, which only the electrons pass through, the determination of the beam energy spread will only be done by using the asymmetric parameterization.

9.1 Adding the Beam Energy Spread to the Re-Weighting Fit

Very few additions have to be made to include the beam energy spread into the measurement. First of all, the beam energy spread has to be included in the production of the Bhabha events. For this purpose the initial energy of the particle $x_{1/2}$ coming from the respective beamstrahlung spectrum is smeared out by multiplying the fractional energy with a random variate $r_{1/2}$ generated by a Gaussian around a mean $\mu = 1.0$ with a corresponding variance $\sigma_{\text{Beamsread}}$. The calculation of the weight and the scaling of the four vectors is then done using the new particle energy $\bar{x}_{1/2} = x_{1/2}r_{1/2}$. For each Monte Carlo Bhabha event the two random variates from the Gaussian r_1 and r_2 are saved.

Secondly, the re-weighting fit is changed to incorporate two new free parameters for the two beam energy spreads σ_e and σ_p . The re-weighting factor w is multiplied by a factor that is the ratio between the Gaussian distribution with the free parameter $\sigma_{e/p}^B$ and the variance the beam energy was created for during the MC-production $\sigma_{e/p}^A$:

$$w = \frac{f_B(x_1, x_2; B) BS(r_1, \sigma_e^B) BS(r_2, \sigma_p^B)}{f_A(x_1, x_2; A) BS(r_1, \sigma_e^A) BS(r_2, \sigma_p^A)}. \quad (9.1)$$

The additional re-weighting factors are used instead of the convolution of the beamstrahlung parameterization with the beam energy spread parameterization. Because there is no analytical function to describe the convolution between the beta-

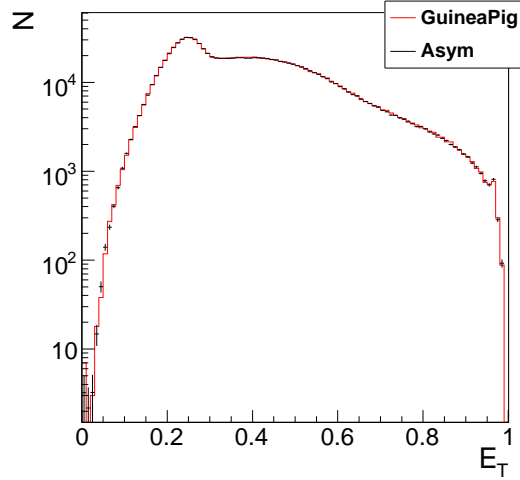


Figure 9.1: The histogram of the transformed reconstructed energy E_T . The peak moves to a lower energy because of the beam energy spread.

distribution and the Gaussian distribution, the computing time for the calculation of the re-weighting factors would increase notably.

Although the beam energy spread does not have to follow a Gaussian profile, only the Gauss-distribution is used here:

$$BS(r; \sigma) = \frac{1}{\sqrt{2\pi}\sigma} \exp\left(-\frac{1}{2} \frac{(1-r)^2}{\sigma^2}\right). \quad (9.2)$$

9.1.1 Effect on Measured Energy Spectra

Because the beam energy spread is a factor 10 smaller than the detector resolution there is no impact on the energies measured by the calorimeter. But the effect is large enough to smear out the difference between the transformed spectra of the reconstructed energies $\sqrt{s_{\text{rec}}}$ from GuineaPig and the parameterization. Before, there was a problem for events, where the energy loss was smaller than 0.0001. This energy difference is a factor 10 smaller than the beam energy spread, which means that the differences in the reconstructed energy spectrum for the parameterizations and for GuineaPig are smeared out and disappear (Figure 9.1). Consequently the merging of the first bins for the reconstructed energy spectrum is removed.

The energy reconstructed by the acollinearity $\sqrt{s_{\text{rec}}}$ is by construction always smaller or equal to the nominal energy. That means that the energy spread added to events without beamstrahlung or bremsstrahlung with $\sqrt{s_{\text{rec}}/s} = 1$ always lowers the resulting reconstructed energy to $\sqrt{s_{\text{rec}}/s} < 1$. For events with acollinear outgoing particles, where the reconstructed energy is $\sqrt{s_{\text{rec}}/s} < 1$, adding the beam spread could increase or decrease the resulting reconstructed energy.

Table 9.1: Results for the re-weighting including a symmetric beam energy spread.

Par.	Arbitrary1	Arbitrary2	Error
a_{peak}	0.4116	0.3984	0.0041
a_{arm1}	0.1979	0.2077	0.0048
a_{arm2}	0.2325	0.2459	0.0048
a_2	12.96	12.84	0.50
a_3	-0.674	-0.701	0.018
a_4	11.78	11.31	0.40
a_5	-0.666	-0.693	0.016
a_6	10.71	10.87	0.64
a_7	-0.670	-0.6491	0.026
a_8	11.54	10.76	0.61
a_9	-0.726	-0.711	0.023
a_{body}	0.1580	0.1480	
σ_e	0.00102	0.00101	0.00001
σ_p	0.00103	0.00101	0.00001

9.2 Measuring a Symmetric Beam Energy Spread

At first, the beam energy spread is assumed to be equal for electrons and positrons:

$$\sigma_e = \sigma_p = 0.001. \quad (9.3)$$

The GuineaPig spectrum from the asymmetric beam parameters is used to generate the Bhabha events and the random variates symbolizing the beam spread are simply multiplied to the energies after beamstrahlung. The MC samples for the re-weighting fit are created with a symmetric beam energy spread of:

$$\sigma_e^A = \sigma_p^A = 0.0011. \quad (9.4)$$

The parameter sets “Arbitrary1” and “Arbitrary2” with the same parameters then before (Table 8.9) are used as the initial energy spectrum due to beamstrahlung.

The beam energy spread is measured with a precision of few percent. The distribution of the events for the different regions show a larger spread around the real value, but is still within 0.5% (Table 9.1). The inclusion of the beam energy spread in the measurement has only a small impact on the measurement of the other parameters.

The beam energy spread can be extracted because of the dependence of the reconstructed energy $\sqrt{s_{\text{rec}}}$ on the size of the beam energy spread.

9.2.1 Threshold Scan with Beam Energy Spread

The determined parameters are used to calculate the expected cross sections for a threshold scan. To calculate the cross sections the convolution between the asymmetric parameterization and the beam energy spread is used (4.10).

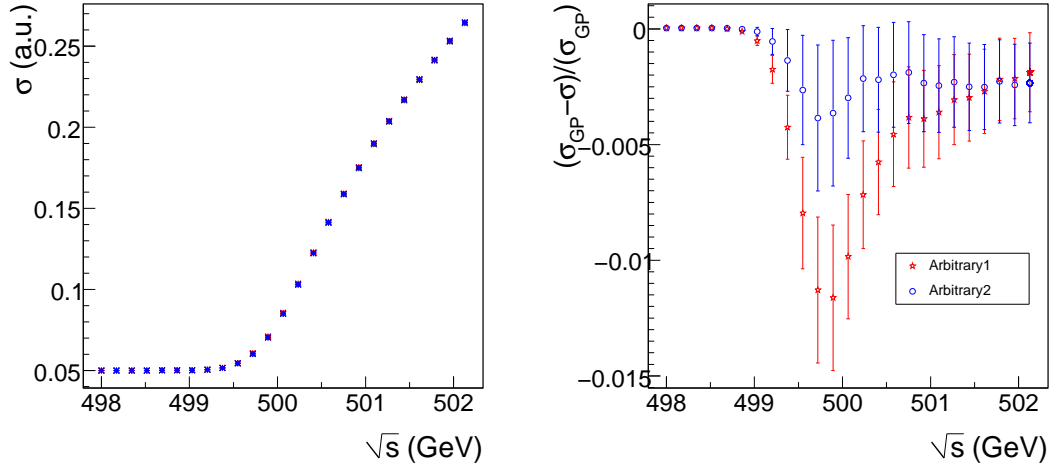


Figure 9.2: The thresholds scans for the measurement of the symmetric beam energy spread around the threshold.

The reference cross sections are calculated by taking the energy distribution of the scattering events from GuineaPig and multiplying them with random variates r_1 and r_2 of Gaussian distributions with the respective variance for the beam energy spread:

$$\sum_{i=1}^N \tilde{\sigma}(\sqrt{x_1^i x_2^i r_1^i r_2^i s}). \quad (9.5)$$

The resulting threshold scans for the interesting region around the threshold are found in Figure 9.2. The parameters returned for the set “Arbitrary1” show a large difference to the expected cross sections from GuineaPig. This difference of 1% at the threshold is caused by the large difference to the correct distribution of the events in the regions. For the set “Arbitrary2”, where the parameters a_{peak} , a_{arm1} and a_{arm2} are much closer to the expected results the difference is smaller than 0.5%.

9.3 Measuring the real Beam Energy Spread

If the undulator based positron source is used, the beam energy spread for the electrons is larger than that for the positrons.:

$$\sigma_e = 0.0014$$

$$\sigma_p = 0.0010$$

The data Bhabha sample is created with these expected beam energy spreads and the asymmetric differential luminosity generated for the asymmetric beam parameters.

For the MC Bhabha samples the beam energy spreads are also created with

Table 9.2: Results from the re-weighting fit including the real beam energy spread.

Par.	Arbitrary1	Arbitrary2	Error
a_{peak}	0.4035	0.3861	0.0048
$a_{\text{arm 1}}$	0.2062	0.2197	0.0054
$a_{\text{arm 2}}$	0.2417	0.2428	0.0053
a_2	12.68	11.95	0.49
a_3	-0.670	-0.759	0.018
a_4	11.15	11.44	0.40
a_5	-0.684	-0.688	0.017
a_6	11.13	9.76	0.55
a_7	-0.653	-0.677	0.025
a_8	11.41	11.37	0.64
a_9	-0.711	-0.689	0.025
a_{body}	0.1485	0.1514	
σ_e	0.00137	0.00139	0.00001
σ_p	0.00107	0.00102	0.00002

different sizes for electrons and positrons:

$$\sigma_e^A = 0.0015$$

$$\sigma_p^A = 0.0011$$

For the differential luminosity due to beamstrahlung the parameter sets “Arbitrary1” and “Arbitrary2” are used again to generate the Bhabha events.

The re-weighting fit is able to reproduce the correct beam energy spreads as well as the distributions of the events in the different regions (Table 9.2). The beam energy spreads are reproduced to within 5% of the correct values for the set “Arbitrary1” and to within 2% for the set “Arbitrary2”.

The re-weighting fit for the parameter set “Arbitrary2” is also slightly better able to describe the cross sections for the differential luminosity from GuineaPig (Figure 9.3). For “Arbitrary2” the cross sections are 0.5% smaller than the cross sections for GuineaPig and the difference diminishes rapidly. For “Arbitrary1” the cross sections are at most 0.6% larger than the ones expected from GuineaPig and the difference does not decrease as rapidly as for “Arbitrary2”.

It seems that the even distribution of the events for the initial differential luminosity described by the parameter set “Arbitrary2” is better able to extract the correct differential luminosity through the threshold scan.

9.4 Mass Measurement

The differential luminosity spectra and beam energy spreads measured by the re-weighting fit with the real beam energy spreads are used in the measurement of the

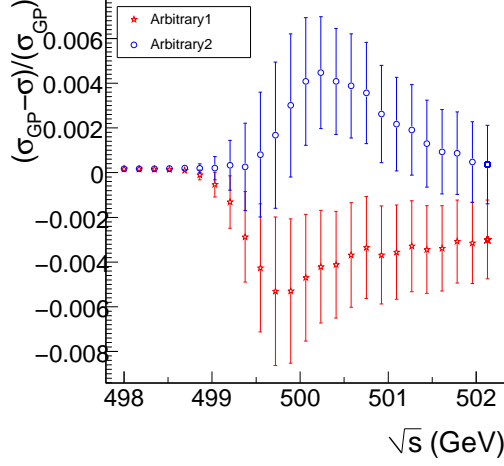


Figure 9.3: The thresholds scans for the measurement of the real beam energy spread around the threshold.

mass of a toy MC particle. The production cross section is given by (4.9):

$$\tilde{\sigma}_{e^+e^- \rightarrow \chi^+\chi^-}(s) \approx \frac{130\text{nb}}{s(\text{GeV}^2)} \cdot \sqrt{1 - \frac{4m_\chi^2}{s}}. \quad (9.6)$$

The measured data points are given by (9.5), the real beam energy spreads for the electrons and positrons are used for the Gaussian variates r_1 and r_2 . For each of the nine data points an integrated luminosity of $L_{\text{int}} = 5 \text{ fb}^{-1}$ is assumed and a small irreducible background is kept. A perfect detector efficiency is assumed, so that all produced particle pairs are counted. The resulting event rates are found in Table 9.4. One of the data points is taken far below the threshold to fix the background.

The fitting function is the function for the expected cross sections:

$$\sigma_L(\sqrt{s}) = \int dx_1 dx_2 L(x_1, x_2) \tilde{\sigma}(\sqrt{x_1 x_2 s}). \quad (9.7)$$

The differential luminosity $L(x_1, x_2)$ is given by the convolution of the asymmetric parameterization and the Gaussian distribution of the beam energy spread. The free parameters for the fit are the mass of the particle m and $\sigma_{\text{Background}}$ for the constant irreducible background. It is assumed that the differential luminosity is the same for all nominal center-of-mass energies used for the threshold scan, both from GuineaPig and the parameterizations.

The error on the mass m due to the parameter uncertainties Δ_j is calculated by fitting the data points once with the parameters A , which results in the mass $m(A)$. By fitting the data points again with the parameters A , where the j -th parameter was changed by one standard deviation of the error Δ_j , the masses $m(A - \Delta_j)$ are found. The variance on the mass $(\Delta m)^2$ is

$$(\Delta m)^2 = (m(A) - m(A - \Delta_j)) C_{jk} (m(A) - m(A - \Delta_k)), \quad (9.8)$$

Table 9.3: Expected event rate for the production of the MC toy particles with an integrated luminosity $L_{\text{int}} = 5\text{fb}^{-1}$ per scanning point.

Energy/GeV	Events
400	33 ± 6
497	33 ± 6
499	33 ± 6
501	117 ± 11
503	206 ± 14
505	272 ± 17
507	329 ± 18
509	381 ± 20
511	426 ± 21
513	468 ± 22

with the correlation matrix of the parameters C_{jk} . The masses found for the different initial parameter sets are:

$$\begin{aligned}
 \text{Arbitrary1} & \quad m_\chi = (250.001 \pm 0.007) \text{ GeV}, \\
 \text{Arbitrary2} & \quad m_\chi = (250.004 \pm 0.006) \text{ GeV}.
 \end{aligned}
 \tag{9.9}$$

The two results are in perfect agreement with the mass of the particle and the uncertainty due to the parameterizations is only 7 MeV, which is much smaller than the desired resolution for mass measurements of $\sigma_m/m = 10^{-4}$.

Of course, this result only uses the differential luminosity spectrum for beam-strahlung and beam energy spread and does not factor in the acceptance of the detector or systematics in the measurement of the beam energy. The final resolution of the mass will be larger, but it is not limited by the measurement of the differential luminosity.

Chapter 10

Conclusion

For some of the physics analyses at the ILC, like threshold scans, the differential luminosity has to be known precisely. Because of the dependence of the beamstrahlung on the geometry of the bunches the differential luminosity has to be measured through Bhabha scattering.

The differential luminosity is smeared by initial and final state radiation, so that a parameterization has to be used to measure the differential luminosity. The parameterization must be able to properly describe the important characteristics like the correlation between the energies of the scattering particles.

A measurement of the differential luminosity is possible through the very precisely reconstructed energy using the acollinearity of Bhabha events. But the study by Mönig [4] showed that the Circe parameterization is not able to describe the correlation between the particle energies and that this lack of correlation is significant.

To include the correlation a new parameterization based on Circe was created. This new parameterization is better able to describe the particle energy spectrum simulated by GuineaPig. The distribution of the scattering events in the three regions (peak, arms and body) of events of the beamstrahlung is described to a precision of less than 0.3% (Table 6.3) instead of a precision worse than 3% for Circe. This improved description of the differential luminosity also results in the threshold scans closer to the reference threshold scans using GuineaPig. CoPa is consistently closer than Circe to the threshold scan from GuineaPig, especially close to the threshold (Figure 6.2(b)).

The difference between Circe and GuineaPig becomes much more important, if the differential luminosity is no longer symmetric. In order to describe an asymmetric differential luminosity the parameterization was expanded further. This asymmetric parameterization is able to describe the distribution of the scattering events simulated by GuineaPig with differing beam parameters (Table 6.4). For the threshold scan only the asymmetric parameterization is able to properly follow the cross sections given by the GuineaPig particle energy spectrum without large offsets (Figure 6.3).

The measurement of the differential luminosity is also possible with the new parameterizations. The determination of the parameters was possible by using the

effective center-of-mass energy, reconstructed through the acollinearity, as well as the absolute particle energies measured by the calorimeter. It was possible to determine the correct distribution of the events in the different regions for the asymmetric differential luminosity.

The re-weighting fit with the three-dimensional histogram might still offer some room for improvement. The χ^2 is only calculated with an approximate error for the bin of the MC histogram. It might be possible to improve the results by running the fit iteratively and using the weights for the minimized χ^2 of the first fit as the base of the error for a following fit.

Not only the differential luminosity due to beamstrahlung, but also the beam energy spreads could be measured by the re-weighting fit. The expected asymmetric beam energy spreads of $\sigma_e/E = 0.0014$ for electrons and $\sigma_p/E = 0.0010$ for positrons could be determined within a precision of 5%. With the initial differential luminosity from the parameterization, where the events were evenly distributed in the different regions (30% in the peak, 25% each for the arms and 20% in the body, “Arbitrary2”) a precision of only 2% of the beam energy spreads was possible (Table 9.2). It can be noted that this parameter set “Arbitrary2” was significantly better able to reproduce the correct results than the other parameter set “Arbitrary1”. For the threshold scan the set “Arbitrary2” shows deviations to GuineaPig of only 0.4% as opposed to 0.6% by the other parameter set (Figure 9.3).

The result for the mass measured through the production threshold scan is an error of 7 MeV on a 250 GeV particle with an integrated luminosity of 5 fb^{-1} per data point. This error on the mass is smaller than the expected precision of the nominal beam energy measurements of $\Delta E_{\text{Beam}}/E_{\text{Beam}} \approx 10^{-4}$ [5].

All of these studies have been done with perfectly aligned beams, without energy jitter or other problems that might affect the differential luminosity. Because the collection of data takes about a month of running the ILC, it can be expected that some variation in the bunch geometry of beam energy will be encountered. How this will affect the determination of the parameters has not been studied.

Appendix A

Calculating the Effective Center-of-Mass Energy from the Angles

Because of the very good resolution of the trackers, the reconstruction of the effective center-of-mass energy is possible with a very high precision by using only the angles of the outgoing lepton pair. The only assumption that has to be made is the direction of the photon, in case of the beamstrahlung, where the beamstrahlung photons are not accessible.

From the momentum conservation follows

$$p_p + p_e = p_1 + p_2 + p_\gamma. \quad (\text{A.1})$$

It is assumed that there was only one photon and that it was radiated off along the beam pipe, i.e. the z-axis. Neglecting the electron masses $m_e \ll E_{\text{beam}}$ so that $p_0 = |\vec{p}| = E$ for all particles. Rotating the system around the z-axis so that everything happens in the xz -plane results in:

$$\begin{pmatrix} E_b + E_b \\ 0 \\ 0 \\ 0 \end{pmatrix} = \begin{pmatrix} E_1 + E_2 + E_\gamma \\ E_1 \sin(-\Theta_1) + E_2 \sin(\Theta_2) \\ 0 \\ E_1 \cos(-\Theta_1) + E_2 \cos(\Theta_2) + E_\gamma \end{pmatrix} \quad (\text{A.2})$$

From the momentum conservation follows for the energy of the outgoing leptons:

$$E_1 = -E_\gamma \frac{\sin(\Theta_2)}{\sin(\Theta_1 + \Theta_2)} \quad (\text{A.3})$$

$$E_2 = -E_\gamma \frac{\sin(\Theta_1)}{\sin(\Theta_1 + \Theta_2)} \quad (\text{A.4})$$

The Mandelstamm variable s equals the center-of-mass energy E_{cm} and

$$s = (p_e + p_p)^2 = 4E_b^2. \quad (\text{A.5})$$

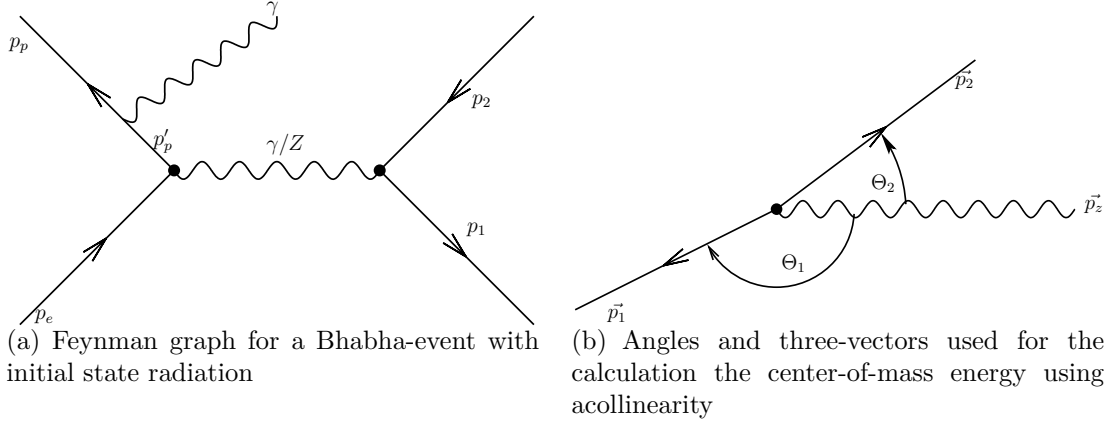


Figure A.1: Drawings for the calculation of $\sqrt{s'}$ using acollinearity

From (A.2) follows

$$s = (E_1 + E_2 + E_\gamma)^2. \quad (\text{A.6})$$

With (A.3)

$$s = \left(-E_\gamma \frac{\sin(\Theta_2)}{\sin(\Theta_1 + \Theta_2)} - E_\gamma \frac{\sin(\Theta_1)}{\sin(\Theta_1 + \Theta_2)} + E_\gamma \right)^2 \quad (\text{A.7})$$

$$s = \frac{E_\gamma^2}{\sin^2(\Theta_1 + \Theta_2)} (\sin(\Theta_1) + \sin(\Theta_2) - \sin(\Theta_1 + \Theta_2))^2 \quad (\text{A.8})$$

For the effective center-of-mass energy $\sqrt{s'}$ only the four-vectors of the outgoing leptons are used, because the energy of the photon is lost:

$$s' = (p_1 + p_2)^2 = p_1^2 + p_2^2 + 2p_1 p_2. \quad (\text{A.9})$$

Again neglecting the masses of the leptons $p^2 = m_e \ll 250 \text{ GeV}$ leads to

$$s' = 2E_1 E_2 (1 - \cos(\Theta_1 + \Theta_2)). \quad (\text{A.10})$$

Using (A.3) again leads to

$$s' = 2 \frac{E_\gamma^2}{\sin^2(\Theta_1 + \Theta_2)} (\sin(\Theta_1) \sin(\Theta_2) (1 - \cos(\Theta_1 + \Theta_2))). \quad (\text{A.11})$$

The following identities are needed for the transformations [24]:

$$\sin(\Theta_1) \sin(\Theta_2) = \frac{\cos(\Theta_1 - \Theta_2) - \cos(\Theta_1 + \Theta_2)}{2}, \quad (\text{A.12})$$

$$\sin(\Theta_1) \cos(\Theta_2) = \frac{\sin(\Theta_1 - \Theta_2) + \sin(\Theta_1 + \Theta_2)}{2}, \quad (\text{A.13})$$

$$\cos(\Theta_1 \pm \Theta_2) = \cos(\Theta_1) \cos(\Theta_2) \mp \sin(\Theta_1) \sin(\Theta_2), \quad (\text{A.14})$$

$$\cos^2(\Theta) + \sin^2(\Theta) = 1. \quad (\text{A.15})$$

Starting from the part that does not cancel with the term from s and expanding the cosine according to (A.14) is expanded to:

$$\begin{aligned} & 2 \sin(\Theta_1) \sin(\Theta_2)(1 - \cos(\Theta_1 + \Theta_2)) \\ &= 2 \sin(\Theta_1) \sin(\Theta_2) - 2 \sin(\Theta_1) \sin(\Theta_2) \cos(\Theta_1) \cos(\Theta_2) + 2 \sin^2(\Theta_1) \sin^2(\Theta_2). \end{aligned}$$

(A.12) and (A.13) are used for the appropriate terms:

$$\begin{aligned} &= \cos(\Theta_1 - \Theta_2) - \cos(\Theta_1 + \Theta_2) \\ & - \frac{1}{2}(\sin(\Theta_1 + \Theta_2) + \sin(\Theta_1 - \Theta_2))(\sin(\Theta_1 + \Theta_2) - \sin(\Theta_1 - \Theta_2)) \\ & + \frac{1}{2}(\cos(\Theta_1 - \Theta_2) - \cos(\Theta_1 + \Theta_2))^2 \\ &= \cos(\Theta_1 - \Theta_2) - \cos(\Theta_1 + \Theta_2) \\ & - \frac{1}{2}(\sin^2(\Theta_1 + \Theta_2) - \sin^2(\Theta_1 - \Theta_2)) \\ & + \frac{1}{2}(\cos^2(\Theta_1 - \Theta_2) + \cos^2(\Theta_1 + \Theta_2) - 2 \cos(\Theta_1 - \Theta_2) \cos(\Theta_1 + \Theta_2)). \end{aligned}$$

(A.15) is used to replace \cos^2 -terms with \sin^2 -terms:

$$\begin{aligned} &= \cos(\Theta_1 - \Theta_2) - \cos(\Theta_1 + \Theta_2) - \cos(\Theta_1 - \Theta_2) \cos(\Theta_1 + \Theta_2) \\ & + \frac{1}{2}(1 - \sin^2(\Theta_1 - \Theta_2) + 1 - \sin^2(\Theta_1 + \Theta_2)) \\ & - \frac{1}{2}(\sin^2(\Theta_1 + \Theta_2) - \sin^2(\Theta_1 - \Theta_2)) \\ &= \cos(\Theta_1 - \Theta_2) - \cos(\Theta_1 + \Theta_2) \\ & - \cos(\Theta_1 - \Theta_2) \cos(\Theta_1 + \Theta_2) \\ & + 1 - \sin^2(\Theta_1 + \Theta_2). \end{aligned}$$

(A.14) is used where applicable:

$$\begin{aligned} &= 1 - \sin^2(\Theta_1 + \Theta_2) \\ & + \cos(\Theta_1) \cos(\Theta_2) + \sin(\Theta_1) \sin(\Theta_2) \\ & - (\cos(\Theta_1) \cos(\Theta_2) - \sin(\Theta_1) \sin(\Theta_2)) \\ & - (\cos(\Theta_1) \cos(\Theta_2) + \sin(\Theta_1) \sin(\Theta_2))(\cos(\Theta_1) \cos(\Theta_2) - \sin(\Theta_1) \sin(\Theta_2)) \\ &= 1 - \sin^2(\Theta_1 + \Theta_2) + 2 \sin(\Theta_1) \sin(\Theta_2) \\ & - \cos^2(\Theta_1) \cos^2(\Theta_2) + \sin^2(\Theta_1) \sin^2(\Theta_2). \end{aligned}$$

(A.15) is used again to replace \cos^2 -terms with \sin^2 -terms

$$\begin{aligned}
&= 1 - \sin^2(\Theta_1 + \Theta_2) + 2 \sin(\Theta_1) \sin(\Theta_2) \\
&\quad - (1 - \sin^2(\Theta_1))(1 - \sin^2(\Theta_2)) + \sin^2(\Theta_1) \sin^2(\Theta_2) \\
&= 1 - \sin^2(\Theta_1 + \Theta_2) + 2 \sin(\Theta_1) \sin(\Theta_2) \\
&\quad - (1 - \sin^2(\Theta_1) - \sin^2(\Theta_2) + \sin^2(\Theta_1) \sin^2(\Theta_2)) + \sin^2(\Theta_1) \sin^2(\Theta_2) \\
&= 1 - \sin^2(\Theta_1 + \Theta_2) + 2 \sin(\Theta_1) \sin(\Theta_2) \\
&\quad - 1 + \sin^2(\Theta_1) + \sin^2(\Theta_2) \\
&= -\sin^2(\Theta_1 + \Theta_2) + 2 \sin(\Theta_1) \sin(\Theta_2) + \sin^2(\Theta_1) + \sin^2(\Theta_2) \\
&= -\sin^2(\Theta_1 + \Theta_2) + (\sin(\Theta_1) + \sin(\Theta_2))^2 \\
&= (\sin(\Theta_1) + \sin(\Theta_2) + \sin^2(\Theta_1 + \Theta_2))(\sin(\Theta_1) + \sin(\Theta_2) - \sin^2(\Theta_1 + \Theta_2)).
\end{aligned}$$

Finally s' becomes:

$$\begin{aligned}
s' = \frac{E_\gamma^2}{\sin^2(\Theta_1 + \Theta_2)} & (\sin(\Theta_1) + \sin(\Theta_2) - \sin(\Theta_1 + \Theta_2)) \\
& \cdot (\sin(\Theta_1) + \sin(\Theta_2) + \sin(\Theta_1 + \Theta_2)).
\end{aligned} \tag{A.16}$$

Dividing (A.16) by (A.8) leaves the fraction of the nominal beam energy that can be calculated using only the angles of the outgoing particles:

$$\frac{\sqrt{s'}}{\sqrt{s}} = \sqrt{\frac{(\sin(\Theta_1) + \sin(\Theta_2) + \sin(\Theta_1 + \Theta_2))}{\sin(\Theta_1) + \sin(\Theta_2) - \sin(\Theta_1 + \Theta_2)}}. \tag{A.17}$$

For the simulation the angles Θ_1 and Θ_2 are calculated from the four vectors of the leptons:

$$\begin{aligned}
\Theta_1 &= \text{acos}(p'_z/|\vec{p}'|), \\
\Theta_2 &= \text{acos}(q'_z/|\vec{q}'|).
\end{aligned} \tag{A.18}$$

Because $\sqrt{s'}$ differs to the real effective center-of-mass energy, if photons are radiated in different directions the effective center-of-mass energy reconstructed through the acollinearity is called $\sqrt{s_{\text{rec}}}$.

Bibliography

- [1] D. Schulte. *Study of Electromagnetic and Hadronic Background in the Interaction Region of the Tesla Collider*. PhD thesis, Universität Hamburg, 1996.
- [2] T. Ohl. CIRCE version 1.0: Beam spectra for simulating linear collider physics. *Comput. Phys. Commun.*, 101:269–288, 1997. doi: 10.1016/S0010-4655(96)00167-1.
- [3] N. Phinney et al., editors. *ILC Reference Design Report Volume 3 - Accelerator*. ILC, 2007.
- [4] K. Mönig. Measurement of the differential luminosity using Bhabha events in the forward tracking region at TESLA, 2000. LC-PHSM-2000-060.
- [5] J. Brau et al., editors. *International Linear Collider Reference Design Report. 1: Executive Summary. 2: Physics at the ILC. 3: Accelerator. 4: Detectors*. ILC, 2007. ILC-REPORT-2007-001.
- [6] A. Djouadi et al., editors. *ILC Reference Design Report Volume 2 - Physics at the ILC*. ILC, 2007.
- [7] J. D. Jackson. *Klassische Elektrodynamik*. Walter de Gruyter, Berlin, New York, 2. verbesserte auflage edition, 1985.
- [8] Global design effort, 2007. URL <http://www.linearcollider.org>.
- [9] T. Behnke. The ILC: The next step in particle physics. *J. Phys. Conf. Ser.*, 53:371–396, 2006. doi: 10.1088/1742-6596/53/1/023.
- [10] M. A. Thomson. Particle flow calorimetry at the ILC, 2006.
- [11] J. Brau et al., editors. *ILC Reference Design Report Volume 1 - Executive Summary*. ILC, 2007.
- [12] Geant4 - a simulation toolkit. URL <http://geant4.web.cern.ch/geant4/>.
- [13] Mokka - a detailed geant4 simulation for the international linear collider detectors. URL <http://polywww.in2p3.fr/activites/physique/geant4/tesla/www/mokka/mokka.html>.

- [14] Modular analysis and reconstruction for the linear collider (marlin). URL http://ilcsoft.desy.de/portal/software_packages/marlin/index_eng.html.
- [15] P. Chen. An introduction to beamstrahlung and disruption. In M. Month and S. Turner, editors, *Frontiers of Particle Beams*, volume 296 of *Lecture Notes in Physics*, Berlin Springer Verlag, pages 495–532, 1988. SLAC-PUB-4379.
- [16] P. Chen. Beamstrahlung and the QED, QCD backgrounds in linear colliders, 1992. Presented at 9th International Workshop on Photon-Photon Collisions (PHOTON-PHOTON '92), San Diego, CA, 22-26 Mar 1992, SLAC-PUB-5914.
- [17] C. Amsler et al. Review of particle physics. *Phys. Lett.*, B667:1, 2008.
- [18] E. W. Weisstein. Beta function, November 2008. URL <http://mathworld.wolfram.com/BetaFunction.html>. From MathWorld – A Wolfram Web Resource.
- [19] E. W. Weisstein. Incomplete beta function, November 2008. URL <http://mathworld.wolfram.com/IncompleteBetaFunction.html>. From MathWorld – A Wolfram Web Resource.
- [20] Root: An object oriented data-analysis framework, 2008. URL <http://root.cern.ch/>.
- [21] F. James and M. Roos. Minuit: A System for Function Minimization and Analysis of the Parameter Errors and Correlations. *Comput. Phys. Commun.*, 10:343–367, 1975.
- [22] S. Jadach, W. Placzek, and B. F. L. Ward. BHWIDE 1.00: O(alpha) YFS exponentiated Monte Carlo for Bhabha scattering at wide angles for LEP1/SLC and LEP2. *Phys. Lett.*, B390:298–308, 1997. doi: 10.1016/S0370-2693(96)01382-2.
- [23] C. Rimbault, P. Bambade, K. Monig, and D. Schulte. Impact of beam-beam effects on precision luminosity measurements at the ILC. *JINST*, 2:P09001, 2007. doi: 10.1088/1748-0221/2/09/P09001.
- [24] I. N. Bronstein, K. A. Semendjajew, G. Musiol, and H. Mühlig. *Taschenbuch der Mathematik*. Verlag Harri Deutsch, Thun, Frankfurt a. M., 5. erweiterte und verbesserte auflage edition, 2001.

List of Figures

2.1	ILC Layout	6
2.2	LDC Overview	9
2.3	Angular spectrum of reconstructed events	10
2.4	Angle vs reconstructed Energy	10
2.5	Particle energy spectra after reconstruction	11
3.1	Gauss surface and amperian loop	14
3.2	Energy spectra simulated with GuineaPig for the different beam parameter sets from Table 2.1. The legend from the plot on the left applies to the plot on the right as well.	17
3.3	These plots show the time slices of a simulated bunch crossing. The histograms show events that happen during the first, second, third and fourth quarter of the bunch crossing respectively. The particles show a larger probability to radiate for events occurring later during the bunch crossing.	18
4.1	Differential luminosity spectrum.	20
4.2	Threshold scan with and without luminosity spectrum	23
4.3	Threshold scan with beam energy spread	24
5.1	Energy spectrum after Beamstrahlung	26
5.2	The beta-distribution part of the Circe parameterization without and with the transformation $t = (1 - x)^{1/5}$	28
5.3	Transformed GuineaPig Spectrum	29
5.4	Fit on the GuineaPig spectrum using Circe.	31
5.5	Comparisons between Circe and GuineaPig	32
5.6	Effective center-of-mass energy spectrum	33
5.7	Relative differences between the threshold scan using GuineaPig and scans, where a Circe parameterization was used as the differential luminosity.	35
6.1	Effect of the correlation between the particle energies on the slopes of the beta-distribution.	38
6.2	Threshold scans with Circe and CoPa.	41

6.3	Relative difference between the threshold scans with Circe, CoPa and Asym and the threshold scan from the asymmetric GuineaPig sample.	43
7.1	Feynman graph and angles for the reconstruction of the effective center-of-mass energy.	46
7.2	Energy spectra of Bhabha-events	47
7.3	Smearred energy spectrum.	49
8.1	The two histograms after the re-weighting fit (left) and their relative difference (right).	55
8.2	The weights for the MC histogram for the lowest χ^2 from the fit where the initial parameters were the real parameters without (left) and with (right) the merging. The large peak is from the events with $x_1 = x_2 = 1.0$.	57
8.3	The two histograms after the re-weighting fit (left) and their relative difference(right), where the bins below $E_T = 0.14$ have been merged.	57
8.4	The resulting threshold scans for the fit without (left) and with (right) the merger.	58
8.5	Threshold-scan resulting from the 1D and 2D re-weighting fit with CoPa.	60
8.6	Histograms used for the 2D re-weighting fit to find the CoPa parameters. The sharp cutoff for $E_T = 0.14$ are due to the merging of the bins.	60
8.7	Left: Threshold scans for the results from the 2D fit. Right: Threshold scans for the results for the 3D fits without the demand of at least 20 entries for a bin.	61
8.8	The three-dimensional histogram used for the re-weighting fit.	62
8.9	Left: Threshold scans for the results from the 2D fit. Right: Threshold scans for the results for the 3D fits with the demand of at least 20 entries for a bin.	63
8.10	Resulting threshold scans for the an asymmetric differential luminosity measured with the symmetric parameterizations Circe and Copa (Left) and the asymmetric parameterization (Right).	66
8.11	Projections of the three-dimensional histogram used for the re-weighting fit. Note that the events from bins with less than 20 entries have been removed prior to the projection, leaving some areas empty. Left: Projection showing the transformed reconstructed spectrum E_T versus the transformed energy spectrum of the positron E_T^- . Right: Projection showing the transformed energy spectrum of the electron E_T^- versus the energy spectrum of the positron E_T^+ .	66
9.1	The histogram of the transformed reconstructed energy E_T . The peak moves to a lower energy because of the beam energy spread.	68
9.2	The thresholds scans for the measurement of the symmetric beam energy spread around the threshold.	70

9.3	The thresholds scans for the measurement of the real beam energy spread around the threshold.	72
A.1	Feynman Graph and Angles	78

List of Tables

2.1	Beam parameters for the ILC at $\sqrt{s} = 500$ GeV [3].	8
5.1	Results for fitting the 1D and 2D Circe parameterization to two particle energy spectra produced by GuineaPig. Both GuineaPig samples were produced with the same beam parameters. The bins are per axis, which means that the bins for the two-dimensional histograms are N_{Bins}^2 . Some of the bins are empty, because of the merging of the bins below $t \approx 0.15$	31
6.1	Probabilities for the different regions of the Energy spectrum due to Beamstrahlung.	38
6.2	Results for fitting the correlated parameterization to two different GuineaPig samples produced with the same beam-parameters, with different numbers of bins per axis.	40
6.3	Probabilities for the different regions of the Energy spectrum due to beamstrahlung.	40
6.4	The probabilities for the case of the asymmetric beam properties and the results for the different parameterizations.	42
6.5	Parameters to describe the asymmetric spectrum from all three parameterizations. The fits were done with 50 bins per axis.	43
8.1	Circe parameters for the differential luminosity input for BHWide (See Section 7.1.1).	54
8.2	The Circe parameters and the reproduced parameters using re-weighting to fit the MC onto the MC Sample.	55
8.3	Parameters reproduced by the re-weighting fit. The parameters found by the direct fit are $a_0 = 0.6288$, $a_2 = 11.81$ and $a_3 = -0.6733$	56
8.4	Parameters for the production of the parameterized energy spectra used as the initial energy for the generation of the Bhabha events. . .	58
8.5	Comparison between the errors from the direct fit to the GuineaPig spectrum and the 1D and 2D-re-weighting fit from CoPa to CoPa. . .	59
8.6	Results for the measurement of the CoPa parameters from the re-weighting fit using two-dimensional histograms. Errors are approximately equal for all results.	61

8.7	Results for the measurement of the CoPa parameters from the re-weighting fit using three-dimensional histograms without the requirement of at least 20 entries in a bin. Errors are approximately equal for all results.	63
8.8	Results for the determination of the CoPa parameters from the re-weighting fit using the three-dimensional histograms with the requirement of at least 20 entries in a bin. Errors are approximately equal for all results.	63
8.9	Parameters from the asymmetric parameterization for the production of the parameterized energy spectra.	64
8.10	Results for the three-dimensional re-weighting fit for the asymmetric parameterization.	65
9.1	Results for the re-weighting including a symmetric beam energy spread.	69
9.2	Results from the re-weighting fit including the real beam energy spread.	71
9.3	Expected event rate for the production of the MC toy particles with an integrated luminosity $L_{\text{int}} = 5\text{fb}^{-1}$ per scanning point.	73

Selbständigkeitserklärung

Hiermit erkläre ich, dass ich die vorgelegte Diplomarbeit eigenständig, ohne unerlaubte fremde Hilfe und nur unter der Zuhilfenahme der angegebenen Quellen verfasst habe.